UNIVERSITY OF SOUTHAMPTON

DEPARTMENT OF ELECTRONICS

BIREFRINGENCE IN SINGLE-MODE OPTICAL FIBRES

by

ARTHUR JOHN BARLOW

A thesis submitted for the degree of
Doctor of Philosphy
November 1982

LIST OF CONTENTS

UNIVERSITY OF SOUTHAMPTON

ABSTRACT

FACULTY OF ENGINEERING AND APPLIED SCIENCE

ELECTRONICS

Doctor of Philosophy

BIREFRINGENCE IN SINGLE-MODE OPTICAL FIBRES

By Arthur John Barlow

The birefringence properties of single-mode optical-fibre waveguides are discussed.

A fibre birefringence measurement system has been developed specifically to measure the birefringence of fibres as a function of temperature, wavelength, twist and bending. By incorporating a birefringence modulator into the system, the measurement speed and sensitivity is substantially increased, particularly for low birefringences.

The fibre spinning technique has been invented to provide a means of manufacturing ultra-low birefringence fibres with extremely high yield. It is shown that spinning averages the intrinsic local birefringence to produce very low overall retardation. A coupled-mode analysis to describe the birefringence properties of spun and twisted fibres is developed and confirmed experimentally. It is now possible to manufacture ultra-low birefringence fibres routinely.

The coupled-mode analysis is subsequently extended to treat the effects of bending, twist and magnetic fields on both linearly- and circularly-birefringent fibres. The predictions are subsequently confirmed experimentally and a thorough understanding of extrinsic effects on fibre birefringence has been established. The design criteria of polarisation-maintaining fibres are discussed.

A novel technique is also described for the measurement of polarisation mode-dispersion, based on the variation of birefringence with wavelength. The dramatic reduction of polarisation-dispersion achieved by spinning is demonstrated, thereby indicating the high suitability of spun fibres to high-bandwidth communications.

The separate identification of the stress and waveguide effects contributing to the intrinsic fibre birefringence has been achieved by observing the changes in birefringence as a function of wavelength and temperature.

ACKNOWLEDGEMENTS

I would like to thank several members of the Southampton University Optical Communications Group who have contributed to the present work. In particular, I owe much to Dr. David Payne for his numerous ideas for further study without which my progress would have been considerably slower. I would also like to thank Dr. Jens Ramskov Hansen for his excellent collaboration with me in the work on spun and twisted fibres. His help in some of these measurements and with the analysis is greatly appreciated. I also thank Max Hadley and Bob Mansfield for their extensive work in developing the fibre spinning process, and Dr. Eleanor Tarbox, Dr. Robin Birch, Dr. Steve Norman, Dr. Rick Calligaro and members of BTRL, Ipswich for supplying all the fibres used in this work. I am indebted to Dr. Gordon Day for numerous stimulating conversations on the effect of external influences on fibres and to Dr. Arthur Hartog and Martin Gold for their suggestions concerning reflectometry in single-mode fibres. Dr. Mike Adams and Dr. Cathy Ragdale have given me much advice on waveguide theory, for which I am very grateful. Thanks are also due to Malcolm Varnham for numerous awkward questions, Dr. Issei Sasaki for several preform refractive-index profiles, and Steve Clift for attenuation measurements and excellent photographic work.

I am especially grateful to both Dr. Abbas Ourmazd and Professor W. A. Gambling for their comments on the thesis manuscript and to Professor Gambling for his overall supervision. I also owe thanks to Nicki Pink for her excellent and patient typing of the manuscript.

I acknowledge the financial support of the Science and Engineering Research Council and the University of Southampton for the duration of this work.

Finally, I would like to thank my wife, Carol, for her encouragement, keen interest and help in preparing this thesis.

CHAPTER 1 INTRODUCTION

The development of optical fibre waveguides has undoubtedly made a great impact upon the telecommunications industry in recent years. Conventional coaxial-cable systems are unable to compete against the far greater information capacity, reduced weight and lower attenuation of optical fibre systems. Optical communication provides a cost-effective solution to the ever-increasing demand for information transfer and numerous systems are already in operation throughout the world.

Optical fibres can also be incorporated into industrial sensors of all types. The chief advantages of optical sensors are the elimination of electrical fire risk and the lack of sensitivity to electromagnetic interference. Integrating the sensing and communication functions into one fibre yields the possibility of all-optical distributed-sensing systems for industry.

In recent years, research in optical communications has shifted its emphasis from multimode fibres towards single-mode fibres which can provide higher transmission bandwidths, greater sensing capabilities and compatability to integrated optical circuits for direct optical processing systems.

This thesis covers birefringence in single-mode fibres, a topic which encompasses both telecommunications and sensor applications of these fibres. The research programme was also to some extent directed towards the development of fibres with special birefringence properties.

1.1 Background to the Research Programme

Initially optical fibre waveguide development centred on multimode structures and relatively low data-rate, short-haul communication systems. However,

it soon became necessary to develop single-mode fibres for higher-performance systems, including submarine systems. These fibres support only one mode, eliminating the intermodal dispersion prevalant in multimode fibres. The resultant high bandwidth (~ 100 GHz km^{-1} nm^{-1}) coupled with the move to the wavelength regions of low material dispersion and low loss at 1.3μm and 1.55μm has enabled repeater spacings in excess of 100km to be achieved in a 140 mbits/s system[1]. The compatibility of single-mode fibres with integrated optical circuits has promoted their development still further.

However, in practice a single-mode fibre can support two modes with orthogonal polarisations and different propagation characteristics, the latter being considerably influenced by external effects such as pressure on the fibre. A single-mode fibre is therefore birefringent and also exhibits a modal group-delay difference which can limit the fibre bandwidth[2]. Thus, for a fixed input polarisation state the output polarisation varies according to the environmental conditions prevailing. This affects the efficient coupling of light into integrated optical devices which are polarisation-sensitive, and the operation of optical phase-coherent detection schemes[3] in advanced communication systems with large repeater-spacings.

A parallel development to the extensive research effort in the telecommunications sector is a widespread exploitation of fibre-optic technology in sensing devices[4]. Single-mode fibres come into their own in this case; interference between the single guided modes in two fibres can be made to occur in a fibre interferometric sensor such as a Sagnac-effect gyroscope. Again it is found that the fibre birefringence properties can greatly upset sensor operation. Conversely, these very properties can be used in polarimetric (single-fibre) sensors as an extremely sensitive measure of magnetic or acoustic fields, for example[4]. The light guidance of

a fibre allows extremely long optical path lengths to be achieved and hence the sensitivity to be increased, as in the Faraday-rotation current monitor device[5]. The same fibre can, of course, also provide an optical telemetry function from the sensor head.

The polarisation behaviour of a single-mode fibre is thus an extremely important parameter to consider in the design of advanced communications and sensor systems.

1.2 The Research Programme

The general objective of the research programme was to investigate the phenomenon of birefringence in single-mode fibres to gain a full understanding of the subject. Possible applications were also examined. As we shall see, the successful use of fibres in both communications and sensors rests to a large extent on the ability to produce structures having special polarisation properties such as very low or very high birefringence. The development of such fibres was therefore a specific aim of the programme. Several other important questions concerned with birefringence were also addressed, notably the measurement of the extreme range of possible fibre birefringence, the environmental sensitivity of birefringent fibres and the evaluation of the bandwidth limitations likely to arise from birefringence.

At the beginning of the programme in 1978 the field was in its infancy and previous work centred largely around experimental observations[6,7,8] but with little firm theoretical backing. However, the requirement for very high birefringence fibres[9] for interferometric sensors and coupling to integrated optical circuits, and ultra-low birefringence fibres[10] for polarimetric sensors such as the Faraday-rotation current monitor, had already been widely recognised. Although little was understood of the origins and mechanism of fibre birefringence, initial efforts to fabricate these fibres were already underway[9,10].

Over the duration of the present research however, the amount of activity increased sharply. The field can now be said to have reached maturity with many important areas having been covered. For example the present understanding of the causes of birefringence and the effects of external parameters appears to be largely complete. The influence of birefringence on bandwidth and its exploitation in several types of fibre sensor have also been investigated. Furthermore, fibres with both ultra-low birefringence and high-birefringence can now be manufactured on a routine basis in the laboratory and will eventually reach production.

The programme described in subsequent Chapters is set out with several distinct divisions. Chapter Two embraces the complete scope of the thesis and presents the important basic concepts. A summary of the origins of fibre birefringence, both internally and extrinsically produced, is presented. The effect of birefringence on bandwidth is also introduced. This Chapter also describes the theoretical modelling techniques for studying fibre birefringence.

Chapter Three is concerned with the experimental aspects and details of the present study. Much of the work has relied on the measurement of birefringence in fibres to provide confirmation of theoretical ideas, such as the effect of twisting on birefringence. The main problems encountered when measuring the large range of magnitudes of fibre birefringence are examined and special techniques to overcome these are described. The reduction of undesired extrinsic effects during the measurement has been achieved by hanging the fibre vertically.

A large part of the research work, described in Chapter Four, is concerned with the development of fibres with very low birefringence which are suitable for high-bandwidth telecommunications and sensors. It is found that conventional techniques for fibre manufacture

have very poor yields for low birefringence. To circumvent this, a new "spinning" technique has been developed which, by imparting a large frozen-in twist to the fibre, guarantees ultra-low birefringence in production. The analysis of twisted, birefringent fibres is therefore an important part of 'spun' fibre development and is discussed in considerable detail.

Chapter Five extends the analysis of Chapter Four to provide a theoretical evaluation of the magnitude and influence of several external effects which can in fact be classified into two different types. In many of these cases direct experimental confirmation is provided by measurements of the properties of fibres deformed in a controlled manner. The results are subsequently applied to fibre telecommunications and sensors. Indeed, this analysis provides a conceptual design strategy for fibre sensors in addition to quantifying environmental influences such as bending on birefringent fibres.

In Chapter Six, the dispersive effects of fibre birefringence are examined, beginning with mechanisms and measurement. Experimental results obtained using a tunable-wavelength source are presented and the effect of twisting and spinning a fibre on its polarisation dispersion is discussed.

It is found that for maximum bandwidth a 'spun' fibre is essential. A subsequent section examines the variation of birefringence with ambient temperature and quantifies this effect to estimate the stability of various polarimetric fibre sensors. In addition, by exploiting the temperature dependence and the dispersion of birefringence, methods of isolating the various sources of fibre intrinsic birefringence are demonstrated for the purposes of diagnostic feedback to birefringent fibre fabrication.

Finally, Chapter Seven concludes the study, outlining the major achievements of the work, the areas for future study and briefly reviewing some very recent developments in the field occurring during the compilation of this presentation.

1.3 References

1. Maylon, D. J., and McDonna, A. P.: "102km unrepeatered momomode fibre system experiment at 140 Mbit/s with an injection locked 1.52 μm laser transmitter", Electron. Lett., 18, 1982, pp. 445-447.

2. Kapron, F. P., Borrelli, N. F., and Keck, D. B.: "Birefringence in dielectric optical waveguides", IEEE J. of Quantum Electron., QE-8, 1972, pp. 222-225.

3. Yamamoto, Y., and Kimura, T.: "Coherent optical fibre transmission systems", IEEE J. of Quantum Electron., QE-17, 1981, pp. 919-935.

4. Giallorenzi, T. G., et al.: "Optical fibre sensor technology", IEEE J. of Quantum Electron., QE-18, 1982, pp. 626-665.

5. Smith, A. M.: "Polarisation and magneto-optic properties of single-mode optical fibre", Appl. Optics, 17, 1978, pp. 52-56.

6. Papp, A., and Harms, H.: "Polarisation optics of index-gradient optical waveguide fibres", Appl. Optics, 14, 1975, pp. 2406-2411.

7. Gambling, W. A., Payne, D.N., and Matsumura, H.: "Birefringence and optical activity in single-mode fibres", Paper presented at Topical Meeting on Optical Fibre Transmission II Williamsburg, February 22-24, 1977.

8. Harms, A., Papp, A., and Kempter, K.; "Magneto-optical properties of index-gradient optical fibres", Appl. Optics, 15, 1976, pp. 799-801.

9. Ramaswamy, V., French, W. G., and Standley, R.D.: "Polarisation characteristics of non-circular core

single-mode fibres", Appl. Optics, 17, 1978, pp. 3014-3017.

10. Norman, S. R., Payne, D. N., Adams, M. J., and Smith, A. M.: "Fabrication of single-mode fibres exhibiting extremely low polarisation birefringence", Electron. Lett., 15, 1979, pp. 309-311.

CHAPTER 2 BIREFRINGENCE IN SINGLE-MODE FIBRES

2.1 Introduction

Any core asymmetry or stress anisotropy within a single-mode fibre will raise the degeneracy between the two orthogonal linearly-polarised modes, to give a slight relative phase-velocity difference between the modes, or linear birefringence[1,2]. If the plane of polarisation of the two modes (corresponding to the geometric axes) varies along the fibre, circular birefringence is also present[1]. Circular birefringence can be regarded as a phase-velocity difference between left- and right-circularly polarised light equal to twice the angle of rotation Ω of the plane of polarisation of the linearly-polarised fibre modes.

Fibre birefringence arises intrinsically, from core asymmetry or internal thermal-stress anisotropy, and extrinsically from stresses or electromagnetic fields applied to the fibre.

Stress introduces birefringence by means of the photo-elastic or stress-optic effect[3] which plays a very important role in fibre birefringence effects.

This Chapter is confined to a general appraisal of birefringence phenomena in fibres to elucidate the most important problems and research objectives concerning the application of birefringent single-mode fibres in practical systems. First, the various sources of birefringence are discussed. It is shown that the instability in fibre properties caused by time-varying external effects is of prime importance in the design of practical fibres. Several means by which these properties may be analysed theoretically are compared. Next, the effect of birefringence on transmission bandwidth will be discussed. Finally, the design objectives for fibres suitable for communication and sensors will be described.

2.2 Origins of Intrinsic Fibre Birefringence

2.2.1 Linear birefringence

(i) Core asymmetry

The most common form of asymmetry is generally assumed to be core ellipticity. In a fibre with an elliptical core, a difference in propagation constants $\beta_1 - \beta_2 = \Delta\beta_G$ between the two linearly-polarised modes arises from a waveguide effect[4]. The resultant birefringence B_G is given by:

$$B_G = \frac{\lambda}{2\pi} \cdot \Delta\beta_G \qquad (2.1)$$

where λ is the wavelength of light. B_G is proportional to the square of the core-cladding index difference $\Delta'n$ and the ellipticity $e = (\frac{a}{b} - 1)$ for $e < 0.2$, where a and b are the core semi-major and semi-minor axes respectively[4-8]. Figure 2.1 shows $B_G/(\Delta'n)^2$ evaluated[9] at the V-value[10] corresponding to the second-order mode cut-off[11] in the elliptical core (V = 2.4 for near-circular step-index fibres). The waveguide shape birefringence B_G has a fixed sign (taken as positive) such that the polarisation direction of the mode with the higher phase-velocity always coincides with the minor axis of the core ellipse.

(ii) Stress anisotropy

The doped-silica regions in a fibre providing the required index profile for light guiding invariably possess different thermal expansion coefficients according to their respective dopant concentrations. Thus as the fibre cools from the drawing temperature, large thermal stresses are set up by differential thermal contraction within the fibre.
Any structural asymmetry such as an elliptical core or cladding will result in anisotropy in the radial and tangential thermal stresses at the core centre. Through the photo-elastic effect, this gives rise to

a stress-birefringence B_S. However, since a fraction of the total light travels in the cladding[10], it is not clear whether the stresses in the cladding will also contribute to B_S. Furthermore this fraction varies with fibre V-value and may therefore affect the variation of B_S with light wavelength[12,13].

The sign of B_S relative to the minor axis of the core can vary according to the shapes and the relative thermal expansion coefficients of the stress-producing regions of the fibre.

In the fibre the total intrinsic linear birefringence B is simply the algebraic sum of B_G and B_S.

$$B = B_G + B_S = \frac{\lambda}{2\pi} . \Delta\beta = \delta n \qquad (2.2)$$

where $\Delta\beta$ is the total difference in propagation constants and δn is the difference in mode effective-indices. When both polarisation modes are launched, the polarisation state (PS) evolves cyclically along the fibre as the modes beat together in phase relationship. The PS is periodically repeated each time the total retardance R(z) for fibre length z , given by

$$R(z) = \Delta\beta z \qquad (2.3)$$

increases by 2π. This occurs at distances along the fibre spaced a "beat-length" apart. The beat-length L_p is given by

$$L_p = \frac{2\pi}{\Delta\beta} = \frac{\lambda}{B} \quad m. \qquad (2.4)$$

and is particularly useful for characterising the birefringence of a fibre.

2.2.2 Circular birefringence

If the linearly-birefringent fibre described above were twisted, the axes of the birefringence would vary in direction along the fibre. It can be shown that the rotating birefringence axes give rise to a rotation or circular birefringence in the fibre as well as modifying the apparent linear birefringence. Although twist is strictly an extrinsic effect, it is possible for a fibre to possess a frozen-in twist imparted while it is still molten, for example during fibre drawing and therefore to exhibit *intrinsic* circular as well as linear birefringence. The effect of twisting a fibre which is already linearly-birefringent will be discussed in Chapter Four.

2.3 External Effects in Fibres

The birefringence of a fibre is sensitive to external effects, such as bends, which cause the output polarisation state to vary randomly with time. While this causes severe operational problems in communication and polarisation-sensitive applications, the sensitivity to external parameters can be used to advantage in fibre sensors. External effects perturb the fibre locally, introducing birefringence in addition to the intrinsic birefringence already present. Since the axes of the birefringence induced will not in general coincide with those of the fibre, power transfer (coupling) and propagation constant changes (beating) between the fibre normal modes will result. External effects may be classified into those inducing linear and circular birefringence respectively.

2.3.1 Effects inducing linear birefringence

(i) Fibre bending

Bending a fibre introduces a stress anisotropy and hence a linear-birefringence $\delta\beta_b$ with a fast axis in the plane of the bend[14] where:

$$\delta\beta_b = \frac{\pi\, CE}{\lambda} \left(\frac{r}{R'}\right)^2 \simeq -\frac{0.75}{\lambda} \left(\frac{r}{R'}\right)^2 \text{ rad m}^{-1} \qquad (2.5)$$

$E = 7.45 \times 10^9$ kg m^{-2}[15] is Young's modulus, $C = -3.19 \times 10^{-11}$ m^2 kg^{-1}[16] is the stress-optic coefficient for bulk silica at $\lambda = 1.064$ μm and r and R' are the fibre outer and bending radii respectively. If the fibre is bent under tension to produce an axial strain ε_z, an additional linear birefringence $\delta\beta_{tc}$ is introduced, again with a fast axis corresponding to the plane of the bend[17], given by

$$\delta\beta_{tc} = \frac{2\pi}{\lambda} CE \frac{(2-3\nu)}{(1-\nu)} \varepsilon_z \left(\frac{r}{R'}\right) \text{ rad m}^{-1} \qquad (2.6)$$

where ν is Poisson's Ratio = 0.164 [15].

$$\therefore \quad \delta\beta_{tc} \simeq -\frac{2.69}{\lambda} \left(\frac{r}{R'}\right) \varepsilon_z \text{ rad m}^{-1} \qquad (2.7)$$

$\delta\beta_b$ and $\delta\beta_{tc}$ add and cause beating and coupling between the two fibre modes, depending on the plane of the bend relative to the fibre birefringence axes (see Chapter Five).

(ii) Side pressure

Pressure applied transversely to the fibre similarly produces a linear birefringence $\delta\beta_p$, with a fast axis in the direction of the applied compression[18,19] given by:

$$\delta\beta_p = \frac{8C}{\lambda}\left(\frac{f}{r}\right) \simeq -\frac{2.55\times10^{-10}}{\lambda}\left(\frac{f}{r}\right) \text{ rad m}^{-1} \quad (2.8)$$

where f is the applied force in kg m^{-1}. Again both 'beating' and 'coupling' between the modes will be produced according to the orientation of the fibre birefringence axes. The fibre coating has a significant effect in reducing pressure sensitivity of the fibre[18,20].

(iii) Electric fields (Kerr Effect)

An electric field can produce linear birefringence via the Kerr Effect[21]. The effect is however, extremely small and may be neglected under most circumstances.

2.3.2 Effects producing circular birefringence

(i) Twist

As mentioned in 2.2.2, twist or precession of the local birefringence axes in a linearly-birefringent fibre results in apparent circular birefringence. Twisting a fibre when cold also produces torsional stresses, which by the photo-elastic effect, give rise to an optical rotation $\Omega(z)$ or circular birefringence $\delta\beta_{circ}$ proportional to the rate of twist ξ given by:

$$\Omega(z) = g'\xi z = \alpha z = \frac{-R_o C}{n}\xi z = \delta\beta_{circ}/2 \quad (2.9)$$

where g' = 0.073 for silica[22,23], $R_o = 3.19 \times 10^9$ kg m^{-2} [15] is the rigidity modulus and n is the refractive index. Note that unlike the precession effect, torsion birefringence arises even if the fibre is isotropic.

(ii) Magnetic fields (Faraday Effect)

For a fibre exposed to a longitudinal magnetic field H, the Faraday effect induces a rotation α_F radians per unit length given by:

$$\alpha_F = V_o H \quad \text{rad m}^{-1} \qquad (2.10)$$

where $V_o \simeq 4.5 \times 10^{-6}$ rad A^{-1} is the Verdet constant for silica[24]. Although this effect is non-reciprocal, for unidirectional propagation α_F can be regarded as equivalent to a normal (reciprocal) optical rotation Ω.

2.3.3 Ambient Temperature

This is a special type of external influence since it only indirectly introduces output polarisation state changes. Both the differential thermal expansion and the stress-optic effect governing the intrinsic stress-birefringence B_S are temperature sensitive. Thus the phase-relationship between the modes is altered by temperature changes, resulting in output state variations. Similarly, the external effects already mentioned, which utilise the stress-optic effect, will be slightly temperature sensitive. Another common cause of polarisation changes is the differential expansion of the fibre and any support structure (e.g. a spool) which introduces highly temperature-sensitive transverse stress-birefringence.

2.4 Modelling of Fibre Birefringence

The polarisation properties of a fibre may be represented theoretically in several ways. On a microscopic (local) level, the fibre exhibits both linear and circular birefringence and often the birefringence axes vary in orientation along the fibre, an effect known as Fast Axis Rotation (FAR)[25]. The macroscopic properties are therefore a very complex combination of these local birefringences, depending on both the intrinsic birefringence and external effects. This combination is altered by changes in the environmental conditions giving rise to the varying output PS described above.

Jones Calculus[26] is frequently used to describe the fibre properties. The fibre is represented as a 2 x 2 matrix [M] and the input vectors E_x, E_y are related to the two output vectors E_x' E_y' by:

$$\begin{bmatrix} E_x' \\ E_y' \end{bmatrix} = [M] \begin{bmatrix} E_x \\ E_y \end{bmatrix} \qquad (2.11)$$

Although Jones Calculus provides mathematical elegance and accuracy, the Poincaré sphere representation is also extremely useful, since it has great visual and conceptual appeal[27]. The sphere is shown in Figure 2.2. Any polarisation state $[E_x, E_y]$ is represented by a point P on its surface. Points on the equator represent linearly-polarised light at various azimuths, 'H' and 'V' representing horizontal and vertical polarisation directions respectively. Similarly, 'L' and 'R' represent left- and right-circularly polarised light, while the upper and lower hemispheres represent general left- or right-elliptically polarised states according to the phase relationship between E_x and E_y. Birefringence has the effect of rotating the sphere[27] so that the input polarisation state P_1 or $[E_x, E_y]$ is transformed into a new output state P_2 or $[E_x', E_y']$. Thus the fibre properties may be represented by either the relationship between P_1 and P_2, or equivalently, by the matrix [M]. A major theorem of Jones Calculus[26] states that any series of local linearly-and circularly-birefringent fibre sections can be uniquely represented by a single retarder of retardation R with a principal axis direction ϕ, followed by a single rotator of rotation Ω. On the Poincaré sphere, this is equivalent to reducing the complex trajectory from P_1 to P_2 to two simple rotations about two axes at right angles[27],

usually about an axis in the equator (equivalent to the retardation R) and the polar axis (equivalent to the rotation Ω) respectively.

The fibre retarder-rotator model given by R, ϕ and Ω applies for a given fibre length, wavelength and point in time and is shown in Figure 2.3. There are always two directions of input linear-polarisation corresponding to the "principal axes" ϕ and $90 + \phi$, where linear-polarisation emerges at the output, through in general rotated with respect to the input. This is the so-called "linear-output/linear-input" condition. In general the principal axes ϕ and $90 + \phi$ do not bear any relation to and are distinct from, the local fast and slow axes given by the fibre geometry. When light is launched along ϕ or $90 + \phi$ the PS may not be linear throughout the fibre because of the local rotation and fast axis rotation. On the Poincaré sphere (Figure 2.4(a)), the input and output state both lie on the equator but are transformed from one to the other along a random trajectory.

The universal retarder-rotator model also possesses two general elliptically-polarised polarisation "eigenstates" which, when presented at the input, are each exactly reproduced at the output. Again of course, the PS may vary considerably along the fibre. On the Poincaré sphere, this is a special case where P_1 and P_2 are coincident but are linked by a general trajectory (see Figure 2.4(b)). In Jones Calculus form this situation is

$$\begin{bmatrix} A \\ B \end{bmatrix} = [M] \begin{bmatrix} A \\ B \end{bmatrix} \qquad (2.12)$$

where A, B are the eigen-vectors of [M] representing the eigenstate. Although external effects modify the birefringence continually, the eigenstates can always be found, but will vary with time[28].

If there were no external effects and the fibre were intrinsically untwisted and therefore uniformly linearly-birefringent, the local axes all along the fibre would coincide with the fibre principal axes ϕ. These axes not only correspond to the eigenstates but are also "normal modes", since light polarised along one of the axes would remain linearly-polarised throughout the fibre. Normal modes, which are generally insensitive to light wavelength, and are length-invariant, are given by

$$U_{1,2} = \left[N_1 \pm iN_2\right] \quad e^{\pm i\gamma z} \qquad (2.13)$$

where N_1 and N_2 are constants and 2γ is the difference in propagation constants between the two modes, in this case $\Delta\beta$.

When the fibre is uniformly twisted, or the two undisturbed fibre modes are coupled uniformly by some disturbance, it is possible to find new normal modes (and identical eigenstates) which are generally elliptically-polarised. Again, light launched in one of the modes propagates without change to the output. In this instance, the input and output state on the Poincaré sphere are identical while the 'trajectory' reduces to a spot (Figure 2.4(c)).When the fibre has length invariant properties the normal modes and polarisation eigenstates are indistinguishable. However, when the external effects or mode-coupling is random, normal modes may only be defined on a local scale, whereas overall fibre eigenstates still exist. It is essential to make this distinction since both the effects of environmental influences and the fibre polarisation mode-dispersion deal with the fibre normal modes.

In this thesis, Jones Calculus, the Poincaré sphere and normal modes will all be used, often in conjunction, to provide complementary conceptual aids for the understanding of birefringence phenomena.

2.5 Polarisation Mode-Dispersion

The variation of the difference in propagation constants $\Delta\beta$ with wavelength (or fibre V-value) gives rise to a group-velocity difference between the modes called polarisation mode-dispersion (PMD). The relative group delay $\Delta\tau_o$ between the two modes is given by:

$$\Delta\tau_o = \frac{L}{c} \cdot \frac{d(\Delta\beta)}{dk} \qquad \text{sec km}^{-1} \qquad (2.14)$$

where L = fibre length and c is the free-space speed of light. $\Delta\tau_o$ represents a significant dispersion or limitation of the fibre transmission bandwidth, particularly when the first-order chromatic-dispersion has been minimised or if a monochromatic source is used. The value $\Delta\tau_o$ depends on the fibre birefringence and is of the order of 5-10 ps km^{-1} in nominally-circular telecommunications fibres.

Note that PMD can only be defined if the fibre possesses normal modes. If the undisturbed fibre modes defining $\Delta\tau_o$ are uniformly coupled, new normal modes are set up and the dispersion becomes

$$\Delta\tau = \frac{L}{c} \cdot \frac{d(2\gamma)}{dk} \quad \text{sec km}^{-1} \qquad (2.15)$$

from equation (2.13). If , however, the modes are randomly coupled, $\Delta\tau$ is no longer a linear function of length since the normal modes are only defined locally within the fibre. The individual dispersions of each section may add constructively or destructively depending on the fast axis rotation along the fibre. It is possible to experience either bandwidth reduction or increase in the presence of random coupling, as shown in Chapter Six.

2.6 Fibres for Practical Applications

(i) Communications

In a communications system, fibre bandwidth is of great importance and the values of polarisation mode-dispersion typically found in fibres present a problem in long-haul high bit-rate systems. Also, coherent detection systems require a stable fibre output PS for heterodyning. As already indicated, both the output state and the PMD are greatly influenced by the prevailing environmental conditions in the fibre cable. However, if by increasing the fibre intrinsic birefringence external effects could be rendered negligible, stability of fibre output state would be ensured. In this case, the fibre would support two linearly-polarised normal modes, only one of which would be launched to avoid PS variations arising from the temperature sensitivity of birefringence. This mode would be transmitted without significant change and the fibre would "maintain" a stable polarisation state despite the external effects. Moreover, though the PMD in a high birefringence fibre might be substantial, polarisation-maintenance would ensure it is inoperative.

The drawback with this approach is that perfect polarisation-maintenance is unobtainable; a finite amount of power is always coupled into the unlaunched mode by bends or twists. Consequently, the output polarisation state will undergo massive excursions due to ambient temperature changes, precluding the use of active polarisation-controllers[29,30] which have a very limited "pull-in" range. Moreover, the PMD is invoked by the coupling resulting in intolerable communications bandwidth reduction. The alternative is to use a low-birefringence fibre. Here, the polarisation excursions would be very small and largely due to external effects other than temperature. This permits the use of a polarisation-controller and the much lower PMD ensures that the effect on fibre bandwidth due to mode-coupling would be negligible.

(ii) Sensors and other Fibre Devices

In two-fibre interferometric sensors[31], efficient interference is obtained only if each fibre preserves polarisation[32]. Thus high-birefringence polarisation-maintaining fibres are required in these applications. For the Sagnac-effect fibre rotation sensor (gyroscope) a single fibre is used for both light paths, so it is sufficient only to insert polarisers at both fibre ends[33] to ensure correct operation. However, the use of a polarisation-maintaining fibre vastly improves the stability of the device.

In contrast, polarimetric (single-fibre) sensors require maximum fibre sensitivity to the desired stimulus. Fibre intrinsic birefringence can interfere with the induced birefringence to reduce sensitivity. For example, linear birefringence quenches the Faraday-rotation[34] in a Faraday-effect current monitor[22,24]. Thus a low-birefringence fibre would be advantageous, but such a fibre would also be very sensitive to any other effects. By using a fibre having birefringence of the same type (i.e. linear or circular) as the birefringence induced by the stimulus, sensitive but *selective* sensing is possible. Since fibre intrinsic birefringence is not easily controlled in practice, it is preferrable to use a low-birefringence fibre into which a controlled amount of retardation or rotation has been introduced by bending or twisting. This principle is used to provide controlled-birefringence fibre elements for fibre devices such as sensors[35], filters and isolators[36]. Any intrinsic fibre birefringence would not only unpredictably modify the required birefringence but would also introduce temperature sensitivity and hence device instability. Thus a low-birefringence fibre is essential.

(iii) Low- and High-Birefringence Fibres

From the discussion above, ultra-low birefringence fibres with $B < 10^{-8}$ (i.e. $L_p > 100m$) are required for

high-bandwidth communications, polarimetric sensors and other fibre devices. On the other hand, high-birefringence fibres with beat lengths of less than 1cm are suitable for interferometric sensors and communications where polarisation must be maintained. The manufacture of fibres with these extreme birefringence properties requires highly specialised fabrication techniques. For example, because it is difficult to control B_S and B_G at low values[37], the fibre "spinning" process[22] has been developed to provide high yields for low-birefringence fibres. "Spun" fibres automatically have negligible birefringence or PMD regardless of the value of B. These fibres have attenuation and other characteristics similar to any nominally-round single-mode fibre. Their development will be described in detail in Chapter Four.

High-birefringence fibres either employ highly-elliptical cores[9] (see Figure 2.1) or have highly-asymmetric stress-producing structures such as elliptical claddings[38]. The latter approach has so far proved extremely promising, with beat lengths of 0.6mm (0.633μm)[39] and losses of 0.8 dB km^{-1} at 1.55μm having already been achieved. It is also possible to design a true "single-polarisation" fibre which supports only only one polarised mode[40] for polarisation-maintenance applications but this has yet to be realised in practice.

In general the PMD in a high-birefringence fibre is high i.e. 100-1000 ps km^{-1}. However, it is possible to substantially reduce this figure by offsetting the PMD's due to stress and ellipticity against each other, but without sacrificing the birefringence[8].

The salient features of both low- and high-birefringence fibres are shown in Table 2.1.

2.7 References

1. Hecht, E., and Zajac, A.: "Optics", Addison-Wesley, 1974.

2. Shurcliff, W. A.: "Polarised light:production and use", Oxford, 1962.

3. American Institute of Physics Handbook, McGraw-Hill, 1972, p.6-233.

4. Schlosser, W.O.: "Delay distortion in weakly guiding optical fibres due to elliptic deformation of the boundary", Bell Syst. Tech. J., 51, 1972, pp. 487-492.

5. Adams, M. J., Payne, D. N., and Ragdale, C.M.: "Birefringence in optical fibres with elliptical cross-section", Electron. Lett., 15, 1979, pp. 298-299.

6. Tjaden, D.L.A.: "Birefringence in single-mode optical fibres due to core ellipticity", Philips J. Res., 33, 1978, pp. 254-263.

7. Love, J.D., Sammut, R.A., and Snyder, A. W.: "Birefringence in elliptically deformed optical fibres", Electron. Lett., 15, 1979, pp. 615-616.

8. Okamoto, K., Hosaka, T., and Sasaki, Y.: "Linearly single polarisation fibres with zero polarisation mode dispersion", IEEE J. of Quantum Electron., QE-18, 1982, pp. 496-503.

9. Dyott, R.B., Cozens, J. R., and Morris, D. G.: "Preservation of polarisation in optical fibre waveguides with elliptical cores", Electron. Lett., 15, 1979, pp . 380-382.

10. Adams, M. J.: "An Introduction to Optical Waveguides", Wiley, 1981.

11. Rengarajan, S. R., and Lewis, J. E.: "First higher-mode cut-off in two-layer elliptical fibre waveguides", Electron. Lett., 16, 1980, pp. 263-264.

12. Rashleigh, S.C., and Marrone, M. J.: "Polarisation-holding in a high-birefringence fibre", Electron. Lett., 18, 1982, pp. 326-327.

13. Barlow, A. J., and Varnham, M. P.: unpublished work.

14. Ulrich, R., Rashleigh, S. C., and Eickhoff, W.: "Bending-induced birefringence in single-mode fibres", Optics Lett., 5, 1980, pp. 273-275.

15. Borrelli, N. F., and Miller, R. A.: "Determination of the individual strain-optic coefficients of glass by an ultrasonic technique", Appl. Optics, 7, 1968, pp. 745-750.

16. Barlow, A. J., and Payne, D. N.: "The stress-optic effect in optical fibres", to be published in IEEE J. of Quantum Electron.

17. Rashleigh, S.C., and Ulrich, R.: "High birefringence in tension-coiled single-mode fibres", Optics Lett. 5, 1980, pp. 354-356.

18. Smith, A. M.: "Single-mode fibre pressure sensitivity", Electron. Lett., 16, 1980, pp. 773-774.

19. Sakai, J., and Kimura, T.: "Birefringence and polarisation characteristics of single-mode optical fibres under elastic deformations", IEEE J. of Quantum Electron., QE-17, 1981, pp. 1041-1051.

20. Yoshizawa, N., Yabuta, T., Kojima, N.,and Nagishi, Y.: "Jacketed optical fibre characteristics under lateral pressure", Appl. Optics, 20, 1981, pp. 3146-3151.

21. Simon, A., and Ulrich, R.: "Evolution of polarisation along a single-mode fibre", Appl. Phys. Lett., 31, 1977, pp. 517-520.

22. Barlow, A. J., Ramskov Hansen, J. J., and Payne, D.N.: "Birefringence and polarisation mode-dispersion in spun single-mode fibres", Appl. Optics, 20, 1981, pp. 2962-2968.

23. Smith, A. M.: "Birefringence induced by bends and twists in single-mode optical fibre", Appl. Optics, 19, 1980, pp. 2606-2611.

24. Smith, A. M.: "Polarisation and magneto-optic properties of single-mode optical fibre", Appl. Optics, 17, 1978, pp. 52-56.

25. Smith, A. M.: "Automated birefringence measurement system" J. Phys. E.: Sci. Instrum., 12, 1979, pp. 927-930.

26. Jones, R. C.: "A new calculus for the treatment of optical systems" (parts I-VII), J. Opt. Soc. Am., 31, 1941, pp. 488-503.

27. Ramachandran, G. N., and Ramaseshan, S.: "Crystal Optics", Handbook of Physics, Vol. 25, Pt. 1, Ch. 1.

28. Monerie, M., and Jeunhomme, L.: "Polarisation mode coupling in long single-mode fibres", Opt. Quantum Elect., 12, 1980, pp. 449-461.

29. Ulrich, R.: "Polarisation stabilisation on single-mode fibre", Appl. Phys. Lett., 35, 1974, pp. 840-842.

30. Kidoh, Y., Suematsu, Y., and Furuya, K.: "Polarisation control on output of single-mode optical fibres", IEEE J. of Quantum Electron., QE-17, 1981, pp. 991-994.

31. Harmer, A. L.: "Principles of optical fibre sensors and instrumentation" paper presented at symposium on "Optical Sensors and Optical Techniques in Instrumentation", Inst. of Measurement and Control, London, 12 November, 1981.

32. Sheem, S. K., and Giallorenzi, T. G.: "Polarisation effects on single-mode optical fibre sensors", Appl. Phys. Lett., 35, 1979, pp. 914-917.

33. Ulrich, R., and Johnson, M.: "Fibre ring interferometer: Polarisation analysis", Opt. Lett., 4, 1979, pp. 152-154.

34. Tabor, W. J., and Chen, F. S.: "Electromagnetic propagation through materials possessing both Faraday rotation and birefringence:experiments with Ytterbium Orthoferrite", J. Appl. Phys., 40, 1964, pp. 2760-2765.

35. Giallorenzi, T. G. et al.: "Optical fibre sensor technology", IEEE J. of Quantum Electron., QE-18, 1982, pp. 626-665.

36. Day, G. W., Payne, D. N., Barlow, A. J., and Ramskov Hansen, J. J.: "Faraday rotation in coiled, monomode optical fibres: isolators, filters and magnetic sensors", Optics Lett., 7, 1982, pp. 238-240.

37. Norman, S. R., Payne, D. N., Adams, M. J., and Smith, A. M.: "Fabrication of single-mode fibres exhibiting extremely low polarisation birefringence", Electron. Lett., 15, 1979, pp. 309-311.

38. Katsuyama, T., Matsumura, H., and Suganuma, T.: "Low loss single-polarisation fibres", Electron. Lett., 17, 1981, pp. 473-474.

39. Birch, R. D.: Private communication.

40. Okoshi, T., and Oyamada, K.: "Single-polarisation single-mode optical fibre with refractive-index pits on both sides of core", Electron. Lett., 16, 1980, pp. 712-713.

Feature	Low-birefringence fibres	High-birefringence fibres
Birefringence B	$<10^{-7}$	$>10^{-4}$
Beat length L_p (@ 1μm)	>10m	< 1cm
Attenuation @ 1.55μm	<<1dB/km	0.8dB/km[38]
core geometry	round, small Δ'	round, small Δ' or elliptical, large Δ'
Polarisation-dispersion	<1ps/km	>0.3ns/km (can be made lower [8])
Sensitivity to external effects	High (cannot maintain polarisation)	Low (can maintain >-30dB extinction ratio over 1km[38])
Temperature sensitivity	generally small	very large
Best performance achieved @ 633nm	L_p=140m (unspun)[37] L_p>360m (spun)[22]	L_p<0.6mm[39]
Proposed Applications	High bandwidth communications, coherent detection, polarimetric devices and sensors	Coherent detection systems, interfacing to integrated optics, interferometric sensors (e.g. gyroscope)

Table 2.1 Properties of ultra-low and ultra-high birefringence fibres.

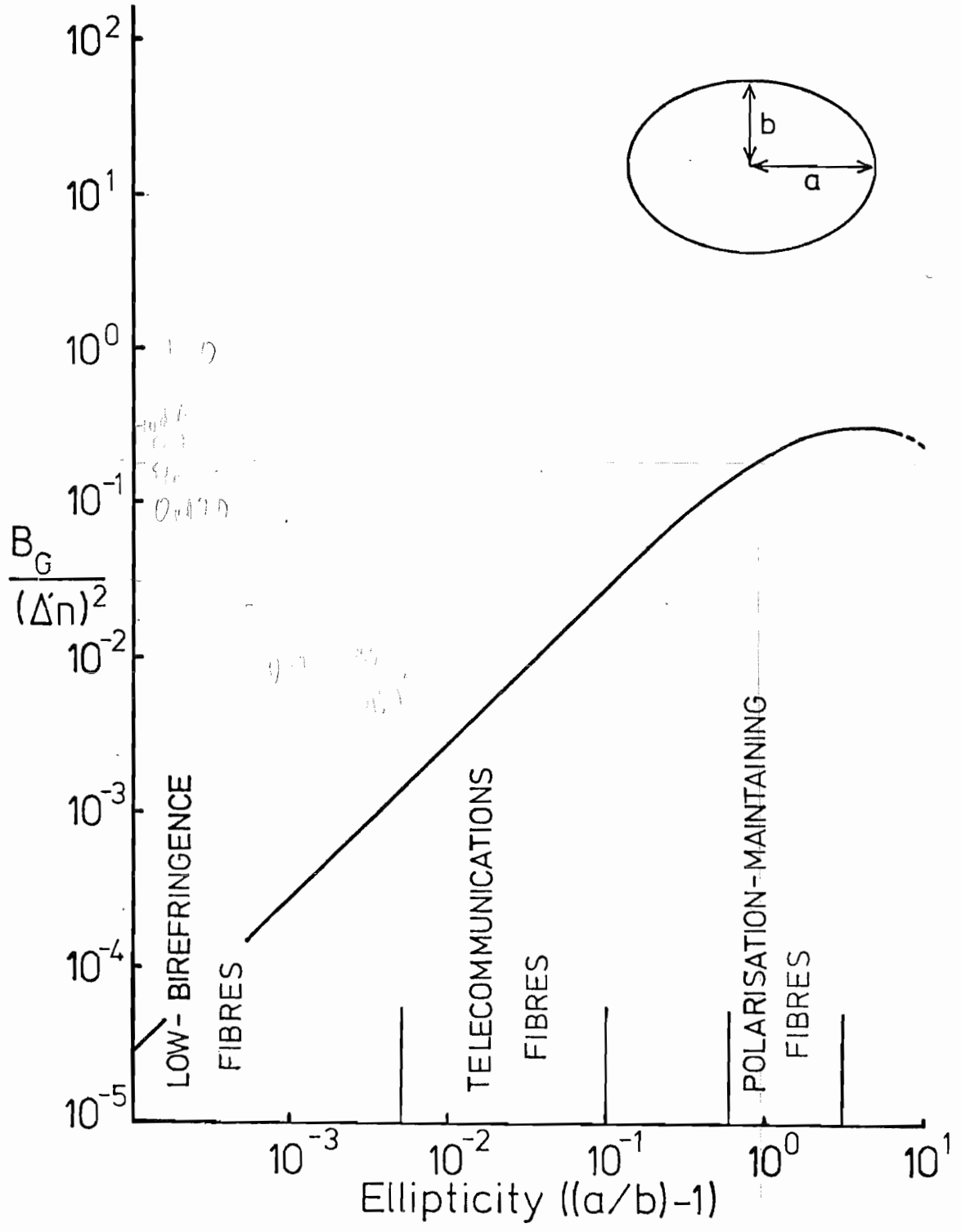

Figure 2.1 Normalised fibre shape birefringence B_G plotted as a function of core ellipticity (a/b-1) for operation at the second-order mode cut-off.

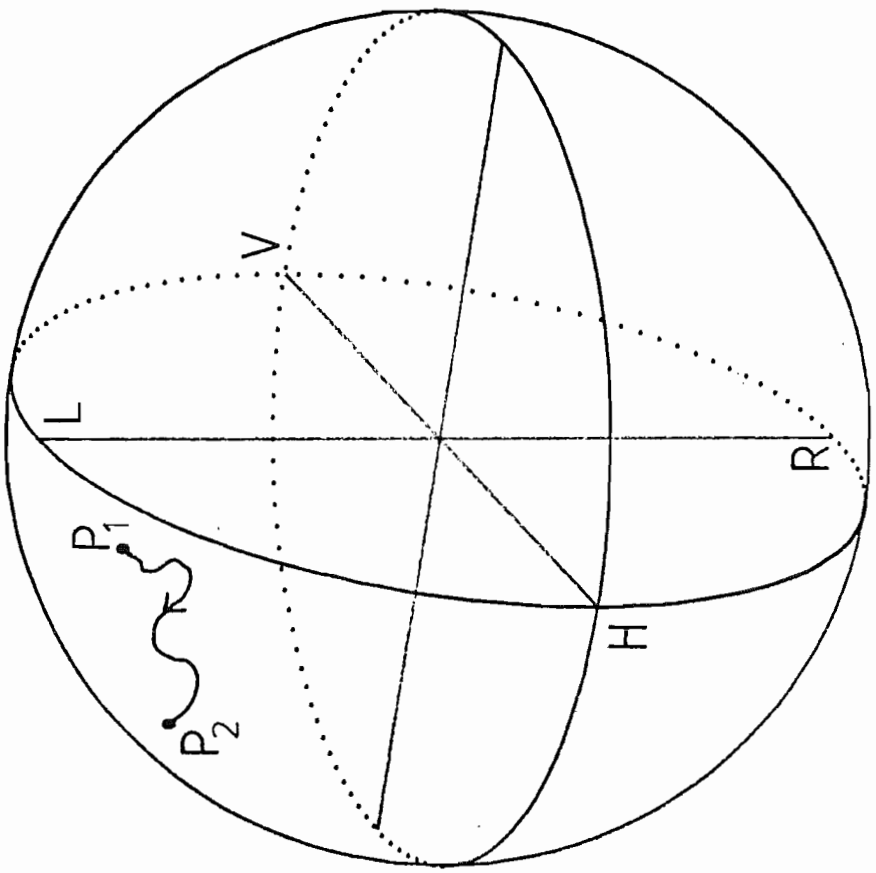

Figure 2.2 The Poincaré sphere representation for polarised light

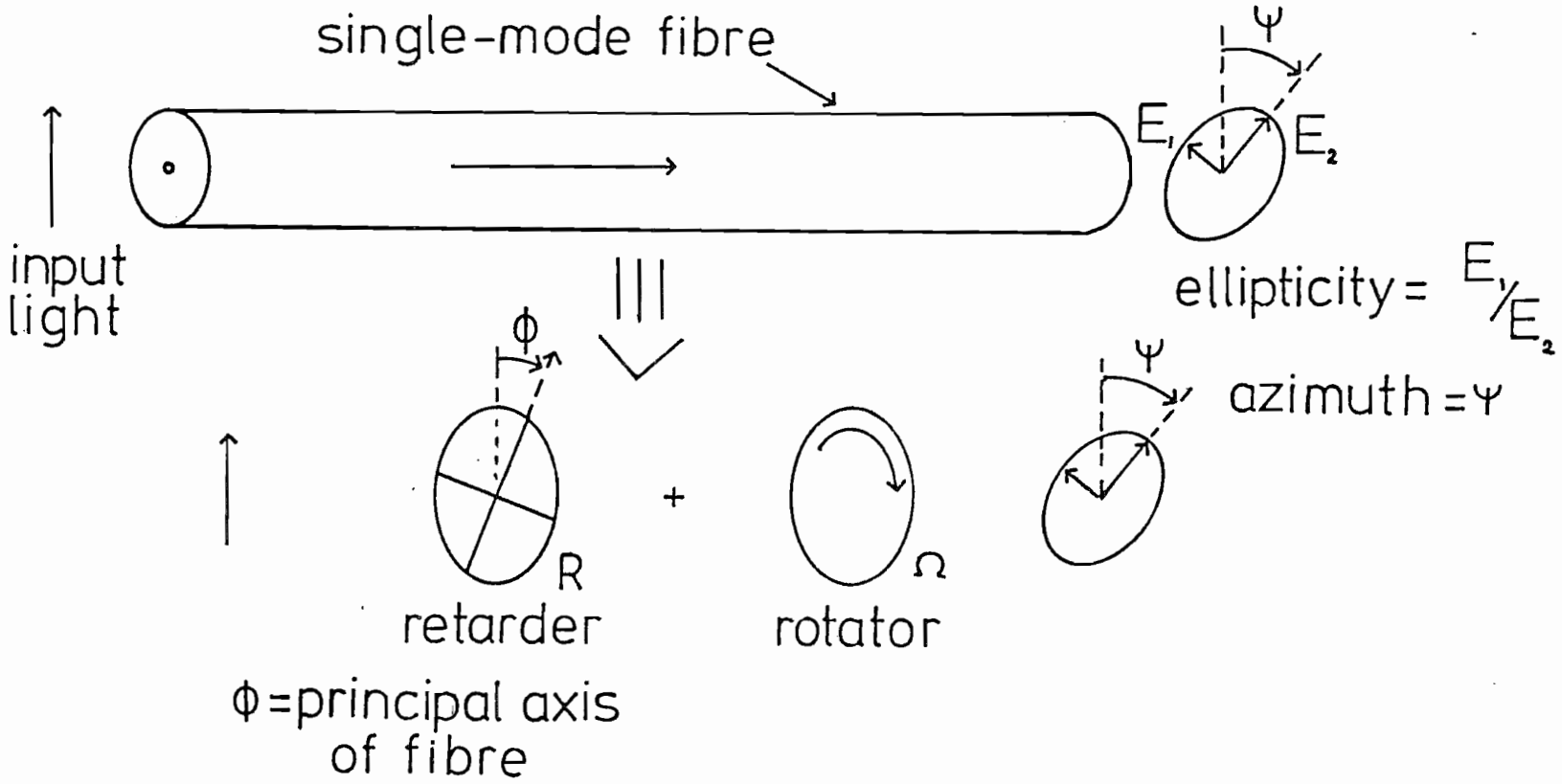

Figure 2.3 Retarder-rotator representation for a birefringent fibre showing the general output elliptical polarisation state.

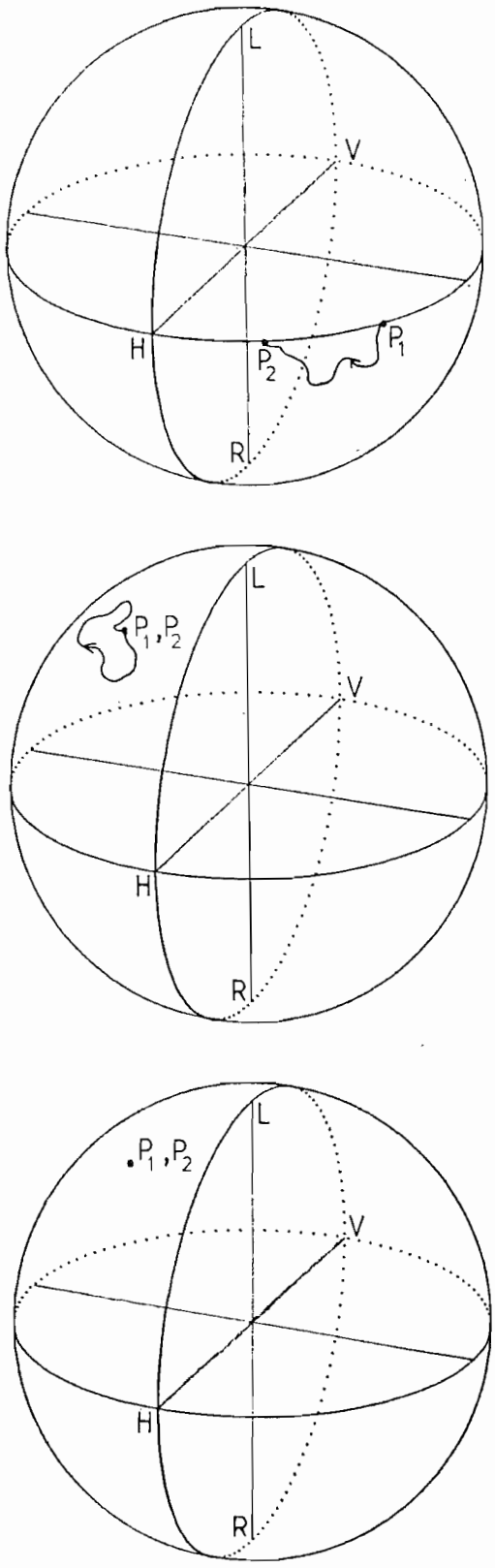

Figure 2.4 The Poincaré sphere showing polarisation evolution along the fibre length when light is launched (a) on one of the principal axes, (b) for polarisation eigenstates and (c) for normal modes.

CHAPTER 3 BIREFRINGENCE MEASUREMENT TECHNIQUES

3.1 Introduction

A central part of any study of birefringence in fibres involves measurements on single-mode fibres. The results are also of importance in the subsequent development and production of fibres for long-distance telecommunications and fibre sensors. This Chapter describes the various techniques available for the determination of birefringence in fibres, concentrating on the specific methods used throughout this study.

Very few methods can adequately cover the enormous potential range of fibre normalised linear birefringence B, which can vary from $\sim 10^{-1}$ [1] to $\sim 10^{-3}$ [2]. Any rotation and twist effects arising must also be detected. However, these effects are negligible in highly-linearly birefringent[3, 4] "polarisation-maintaining" fibres[2,5-14] and a simple linear retardation measurement may suffice (Section 3.2). In general, particularly in ultra-low birefringence fibres suitable for the Faraday current monitor, or twisted fibres, the effects of the rotation are not insignificant[15,16,17]. Consequently, the fibre must be described by the universal retarder/rotator model introduced in Chapter Two. Considerable emphasis has been placed on the development of a suitable technique to measure the parameters retardation R, rotation Ω and principal axis direction ϕ in a fibre.

3.2 Experimental Methods for High-Birefringence Fibres

The birefringence of predominantly linearly-birefringent fibres (with $L_p < 0.5$m) can be measured using the Tardy and Friedel or Senarmont methods, commonly employed in polarisation microscopy[18] and photo-elastic stress analysis[19, 20, 21]. These methods utilise $\lambda/4$ plates or compensators[22] and are not usually sensitive to any rotation which may unexpectedly be present[23].

3.2.1 Fibre birefringence determination by Rayleigh scattering

The preceding methods require access to the fibre ends, but this limitation can be avoided by making use of polarisation-dependent dipole Rayleigh scattering[3, 9] of the light propagating along the fibre. The light-scattering dipoles radiate with nulls in the direction of their axes, so that the fibre appears dark when viewed in the direction of linear polarisation. When both fibre polarisation modes are launched, inter-mode beating gives rise to a periodic variation in polarisation state (PS) along the fibre, which can be observed as a series of light and dark bands of the Rayleigh-scattered light with a spatial period equal to the beat length. Naturally this "beat" pattern is not set up if only one of the modes is launched i.e. input light polarised parallel to fibre principal axis. "Beats" are usually observed using linearly-polarised input light at 45 degrees to the principal axes, or circularly-polarised light. The fibre is laid upon a black plate covered in index-matching liquid to reduce internal reflections, giving maximum "beat" visibility. Figure 3.1 shows the "beat" pattern obtained at 633nm in a highly-elliptical high-birefringence fibre with a 4 mm beat length[24, 25].

The method is only suitable for visible and near infra-red wavelengths, because of the λ^{-4} dependence of scattering intensity. Although beat lengths less than 0.5mm or greater than ~20mm are difficult to observe, Rayleigh-scattering provides a simple non-destructive method.

An interesting extension of this technique occurs in Polarisation Optical Time-Domain Reflectometry (POTDR)[26]. In conventional OTDR some of the Rayleigh scattered light is returned to the launch point, where the intensity can be used to determine the local fibre attenuation by time-resolving the signal. However

the scatter return also mirrors the PS at any position, so that analysis of the backscattered light with a polariser (POTDR) reveals the evolution of the PS along the fibre[27] and hence the beat length[28, 29]. The spatial resolution in beat length is limited to ~1m. but the technique has been widely proposed for distributed remote environmental sensing[30, 31, 32] or for the location of birefringence "hot spots" (kinks, twists etc.) in long fibre cables[26].

3.2.2 Birefringence modulation techniques

Modulation of the local polarisation state in a fibre using external magnetic or electric fields[33] or stresses[34] produces a corresponding variation in the fibre output PS[16]. A non-destructive measurement of fibre birefringence can be performed by observing the output polarisation whilst the point of modulation is scanned along the fibre. Although fibre twist effects can be measured in this way[16], at least one complete birefringence beat must be observed, thus limiting the technique to beat lengths of ~1m or less.

3.3 Measurements on Low-Birefringence Fibres

3.3.1 Measurement technique

The measurement methods described in Section 3.2 are largely unsuitable for fibres where the beat length exceeds ~1m, since the rotation effects are no longer negligible. The retardation R, rotation Ω and principal axis direction ϕ which must be used to describe such a fibre are determined by analysis of the output polarisation state for a given input (linear) polarisation.

The output polarisation is measured with a simple analyser, $\lambda/4$ retardation plate/analyser or a Soleil compensator/analyser[35] with a single detector, or a polarising beamsplitter and two detectors[3, 4]. These methods usually require a lens to collimate the fibre output beam. When the fibre birefringence is small this lens, inevitably birefringent, must be replaced by simple dichroic analyser and wide-area detector.

However, dichroic polarisers are unsatisfactory at wavelengths beyond ~700nm so that a prism polariser (e.g. Glen-Thomson) and lens are necessary.

The basic apparatus thus consists of an unpolarised light source (usually a laser), input polariser, output analyser and photo-detector, as shown in Figure 3.2. The polariser provides linearly-polarised input light at any azimuthal angle, Θ_o.

If the fibre is represented by a retarder of retardation R and principal axis ϕ, followed by a rotator of rotation Ω, the Jones calculus equation is written[15, 36]:

$$\begin{bmatrix} E_x \\ E_y \end{bmatrix} = \begin{bmatrix} A & -B^* \\ B & A^* \end{bmatrix} \cdot \begin{bmatrix} \cos\Theta_o \\ \sin\Theta_o \end{bmatrix} \qquad (3.1)$$

where $A = \cos\frac{R}{2}.\cos\Omega + i\sin\frac{R}{2}.\cos(2\phi+\Omega)$ (3.2)

$$B = \cos\frac{R}{2}.\sin\Omega + i\sin\frac{R}{2}.\sin(2\phi+\Omega) \qquad (3.3)$$

and E_x, E_y are the electric vectors in the x and y directions after fibre length z.

It can be shown[36] that equation (3.1) represents an output polarisation ellipse with angle ψ with respect to the positive x axis. The intensities I_{max} and I_{min} along the major and mimor axes respectively are measured using the analyser at ψ and $\psi+90^o$. The ellipse polarisation P is:

$$P = \frac{I_{max} - I_{min}}{I_{max} - I_{min}} = \sqrt{1 - \sin^2 R . \sin^2 \left[2(\theta_o - \phi) \right]} \qquad (3.4)$$

with

$$\psi = (\phi + \Omega) + \tfrac{1}{2} \tan^{-1} \left[\tan\{2(\theta_o - \phi)\} \cos R \right] \qquad (3.5)$$

Polarised light launched into the fibre parallel to the principal axis, i.e. $\theta_o = \phi$, results in a linearly-polarised output (see Chapter Two) with $P = 1$ and $I_{min} = 0$ at an angle

$$\psi = \phi + \Omega \qquad (3.6)$$

This is the familiar "linear-output/linear-input" condition, which can be detected as an output "null" using the analyser at an angle of $(\phi + \Omega + 90^o)$. The rotation is given by the difference in analyser and polariser angles (Figure 3.2) , whilst the input polariser direction is the principal axis direction. In practice, since the magnitudes of ϕ and Ω are unknown, the polariser and analyser are rotated independently, iterating these rotations, until the absolute best null is obtained at the detector, thus indicating the above "linear-output/linear-input" condition. This procedure becomes insensitive and time-consuming if $R < \sim 5^o$ since $P \simeq 1$ for all θ_o.

Next, the input polariser is rotated to lie at 45^o to the principal axes i.e. $\theta_o - \phi = 45^o$, to give

$$P = \cos R \qquad (3.7)$$

$$\psi = \phi + \Omega + 45^o \qquad (3.8)$$

Measurement of P thus directly gives the fibre retardation R, modulo 2π . The number of beats, or units of 2π phase difference in R which occur over the fibre length, can be determined by "cutting-back" the fibre and

repeating the measurements[37]. If required, the sign of R, i.e. if ϕ is the 'fast' or 'slow' axis, must be inferred.

3.3.2 Retardation measurement using a Soleil Compensator

The sensitivity of the measurement of R at low R values can be increased using a Soleil compensator. After finding the fibre principal axes by the above iterative technique, the compensator is inserted before the fibre at 'A' in Figure 3.2, with its axes parallel to those of the fibre so that its retardation is linearly additive to the fibre retardation R. The compensator retardation can be set to 'bias' the total retardation by a known amount to $\sim 45^{o}$ [37] where the measurement of P, and hence R, is very sensitive. Alternatively, the compensator can be set to exactly oppose the fibre retardation giving a total retardation of zero ($\pm 2\pi$). At the zero-retardation point, the polarisation P is unity which results in a null in I_{min} when $\theta_o - \phi$ is set to 45^{o}. Using the compensator in two orthogonal azimuthal directions and subtracting the retardations necessary for exact compensation removes the quite substantial compensator zero calibration error.

Retardation measurement with the compensator in conjunction with the iteration technique for the determination of ϕ and Ω, requires the detection of nulls only, not absolute intensities, thereby reducing errors arising from laser source/fibre launch fluctuations.

3.3.3 External effects and fibre birefringence measurements

Special attention has been paid to the minimisation, during birefringence measurements, of external influences on the intrinsic fibre properties such as twists or stress. For example, considerable fibre stresses are introduced when spring clamps or magnetic rubber strips are used to anchor the fibre in its metal V-groove[38]. Alternative anchoring methods were adopted to minimise

these stresses, namely "plasticine" or silicone rubber adhesive.

Twist and side-pressure can also arise when the fibre is laid out on a flat surface[15, 39] giving rise to inconsistent measurement results. These effects can be consistently reduced to negligible levels by hanging the fibre vertically so that only the input end is anchored and the fibre hangs freely. In this way the clamping stress and twist are miminised. The axial tension caused by the weight of the fibre is very small and, moreover, neither produces any differential photo-elastic effect[20] nor significantly changes the light propagation characteristics[40]. The low fibre stress levels achieved by hanging the fibre freely enables the effects of known applied disturbances, such as bends, to be measured. Fibre twist experiments may be performed by holding the lower fibre end in a rotatable mount using silicone rubber adhesive. The vertical system ensures that any twist introduced is uniform.

The effects of the standard primary coating of silicone rubber on the properties of a typical low-birefringence fibre[41] were shown to be negligible by comparing results before and after the fibre coating was removed. It appears, therefore, that despite shrinkage during the coating process, the coating imparts neglible stress or twist to a glass fibre.

3.3.4 Experimental arrangement

The basic experimental arrangement using a He-Ne laser is shown in Figure 3.3. Later sections describe the modifications of this system to include measurements as a function of wavelength and temperature.

The vertical optical bench is ~3m long. Randomly-polarised light from the 1mW He-Ne laser (0.633μm) is first passed through an optional OG570 filter to remove the blue

laser-discharge light which might otherwise be inadvertently launched into the fibre. The beam is chopped mechanically at ~260Hz, using a chopper blade equipped with a photo-switch to derive a reference signal.

A pellicle beamsplitter permits focusing of the laser beam onto the fibre front face by projecting the front-face reflection onto a screen. A dichroic polariser and optional Soleil-Babinet compensator precede a x10 strain-free polarising-microscope objective lens which focuses the light into the core of the fibre. The fibre hangs freely, fixed in the groove of a micromanipulator. The lower end of the fibre is held loosely in position over the dichroic analyser and $1cm^2$ silicon p-i-n photo-diode by an iris diaphragm, which also serves to block stray light from the fibre and other components. Stripping of cladding-modes is performed by removing any silicone coating on a short section of the fibre and placing it between two glass plates containing index-matching liquid, held by capillary action. A telescopic tube protects the fibre from draughts. To determine P, the intensities I_{min} and I_{max} must be accurately measured, even though they may differ by up to four orders of magnitude. The detection electronics is therefore designed to have maximum dynamic range. However to reduce phase distortion in the intensity waveform caused by the photo-diode capacitance, a constant value of diode load resistance must be used for all intensity measurements. The switched matched-T attenuator of (60 $\pm$0.5)dB provides this, whilst vastly extending the limited range of available gains in the low-noise amplifier.

The phase-sensitive detector provides sensitive and accurate intensity measurements from ~1mW to ~1nW even in high ambient-light levels. The noise of the detection system is negligible in this range.

3.4 Estimation of the Minimum Measurable Birefringence

Fibresexhibiting less than a few degrees of phase retardation[42] are examined using the system described above. It is therefore important to evaluate and improve the smallest birefringence measurement possible with this system.

3.4.1 Cladding modes

Some cladding modes, which are generally unpolarised, are invariably launched into the fibre under test.

These modes must be well stripped using index-matching oil in order not to affect greatly the fibre (single-mode) output after the analyser which, for a null, can be exceedingly small (~1 μW). The intensity of the cladding modes becomes significant in short pieces of fibre and gives a lower length limit for fibre measurement of ~0.5m.

3.4.2 Higher-order modes

In a near-circular fibre the first higher-order linearly-polarised LP_{11} mode has a cut-off at V = 2.405 and is made up of several composite modes[43] which are not individually linearly-polarised. These are often launched with unequal efficiency[44], giving the LP_{11} mode vastly different polarisation properties from the lowest-order LP_{01} mode. Thus measurements of fibre birefringence are restricted to the single-mode region.

3.4.3 Optical components

The quality of the optical components used is typically the limiting factor in ultra-low birefringence measurements. For example, the finite extinction ratio of $\sim 10^{-4}$ of the dichroic polarisers gives an effective maximum P of ~0.9998 i.e. a minimum measured R of ~1.2°

for the fibre and lens even when the fibre output is perfectly linearly-polarised (true P = 1). In effect the finite light leakage through the polarisers reduces the polarisation P at the fibre output and hence the depth of polarisation nulls. This affects the accuracy of the principal axis position, found by iterating for the best null, particularly at low R values, as well as the accuracy of the compensator nulling technique (sub-section 3.3.2), and the value of R itself.

Vibration of the vertical bench, and laser output variations give rise to a time-varying fibre output power which can be averaged by the phase-sensitive detector, using time-constants of 1-3 secs. to give < 1% intensity measurement error. By far the largest source of error is the birefringence of the polariser (~1°) and the "strain-free" input objective lens (~2° - 3°). These cannot easily be compensated in measurements since the apparatus is frequently dismantled to accommodate new elements (furnaces, tunable light sources etc). The input lens sets the primary lower limit for fibre retardation measurements to ~ 5° or 2° - 3°/m for the 2m maximum test fibre length. The addition of an output lens further degrades this limit. It is possible, but unlikely, that an alternative input lens may lead to substantial improvements in the system performance. However, the present measurement system is more than adequate for the vast majority of the experiments presented in this work.

3.5 Measurements of Birefringence as a Function of Temperature and Wavelength

The isolation of the stress and shape contributions to the birefringence in a fibre can be achieved (see Chapter 6) by measuring fibre birefringence as a function of either temperature or wavelength. The necessary modifications to the basic apparatus are described below.

3.5.1 Temperature

To vary the temperature of a length of fibre under test, a tube furnace was used. This consists of a 1" diameter copper tube 1 metre long with ceramic-insulated windings, lagged (Figure 3.4) with a 1½" layer of "Kaowool" silica fibre. Chromel-alumel thermocouples are fixed at regular intervals along the tube. Convection through the furnace whilst it is mounted on the vertical bench is minimised by iris diaphragms at the top and bottom of the tube which close round, but not touch, the fibre hanging inside the furnace. A temperature controller was used to maintain the furnace temperature to within $\pm$ 1^{o}C of any set temperature up to 400^{o}C maximum. The average fibre temperature profile and the lengths of test fibre outside the furnace are compensated for in experiments. The furnace is also useful for stabilising the fibre against ambient temperature fluctuations, which would otherwise modify the birefringence properties during the course of an experiment.

3.5.2 Wavelength

For the measurement of birefringence as a function of wavelength, a tunable fibre stimulated-Raman laser[45] is substituted for the He-Ne laser shown in Figure 3.3. The fibre is pumped by a Q-switched Nd:YAG laser (λ=1.064μm) producing 300ns, 1000W peak-power pulses with a repetition rate of 1kHz. The Raman fibre is ~ 400m long to produce a wide range of usable output wavelengths[46]. The fibre V-value is 2.4 at 1.0 μm and the loss is < 1dB/km over the range 1.0μm to 1.24μm with a hydroxyl-ion loss peak of ~ 10dB/km at 1.39μm[47]. In the fibre, the 1.064μm pump input power exceeds the threshold set by the Raman gain and the fibre loss. Thus pump power is depleted gradually along the full fibre length as it is Raman-shifted into the first Stokes order centred at 1.12μm. In silica fibres, this order is relatively broad. Further broadening will occur as the first peak is also Raman-shifted to consecutively higher orders at

1.18, 1.24 and 1.30μm. Thus, a near-continuous overall fibre output spectrum arises. Further Raman conversion beyond $\lambda \approx 1.36\mu m$ is prevented because the fibre loss rises sharply. Anti-Stokes shifting of the pump to shorter wavelengths also occurs. The total output is almost continuously tunable in the range 0.95 to 1.36μm.

The experimental arrangement for birefringence measurements using the Raman source is shown in Figure 3.5. Prism polarisers and both input and output lenses are necessary. The analysed light passes via a grating monochromator, to a germanium p-i-n photodiode detector and transimpedance amplifier[48]. This detection arrangement gives maximum system throughput but is slightly polarisation sensitive, and thus precludes the measurement of absolute intensities I_{min} and I_{max}. However, null detection sensitivity is barely affected and the retardation may be measured using a compensator, as described previously. A linear gate is used to sample and hold the height of the optical pulse from the fibre. A gate trigger is derived optically from the YAG laser output via a digital delay to compensate for the optical propagation delay in the Raman fibre. Part of the Raman output is "picked off" by the beamsplitter to pass through a second monochromator, detector/amplifier, and linear gate to provide ratiometric compensation for the Raman output fluctuations at the test wavelength. A polarisation null is detected as a minimum in the ratiometer output voltage, the procedures for measuring ϕ, Ω and R being exactly as described previously.

3.6 Birefringence Measurements using a Photo-Elastic Modulator

3.6.1 The photo-elastic modulator

The preceding simple, analyser-polariser method is not sufficiently sensitive, particularly for low birefringence measurements, because the birefringence to be measured is static. A large increase in sensitivity may be obtained by modulating the system birefringence[49],

for example, by using a photo-elastic modulator[50, 51]. This section describes the first known application of such a device to fibre birefringence measurement.

In the photo-elastic modulator, an oscillating strain-birefringence is set up in a fused silica optical element using a piezo-electric quartz crystal driver. The silica element behaves as a retardation plate whose retardation varies sinusoidally with time. The modulator assembly is placed after the test fibre, where beam alignment is less critical. This avoids variations in fibre launch efficiency arising from the vibration of the silica element.

3.6.2 Theory and measurement technique

The determination of the fibre retardation R, principal axis ϕ and rotation Ω using the modulator is as follows. Linearly-polarised light of intensity I_o is launched into the fibre with an azimuthal angle of θ_o using the prism polariser, while the modulator and prism analyser rotate as one with a fixed relative orientation of 45^o (see Figure 3.6). In this case the principal axis ϕ is taken as the reference direction ($\phi \equiv 0$). The Jones calculus equation is

$$\begin{bmatrix} E_x \\ E_y \end{bmatrix} = [A].[B].\begin{bmatrix} \cos\Omega & -\sin\Omega \\ \sin\Omega & \cos\Omega \end{bmatrix}.\begin{bmatrix} e^{\frac{iR}{2}} & 0 \\ 0 & e^{\frac{-iR}{2}} \end{bmatrix}.\begin{bmatrix} \cos\theta_o \\ \sin\theta_o \end{bmatrix}.\sqrt{I_o} \qquad (3.9)$$

where

$$[A] = \begin{bmatrix} \cos^2(r - 45) & \cos(r - 45).\sin(r - 45) \\ \cos(r - 45).\sin(r - 45) & \sin^2(r - 45) \end{bmatrix} \qquad (3.10)$$

represents the analyser and

$$\left[B\right] = \begin{bmatrix} \cos^2 r.e^{\frac{i\delta}{2}} + \sin^2 r.e^{\frac{-i\delta}{2}} & 2i.\cos r.\sin r.\sin\frac{\delta}{2} \\ 2i.\cos r.\sin r.\sin\frac{\delta}{2} & \cos^2 r.e^{\frac{-i\delta}{2}} + \sin^2 r.e^{\frac{i\delta}{2}} \end{bmatrix}$$

(3.11)

represents the modulator. The modulator is orientated at angle r and its retardation δ is given by

$$\delta = K.\ \sin\ \omega\ t \qquad (3.12)$$

where K is the amplitude of modulation (set to some arbitrary value, e.g. 1/4 of the operating wavelength) and $\omega = 2\pi f$, f being the frequency of modulation (50kHz). Simplifying equation (3.9) gives the intensity $I = |E_x|^2 + |E_y|^2$ falling onto the detector:

$$I = \frac{I_o}{2} \cdot \left[1 + \sin R\ .\ \sin\delta.\ \sin 2\Theta_o + \cos\delta.\ \cos 2\Theta_o.\sin(2r-2\Omega) - \cos R\ .\ \sin 2\Theta_o.\cos\delta.\cos(2r-2\Omega) \right]$$

(3.13)

Expansion of $\sin\delta$ and $\cos\delta$ to 4th order in ωt, using equation (3.12), yields only odd and only even harmonic terms in ωt respectively. Thus, defining the intensity modulation component at ω as W_1 and that at 2ω as W_2 we obtain:

$$W_1 = \frac{I_o}{2} \cdot \left[K - \frac{K^3}{8} \right].\ \sin\ R.\ \sin\ 2\Theta_o \qquad (3.14)$$

$$W_2 = \frac{I_o}{2}.\left[\frac{K^2}{4} - \frac{K^4}{48}\right].\left\{\cos 2\theta_o.\sin(2r-2\Omega) - \cos R.\ \sin 2\theta_o.\cos(2r-2\Omega)\right\} \qquad (3.15)$$

W_1 and W_2 are measured using phase-sensitive detectors operating at f and 2f respectively. Calculation of the sensitivities S_1 and S_2 of the signals W_1 and W_2 respectively, to a change in θ_o yields:

$$S_1 = \frac{d\,W_1}{d\,\theta_o} = I_o.\left[K - \frac{K^3}{8}\right].\sin R.\ \cos 2\theta_o \qquad (3.16)$$

and

$$S_2 = \frac{d\,W_2}{d\,\theta_o} = I_o.\left[\frac{K^2}{4} - \frac{K^4}{48}\right].\{-\sin 2\theta_o\ \sin(2r-2\Omega) - \cos R.\ \cos 2\theta_o.\ \cos(2r-2\Omega)\} \qquad (3.17)$$

From equation (3.14), W_1 neither contains terms in r nor Ω, so that the 50kHz component is independent of the orientation of the modulator/analyser assembly. Therefore by initially rotating of the input polariser, a zero in the 50kHz component W_1 can always be obtained, corresponding to $\theta_o = 0$. The input polariser must then be orientated along the fibre principal axis ϕ(the reference direction). Note that from equation (3.16), the sensitivity of this rotation procedure, S_1, is proportional to sinR. The principal axis position can thus be quickly and accurately found, even for small R's, providing the detection gain is increased. Naturally $S_1 \to 0$ at $R = 0$, but in this case there is no principal axis.

Next, retaining the input polariser position $\theta_o = 0$, the modulator/analyser assembly is rotated until W_2 is also zero, corresponding to $r = \Omega$, from equation (3.15). W_1 remains zero. The sensitivity of this procedure $\left|\frac{d\ W_2}{d(r-\Omega)}\right|$ is a maximum for $\theta_o = 0$ and $r - \Omega = 0$, and is independent of the value of R. The rotation Ω can thus be found very accurately from the difference in modulator and input polariser positions.

The input polariser is now rotated by 45^o to give $\theta_o = +45^o$, while the modulator position is left unaltered (i.e. $r - \Omega = 0$). In this condition $W_2 \propto \cos R$ and $W_1 \propto \sin R$. Detecting the ratio W_1/W_2 gives a calibrated output proportional to $\tan R$ independent of variations in the input intensity I_o or fibre launch efficiency. Note that unlike the previous method, the sign of R with respect to the principal axis position ϕ just measured may be determined. Another advantage is that in the case of $\theta_o = 45^o$ and $r - \Omega = 0^o$, the sensitivities S_1 and S_2 of W_1 and W_2 to θ_o and those of W_1 and W_2 to $r - \Omega$ all approach zero. This means that the measurement of R using W_1/W_2 has large tolerances to the settings of θ_o and $r - \Omega$. This is particularly useful for ultra-low fibre retardations R where it becomes more difficult to determine accurately ϕ and Ω.

The range of R values measurable is limited by the detection system dynamic range using the ratio output $W_1/W_2 \equiv \tan R$. However, using a Soleil compensator to give zero total system retardation as described in sub-section 3.3.2 substantially reduces this problem. Moreover since $W_1 = 0$ is a sufficient condition for detecting $R_{TOTAL} = 0$ and is independent of I_o, ratio detection becomes superfluous. With W_2 no longer of concern, the signal gain may be increased to optimise the detection of a zero in W_1.

The detection system requirements using the modulator then reduce to the sensing of a zero in the 50kHz and

100kHz detector signals to find ϕ and Ω and a subsequent zero in 50kHz signal to determine R. Moreover, unlike the preceeding method, the modulator technique can determine the principal axis position ϕ and rotation Ω without a time-consuming iteration procedure. The method is therefore extremely fast and is much more accurate and sensitive, particularly at low R values.

3.6.3 Detection system

The detection system for the modulator technique using a c.w. source is shown in Figure 3.7. The signal from the $1cm^2$ silicon photodiode is greatly amplified to give sensitive detection of the zeros in the 50kHz and 100kHz components. In the 50kHz channel the amplified signal passes via a 40dB attenuator to a coherent tracking filter with a 3Hz bandwidth and a gain of 40dB at 50kHz. The filter prevents phase-sensitive detector input overload by rejecting the large 100kHz signal which arises when the compensator is used to set zero total retardation. For the 100kHz channel, the amplified signal passes directly to a lock-in amplifier, operating in "2f" mode, whose sensitivity is adjusted to match that of the 50kHz channel. A stable 50kHz reference signal for the channels is derived from the modulator controller. If required, source intensity compensation is provided by the ratiometer and voltmeter.

3.6.4 Operation of the modulator system using a tunable wavelength source

The tunable source used for the modulator system is the Q-switched Nd:YAG laser/Raman fibre described in Section 3.5. The modified experimental arrangement using the modulator is shown in Figure 3.8. As before, the test fibre output passes via the monochromator to a Ge-pin photodiode and transimpedance amplifier. As a result of the 50kHz and 100kHz modulation components introduced by the modulator, the 1kHz-rate 300ns output pulses will have randomly-varying heights.

To extract the required 50kHz and 100kHz modulation components W_1 and W_2 from these pulses, a sampling technique is used. A 1kHz clock is obtained by dividing the 50kHz modulator drive reference signal. This triggers the laser Q-switch controller, via a delay generator, to phase-lock the laser pulses to the modulation. The delay generator and its associated sampling controller are used to increase the delay of each successive laser trigger pulse by an additional 200ns with respect to a reference point in the 50kHz reference waveform. The correspondingly delayed optical pulses thus sample the complete 20μs cycle of the 50kHz and 100kHz modulation components W_1 and W_2 to be detected. By detecting the height of 100 successive optical pulses using a linear gate (as described in Section 3.5.2), a complete cycle of the "replica modulation waveform" can be built up in 100ms. Then the sampling control resets the delay to sample the modulation a second time. The "replica waveform" has a 100ms period, so contains sampled frequency components $\bar{W}_1$ and $\bar{W}_2$ at 10Hz and 20Hz respectively. These signals represent the actual optical modulation components W_1 and W_2 at 50 and 100kHz. $\bar{W}_1$ and $\bar{W}_2$ are measured using the two-channel phase-sensitive detection system of Figure 3.7 which now operates at 10Hz and 20Hz. A 10Hz reference for this system is derived from the 50kHz modulator drive signal using a second linear gate. The amplifier is equipped with a 33Hz low-pass filter which rejects much of the high-frequency noise appearing on the "replica waveform" due to pulse-to-pulse laser intensity fluctuations.

In operation, the 10Hz and 20Hz components $\bar{W}_1$, and $\bar{W}_2$ play the same respective roles as the 50kHz and 100kHz frequency components W_1 and W_2 in the c.w. procedure described previously.

3.6.5 Measurement limitations

In the practical system, the maximum measurement sensitivity is limited by photodiode shot-noise and source laser noise (a particular problem when using the fibre Raman source described in Section 3.5). Any such noise occurring within the pass-band of either detector channel causes intolerably large output fluctuations at very high signal gains. For $R < 0.1^{\circ}$ the 50kHz component W_1 becomes so small as to be swamped by noise, and principal axis determination is impossible. However, for moderate R values, the maximum zero detection sensitivity obtained gives a resolution for R, ψ or Ω better than 0.1°, limited largely by the finite resolution of the vernier scales on the optical components.

The limitations of the simple polariser-analyser technique (see Section 3.4) [52] also apply to the modulator the major drawback being the intrinsic birefringence of the polarisers, modulator ($\sim 0.3^{\circ}$), input and output lenses.

Although there is little improvement in the lower measurement limit of $\sim 5^{\circ}$ of the preceding method, the higher-speed and sensitivity provided by the modulator is a great advantage. Moreover, in the event that ultra-low birefringence lenses could be obtained, the modulator technique is by far the superior method for ultra-low and medium birefringence fibre measurements. It is also ideally suited to automation[53, 54].

3.7 Summary

There are several techniques available for measurement of fibre birefringence according to its magnitude, which can vary over some 6 orders.

In high-birefringence fibres with beat length L_p < ~20mm, observation of the Rayleigh-scattering beat pattern is suitable. In contrast, for medium and low birefringence a polariser-analyser technique has been adopted. This can provide accurate measurements in fibres at various temperatures and wavelengths and is used to obtain the majority of the experimental results presented in this work. More recently, the first known application of a photo-elastic modulator to optical fibres for more sensitive measurement of very low birefringence as well as high birefringence has been developed as a routine technique.

By hanging the test fibre vertically, minimisation of external influences on the fibre has been achieved. For ultra-low birefringence measurements the input lens birefringence provides the major practical limitation of any measurement technique.

3.8 References

1. Norman, S. R., Payne, D. N., Adams, M. J., and Smith, A. M.: "Fabrication of single-mode fibres exhibiting extremely low polarisation birefringence", Electron. Lett., 15, 1979, pp. 309-311.

2. Katsuyama, T., Matsumura, H., and Suganuma, T.: "Low loss single-polarisation fibres", Electron. Lett., 17, 1981, pp. 473-474.

3. Papp, A., and Harms, H.: "Polarisation optics of index-gradient optical waveguide fibres", Appl. Optics, 14, 1975, pp. 2406-2411.

4. Smith, A. M.: "Polarisation and magneto-optic properties of single-mode optical fibre", Appl. Optics, 17, 1978, pp. 52-56.

5. Stolen, R. H., Ramaswamy, V., Kaiser, P., and Pleibel, W.: "Linear polarisation in birefringent single-mode fibres", Appl. Phys. Lett., 33, 1978, pp. 699-701.

6. Ramaswamy, V., Kaminov, I. P., and Kaiser, P.: "Single polarisation optical fibres: Exposed cladding technique", Appl. Phys. Lett., 33, 1978, pp. 814-816.

7. Kaminov, I. P., Simpson, J. R., and Presby, H. M.; "Strain birefringence in single polarisation germanosilicate optical fibres", Electron. Lett., 15, 1974, pp. 677-679.

8. Ramaswamy, V., Stolen, R. H., Divino, M. D., and Pleibel, W.: "Birefringence in elliptically clad borosilicate single-mode fibres", Appl. Optics, 18, 1974, pp. 4080-4084.

9. Kaminov, I. P.: "Polarisation in optical fibres", IEEE J. of Quantum Electron., QE-17, 1981, pp. 15-22.

10. Okoshi, T.: "Single-polarisation single-mode optical fibres", IEEE J. of Quantum Electron., QE-17, 1981, pp. 871-884.

11. Dyott, R. B., Cozens, J. R., and Morris, D. G.: "Preservation of polarisation in optical-fibre waveguides with elliptical cores", Electron. Lett., 15, 1979, pp. 380-382.

12. Hosaka, T., Okamoto, K., Sasaki, Y., and Edahiro, T.: "Single-mode fibres with asymmetrical refractive index pits on both sides of core", Electron. Lett., 17, 1981, pp. 191-193.

13. Hosaka, T., Okamoto, K., Miya, T., Sasaki, Y., and Edahiro, T.: "Low-loss single-polarisation fibres with asymmetrical strain birefringence", Electron. Lett., 17, 1981, pp. 530-531.

14. Kitayama, K., Seikai, S., Uchida, N., and Akiyama, M.: "Polarisation-maintaining single-mode with azimuthally inhomogeneous index profile", Electron. Lett., 17, 1981, pp. 419-420.

15. Kapron, F. P.,Borrelli, N. F., and Keck, D. B.: "Birefringence in dielectric optical waveguides", IEEE J. of Quantum Electron., QE-8, 1972, pp. 222-225.

16. Simon, A., and Ulrich, R.: "Evolution of polarisation along a single-mode fibre", Appl. Phys. Lett., 31, 1977, pp. 517-520.

17. Barlow, A. J., Ramskov Hansen, J. J., and Payne, D. N.: "Birefringence and polarisation mode-dispersion in spun single-mode fibres", Appl. Optics, 20, 1981, pp. 2962-2968.

18. Hartshorne, N. H., and Stuart, A.: "Crystals and the polarising microscope", Edward Arnold, 1970.

19. Durelli, A. J., and Riley, W. F.: "Introduction to Photomechanics", Prentice-Hall, 1965.

20. Kuske, A., and Robertson, G.: "Photoelastic stress analysis", Wiley, 1974.

21. Jerrard, H. G.: "Optical compensators for measurement of elliptical polarisation", J. Opt. Soc. Am., 38, 1948, pp. 35-59.

22. Machida, S., Sakai, J., and Kimura, T.: "Polarisation conservation in single-mode fibres", Electron. Lett., 17, 1981, pp. 494-495.

23. Gambling, W. A., Payne, D. N., and Matsumura, H.: "Birefringence and optical acitivity in single-mode fibres", Paper presented at Topical Meeting on Optical Fibre Transmission II, Williamsburg, February 22-24, 1977.

24. Birch, R. D.: Private Communication.

25. Barlow, A. J., and Payne, D. N.: "Birefringence testing in single-mode fibres manufactured with controlled polarisation characteristics", paper presented at colloquium on "Test Equipment for Optical Fibre Communication Systems", IEE, London, 28 May 1981.

26. Rogers, A. J.: "Polarisation optical time-domain reflectometry", Electron. Lett., 16, 1980, pp. 489-490.

27. Hartog, A. H., Payne, D. N., and Conduit, A. J.: "Polarisation optical time-domain reflectometry: Experimental results and application to loss and birefringence measurements in single-mode optical fibres", Post-deadline paper presented at Sixth European Conference on Optical Communication, York, September 16-19, 1980.

28. Nakazawa, M., Horiguchi, T., Tokuda, M., and Uchida, N.: "Polarisation beat length measurement in a single-mode optical fibre by backward Rayleigh scattering", Electron. Lett., 17, 1981, pp. 513-515.

29. Kim, B. Y., and Choi, S. S.: "Analysis and measurement of birefringence in single-mode fibres using the backscattering method", Optics Lett., 6, 1981, pp. 578-580.

30. Rogers, A. J.: "Polarisation-optical time-domain reflectometry - a technique for the measurement of field distributions", Appl. Optics, 20, 1981, pp. 1060-1074.

31. Kim, B. Y., and Choi, S. S.: "Backscattering measurement of bending-induced birefringence in single-mode fibres", Electron. Lett., 17, 1981, pp. 193-194.

32. Ross, J. N.: "Polarisation optical time domain reflectometry" paper presented at colloquium on Optical Fibre Sensors, IEE, London, May 26, 1982.

33. Ulrich, R., and Simon, A.: "Polarisation optics of twisted single-mode fibres", Appl. Optics, 18, 1979, pp. 2241-2251.

34. Chinone, N., and Ulrich, R.: "Elasto-optic polarisation measurement in optical fibre", Optics. Lett., 6, 1981, pp. 16-18.

35. Imoto, N., and Ikeda, M.: "Polarisation dispersion measurement in long single-mode fibres with zero dispersion wavelength at 1.5 μm", IEEE J. of Quantum Electron., QE-17, 1981, pp. 542-545.

36. Matsumura, H.: "Birefringence and optical activity in phosphosilicate glass fibres", University of Southampton, internal report, (unpublished), November 1976.

37. Smith, A. M.: Private Communication.

38. Kumar, A., and Ulrich, R.: "Birefringence of optical fibre pressed into a V groove", Optics Lett., 6, 1981, pp. 644-646.

39. Ramaswamy, V., Standley, R. D., Sze, D., and French, W. G.: "Polarisation effects in short length, single-mode fibres", Bell Syst. Tech. J., 57, 1978, pp. 635-651.

40. Leminger, O. G.: "Stress birefringence in single-mode fibre", Electron. Lett., 13, 1977, pp. 370-371.

41. Calligaro, R. B.: Unpublished work.

42. Barlow, A. J., Payne, D. N., Hadley, M. R., and Mansfield, R. J.: "Production of single-mode fibres with negligible intrinsic birefringence and polarisation mode-dispersion", Electron. Lett., 17, 1981, pp. 725-726.

43. Adams, M. J.: "An Introduction to Optical Waveguides", Wiley, 1981.

44. Kato, Y., Kitayama, K., Seikai, N., and Uchida, N.: "Novel method for measuring cut-off wavelength of HE_{21}-, TE_{01}-, and TM_{01} modes", Electron. Lett., 15, 1979, pp. 410-411.

45. Lin, C., Cohen, L. G., Stolen, R. H., Tasker, G. W., and French, W. G.: "Near infra-red sources in the 1-1.3μm region by efficient stimulated Raman emission in glass fibres", Optics Comm., 20, 1977, pp. 426-428.

46. Ohmori, Y., Sasaki, Y., and Edahiro, T.: "Fibre length dependence of critical power for stimulated Raman scattering", Electron. Lett., 17, 1981, pp. 593-594.

47. The fibre was kindly supplied by BTRL, Ipswich.

48. Conduit, A. J.: Private Communication.

49. Koeman, B., and Joneschitz-Kriegl, H.: "Analysis of slightly elliptically polarised light" , J. Phys. E: Sci. Instrum., 12, 1974, pp. 625-628.

50. Kemp, J. C.: "Piezo-optical birefringence modulator: new use for a long-known effect", J. Opt. Soc. Am., 59, 1969, pp. 950-954.

51. Wong, C. F.: "Birefringence measurement using a photo-elastic modulator", Appl. Optics, 18, 1974, pp. 3496-3499.

52. Vasil'ev V. I., and Samsonova, S. A.: "Influence of birefringence of the glasses of a polarimeter cell on the accuracy of the polarisation plane rotation measurement", Sov. J. Opt. Tech., 48, 1981, pp. 255-258.

53. Smith, A. M.: "Automated birefringence measurement system", J. Phys. E: Sci. Instrum., 12, 1979, pp. 427-430.

54. Yen, Y., and Ulrich, R.: "Birefringence measurement of fibre-optic devices", Appl. Optics, 20, 1981, pp. 2721-2725.

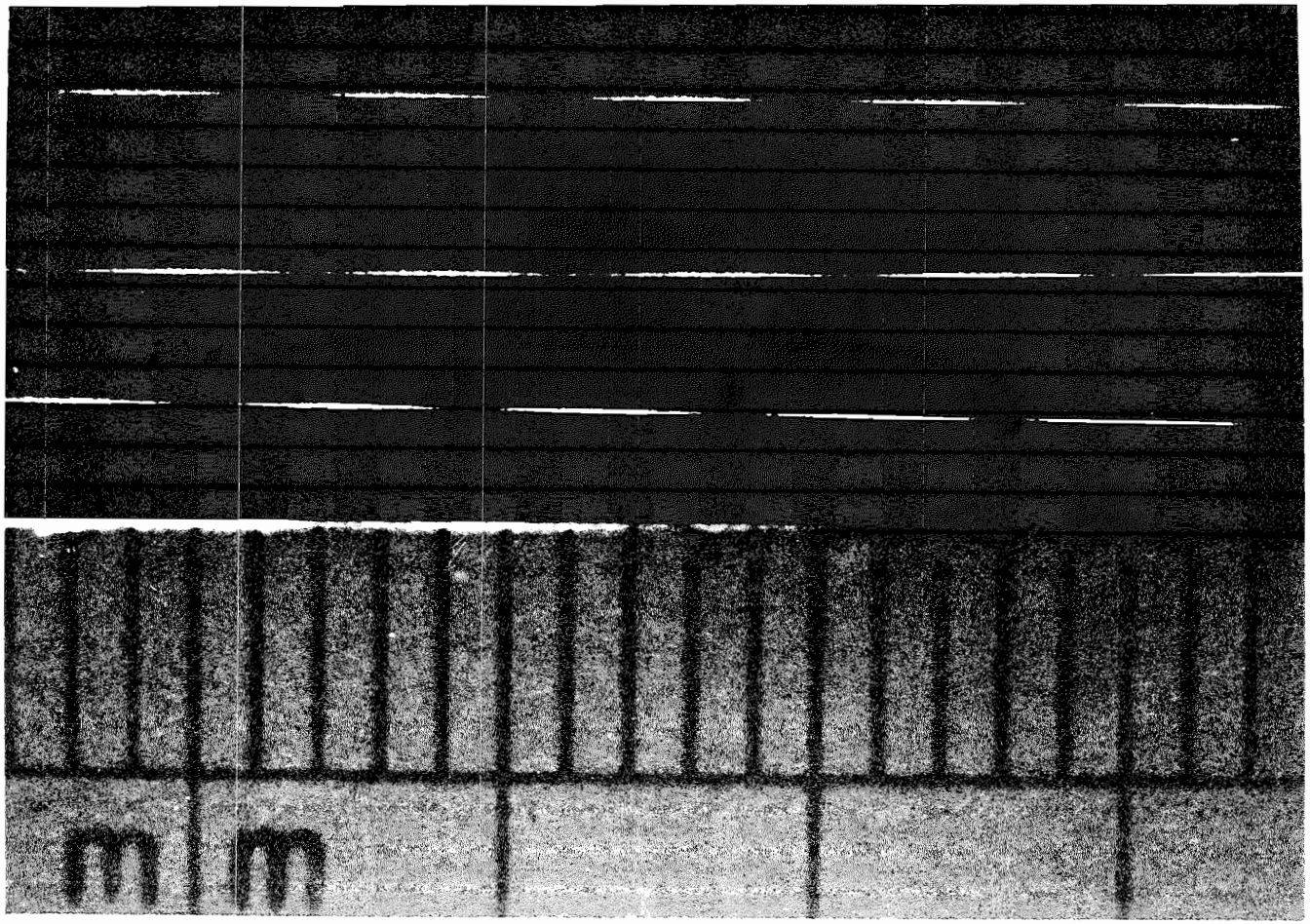

Figure 3.1 The Rayleigh Scattering 'beat' pattern obtained at 633nm in a high-birefringence fibre of 4 mm beat length.

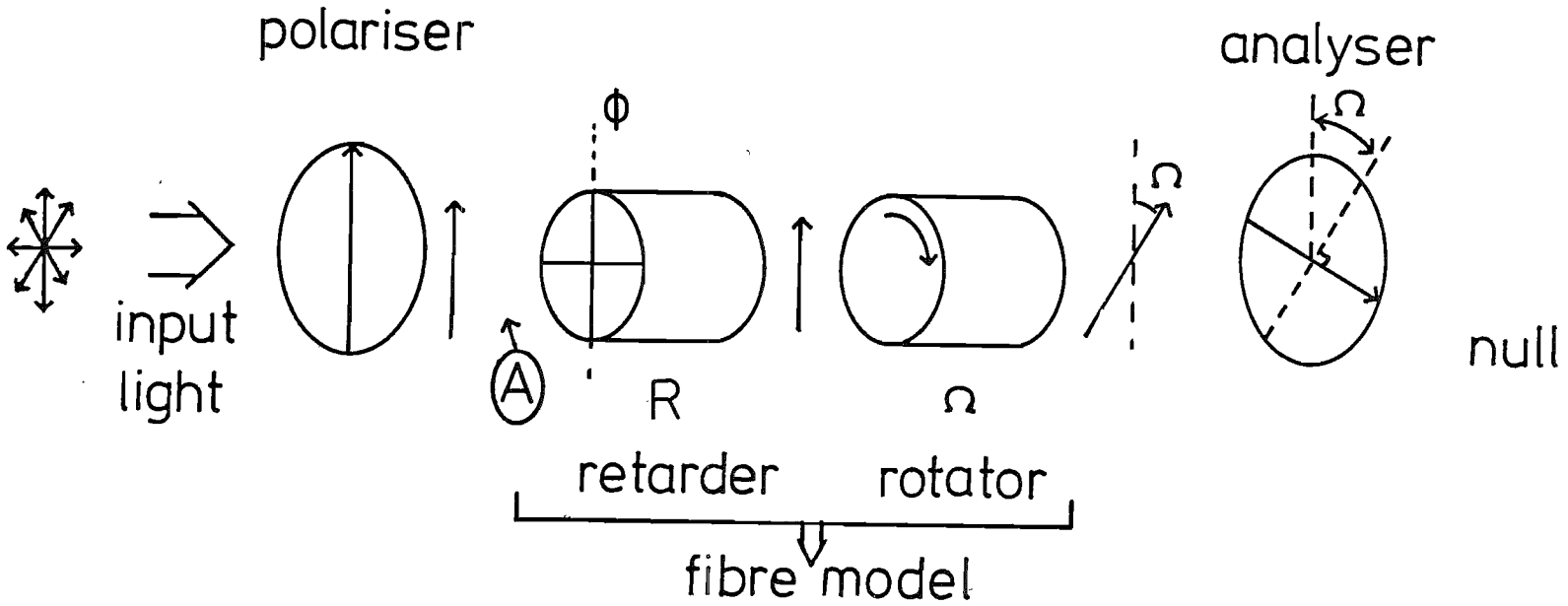

Figure 3.2 The measurement of fibre birefringence using polarisers (input and output lenses have been omitted for clarity).

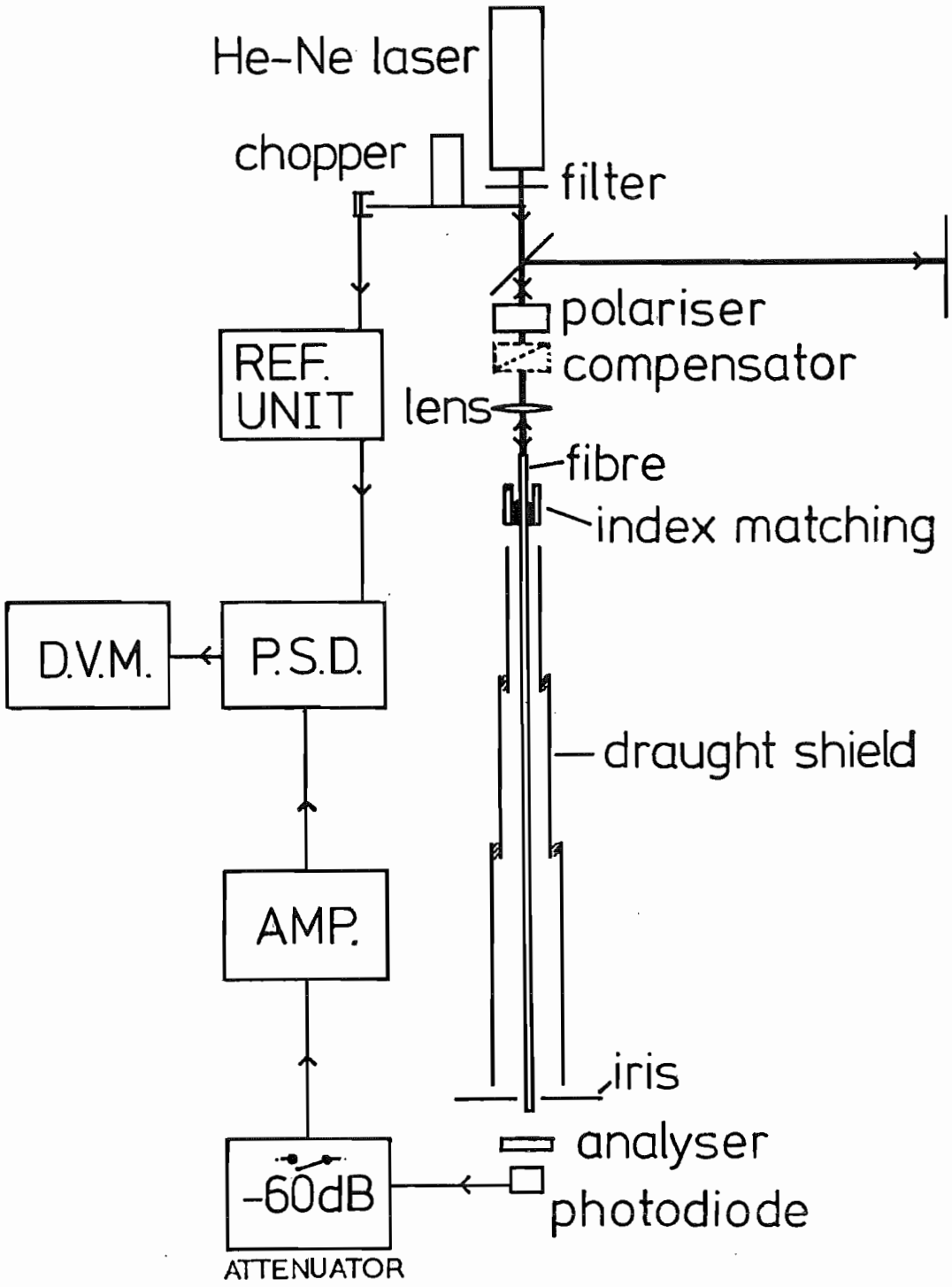

Figure 3.3 The vertical experimental arrangement using a Helium-Neon Laser to measure birefringence in a single-mode fibre.

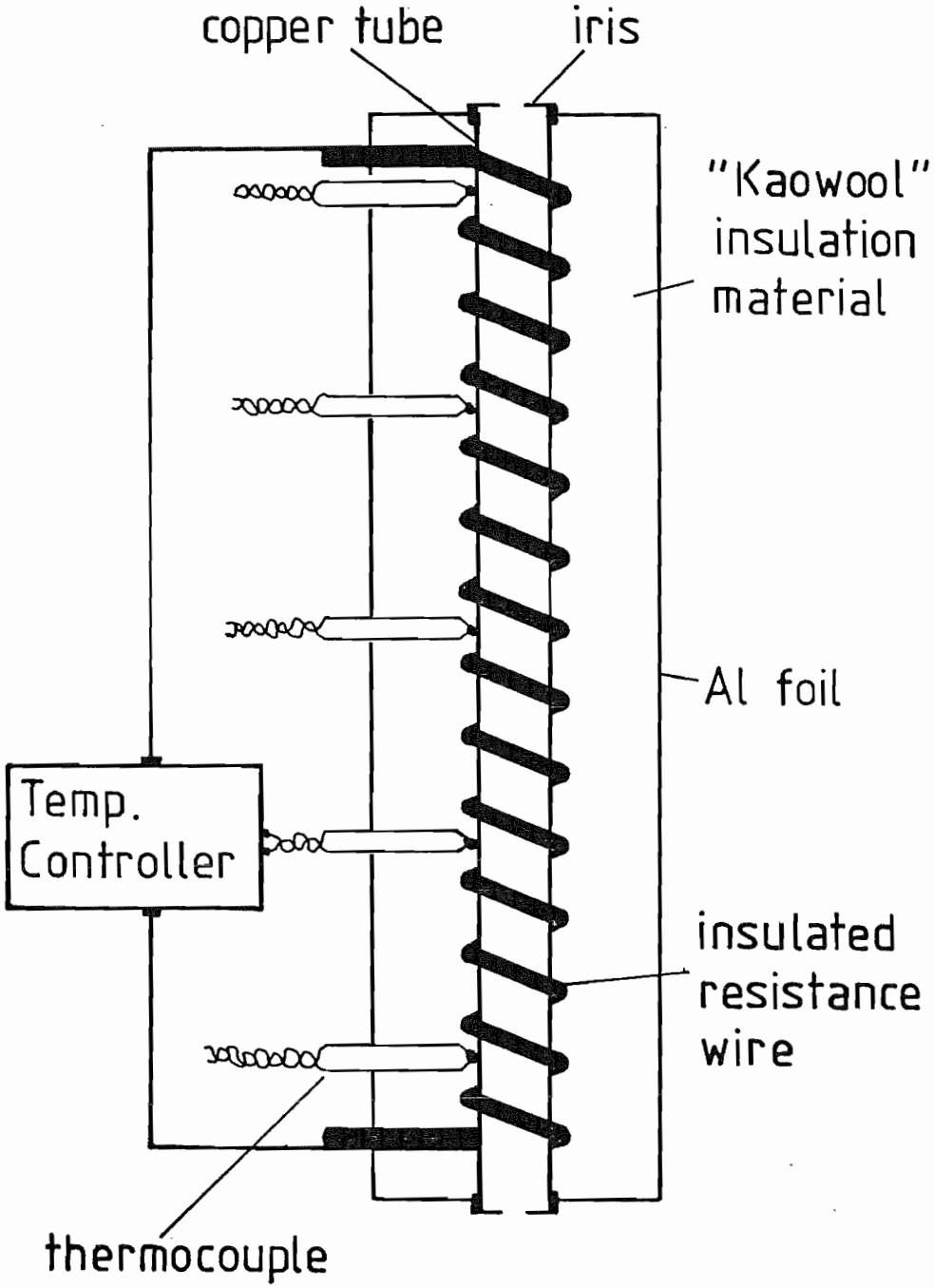

Figure 3.4 Diagram of 1-metre tube furnace used when measuring fibre birefringence as a function of temperature.

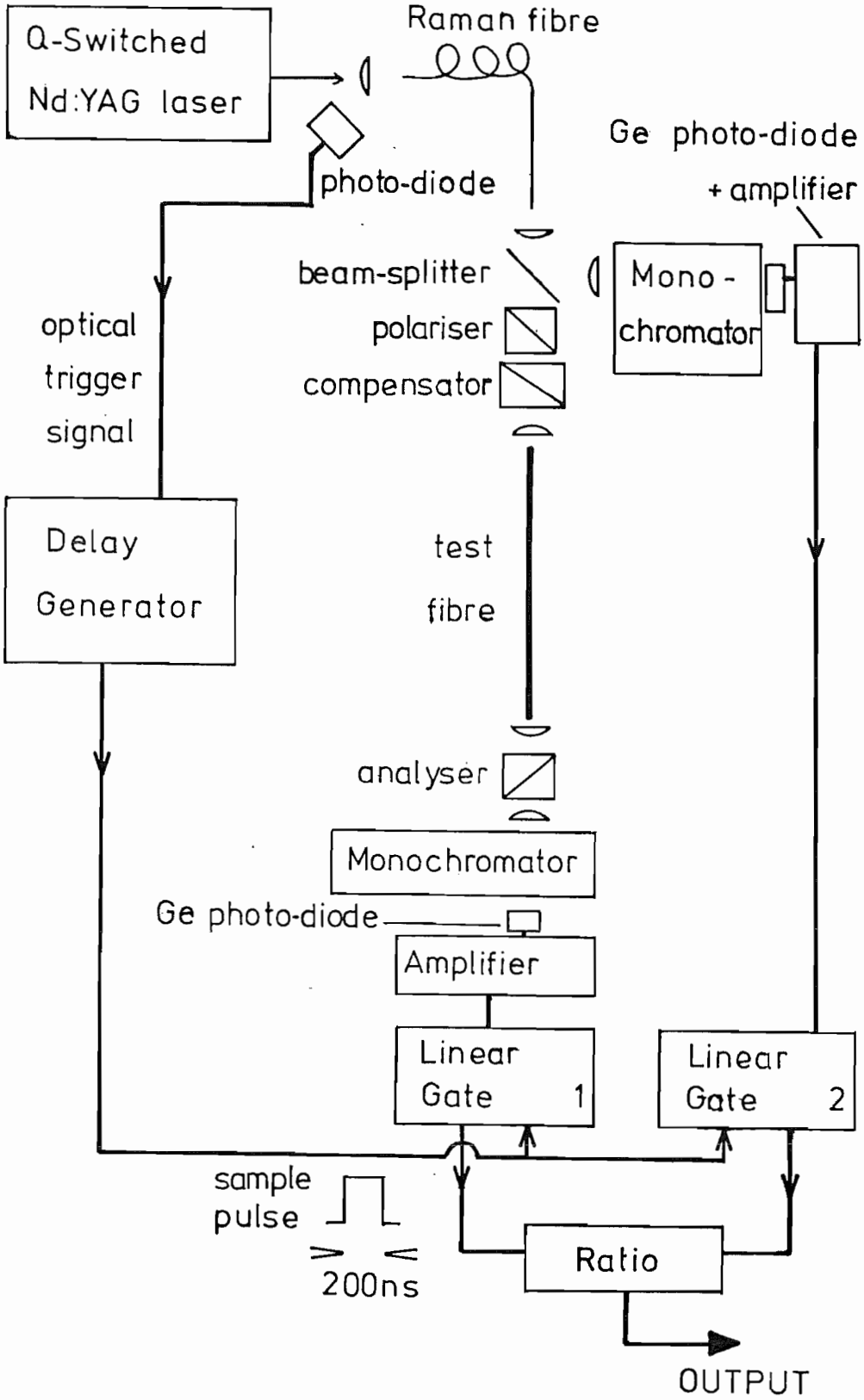

Figure 3.5 Fibre birefringence measurement apparatus using a tunable-wavelength Nd:YAG laser/Raman fibre source.

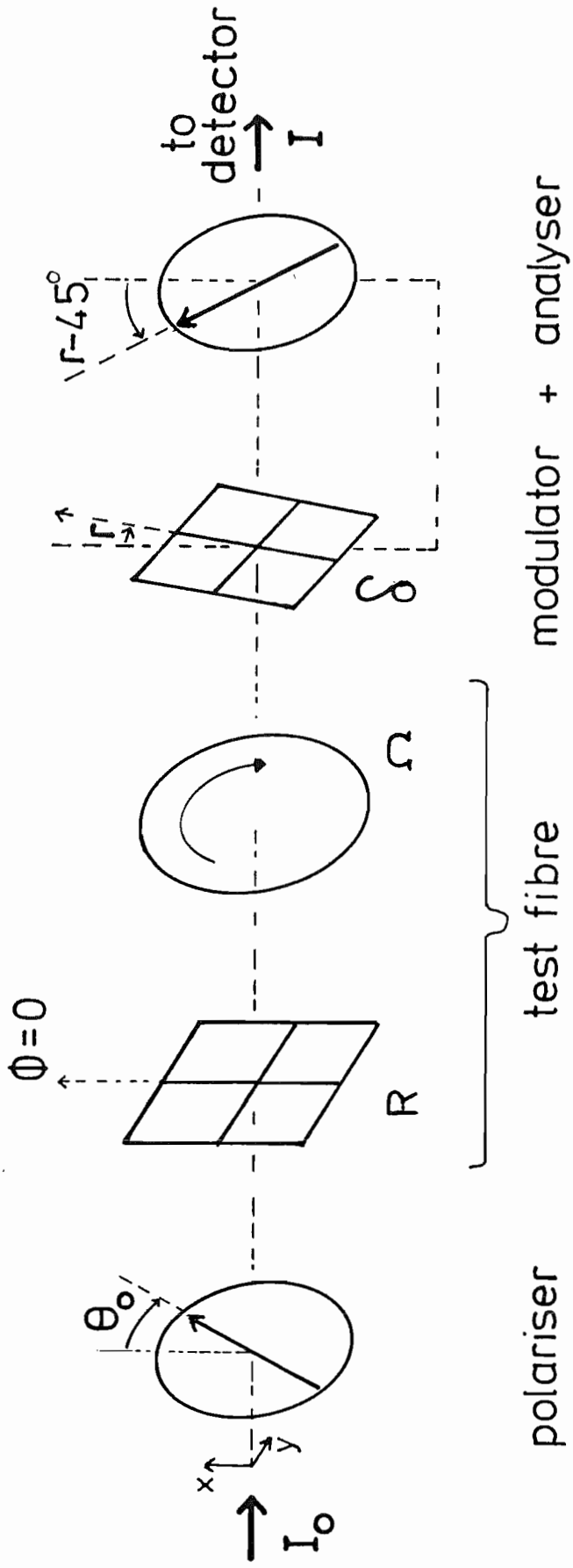

Figure 3.6 Optical arrangement for fibre birefringence measurement using a photo-elastic birefringence modulator. Modulator and analyser rotate as one assembly.

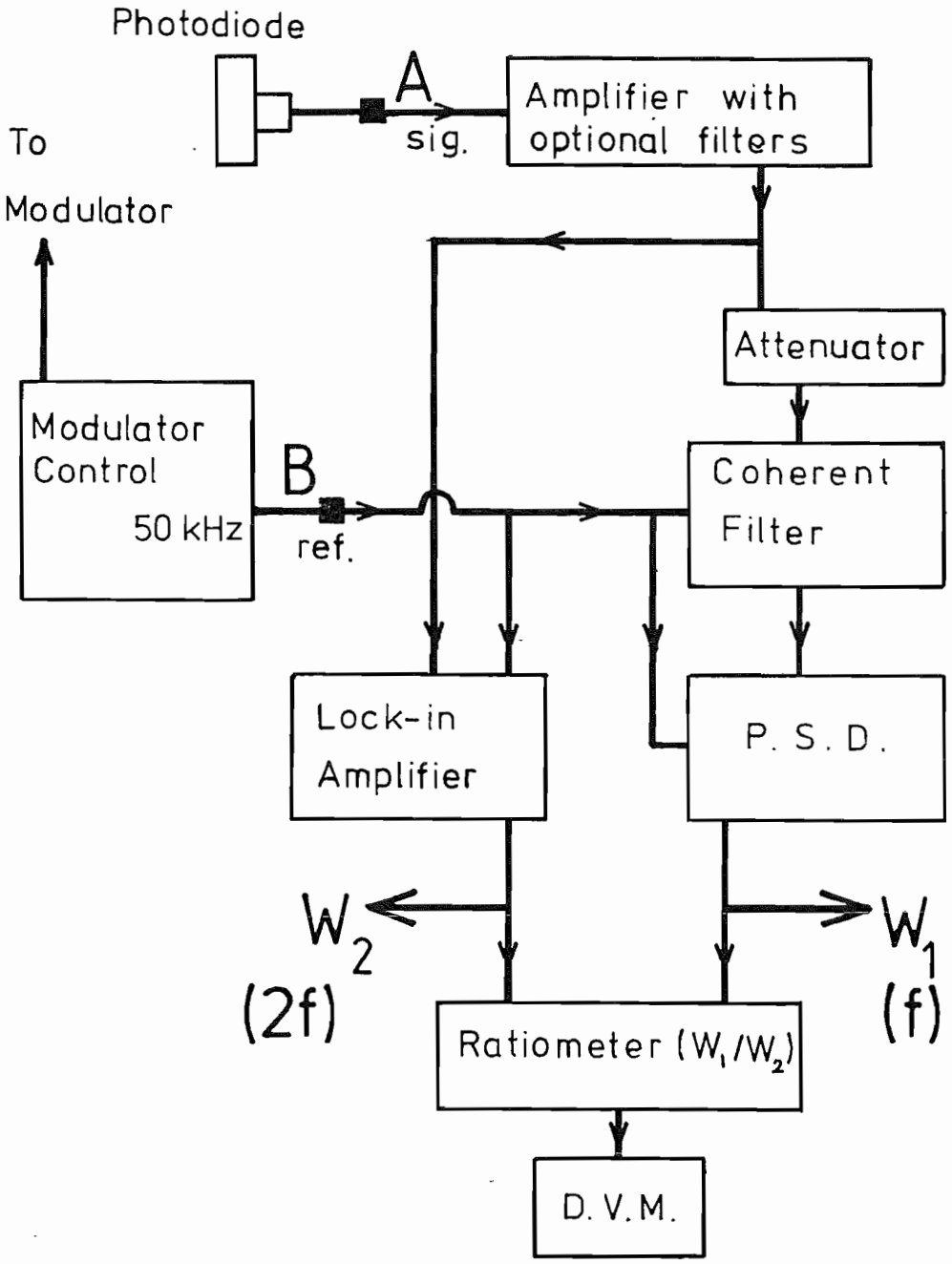

Figure 3.7 The dual-channel phase-sensitive detection system used with the photo-elastic modulator.

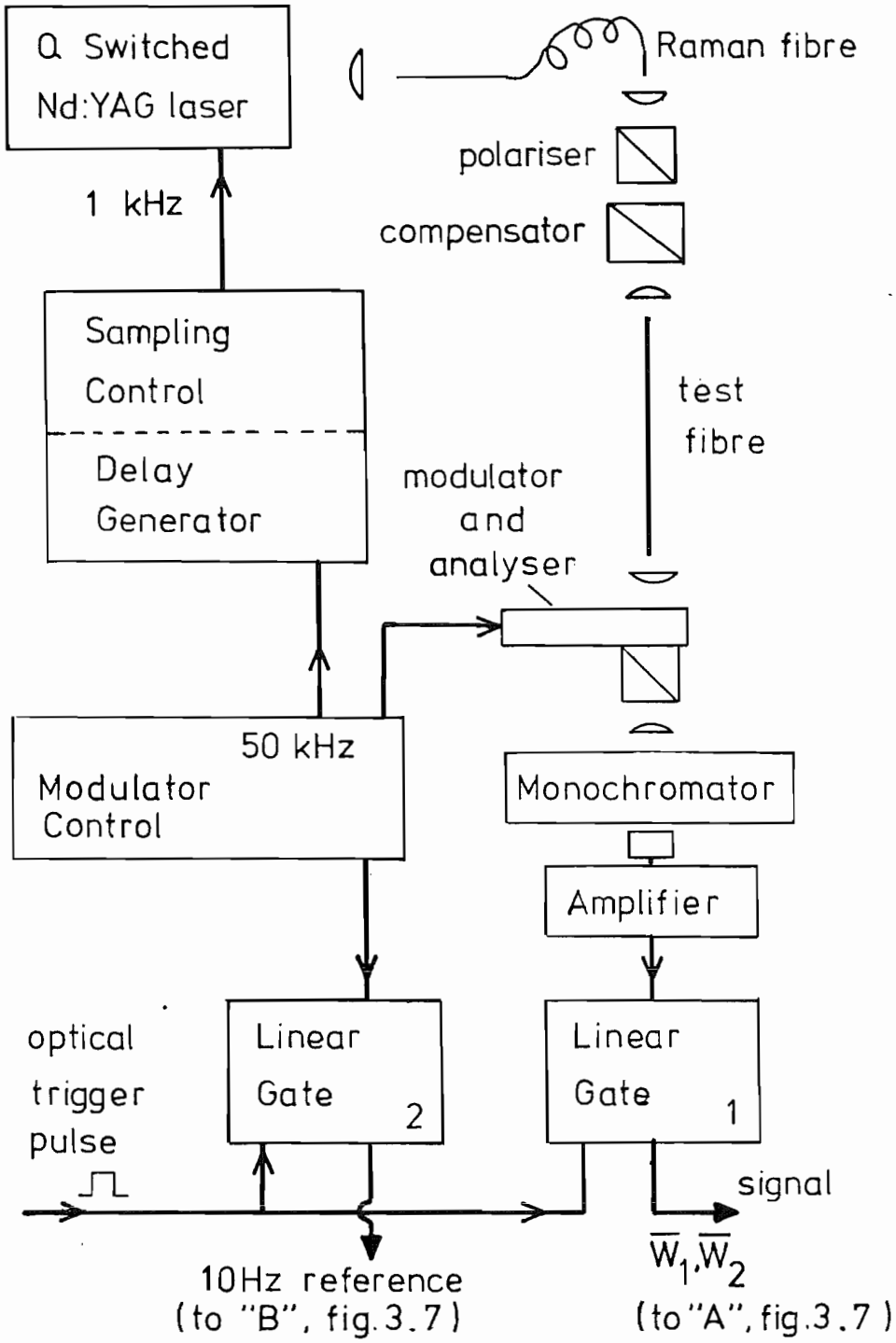

Figure 3.8 Apparatus for the measurement of birefringence in a fibre using a photo-elastic modulator and Raman fibre source. The sampled modulation components $\overline{W_1}$, $\overline{W_2}$ are measured using the detection system shown in Figure 3.7.

CHAPTER 4 THE DEVELOPMENT OF LOW-BIREFRINGENCE FIBRES

4.1 Introduction

Low-birefringence single-mode optical fibres were initially developed[1, 2] for use in the Faraday current monitor device, to give maximum Faraday rotation sensitivity[3, 4, 5, 6, 7]. It is now recognised that low-birefringence fibre is essential to the design and stable operation of controlled birefringence fibre polarimetric devices such as polarisation controllers[8], filters[9, 10] isolators[11, 12] and sensors[12, 13, 14]. Furthermore, fibre telecommunication bandwidth[15] may be reduced by polarisation mode-dispersion. This is negligible in low-birefringence fibres[16, 17] which are therefore potentially useful in high-bandwidth communications.

An evolutionary development of ultra-low birefringence fibres with $B < 10^{-8}$ has occurred within the last five years, centring around two distinct types, (i) the 'conventional' untwisted fibre and (ii) the 'spun' fibre. In 'conventional' fibres, the intrinsic fibre birefringence B itself is designed to be the absolute minimum possible. This is achieved in the CVD fabrication technique by careful reduction of the preform ellipticity and thermal stress which contribute to fibre birefringence. On the other hand, a 'spun' fibre allows the retention of a relatively large intrinsic anisotropy within the fibre, achieving ultra-low overall birefringence by means of a spin averaging affect on the anisotropy, similar to a twist[18].

In this Chapter, both these types of low-birefringence fibre are discussed in detail. Although birefringence as low as 4.5×10^{-9} can be obtained in 'conventional' fibres[2], the main drawback is lack of reproducibility. This is attributed largely to the poor control available in the CVD process. This problem can be all but eradicated by adopting the technique of fibre spinning. By its very

nature, the ability of spinning to produce ultra-low birefringence is not affected by quite considerable variations in fibre intrinsic birefringence.

4.2 Conventional Low-Birefringence Fibres

In designing 'conventional' low-birefringence fibres, the aim is to reduce the intrinsic birefringence B to an insignificant level by minimising both the waveguide shape birefringence B_G and the stress contribution B_S.

It is possible to calculate the contribution B_G due to core ellipticity e for operation at the higher-mode cut-off. At low ellipticity values[19] B_G is proportional to $(\Delta' n)^2 . e$, where Δ' is the normalised core-cladding refractive index difference, and n the refractive index of the core. A large reduction in B_G can thus be obtained by maintaining good core circularity and reducing Δ'^2. However, to obtain a reasonably low fibre bend and microbend loss[20], Δ' must be greater than ~0.003.

Minimisation of the stress birefringence B_S entails reducing the overall stress levels in the fibre core, for example by matching the cladding and core thermal expansion coefficients through suitable adjustment of their respective dopant levels[2, 21]. Moving these thermal expansion coefficients closer to that of the (silica) substrate, i.e. using a low Δ' value, also reduces fibre stress levels.

In a fibre with an ellipticity of <0.1% and $\Delta' = 0.0034$, a birefringence $B = 4.6 \times 10^{-9}$ was obtained[2], corresponding to a beat length $L_p \simeq 140$m at $\lambda = 0.633\mu$m. This fibre possessed a boron-doped silica cladding, a Germania-doped silica core with a silica substrate. Table 4.1 shows the birefringence properties of several similar fibres, both coated and uncoated[22].

B_G and B_S normally act in unison i.e. have the same 'fast' axis direction, when the expansion coefficient of the core exceeds that of the cladding. However, in the fibres of Table 4.1, the shape contribution B_G as predicted by Ref. 19, is consistently larger than the total birefringence B, indicating that a larger stress contribution B_S *opposes* B_G. There are several possible explanations of this situation. First, any cladding and core ellipticities may not be orientated in the same direction. Secondly, the dopant concentrations actually present in the preform vary according to preform deposition and gas delivery conditions[23]. However, these two effects would give a random sign for B_S from fibre to fibre; the consistency of B_S opposing B_G rather points to another effect. It has been shown[24] that in the three-layer core/cladding/substrate structure of these fibres that B_S can oppose B_G when the core and cladding elliptic axes are orientated in the same direction if the core expansion coefficient is substantially lower than than of the cladding[25]. This could arise, for example, (i) if the calculated dopant concentrations in the preform for stress matching are subject to systematic error[21] or (ii) as a result of out-diffusion of the volatile core dopants during collapse of the fibre preform[23]. Out-diffusion depletes the deposited core layers of dopant to yield fibres with cores of consistently lower equivalent expansion coefficient than intended, thereby reversing the sign of B_S. A central dip in the refractive index profile (RIP) also arises from out-diffusion, providing a measure of the extent of the depletion. Figure 4.1 shows a typical RIP obtained in fibre GSB4 using the spatial-filtering technique[26]. Maintaining a dopant-rich atmosphere inside the preform tube during collapse[23, 27] can reduce the out-diffusion. This was not performed for the fibres of Table 4.1[22] and is thought to be the major reason for B_S consistently opposing B_G in these fibres.

Further evidence that B_S does indeed oppose B_G in these fibres was provided by gently heating the fibres to reduce the internal thermal stress[22], whereupon the fibre birefringence increased.

The low birefringence in many of the fibres of Table 4.1 can always be attributed to exceptionally good control of core ellipticity, but in addition, to a substantial cancellation of the stress and ellipticity effects. In effect, fibres such as GSB6 can exhibit low-birefringence despite their considerable core ellipticity.

4.3 Low-Birefringence Reproducibility in 'Conventional' Fibres

From Table 4.1, the reproducibility of low fibre birefringence i.e. $B < 10^{-8}$ is unsatisfactory. Evidently the fibre core and cladding ellipticities, dopant concentrations and hence thermal expansion coefficients cannot be accurately and repeatedly controlled to guarantee low birefringence in conventional fibres, as already outlined above. The problem is compounded by geometry variations along the length of the preform. This results in some sections of a fibre (e.g. GSB4) exhibiting different birefringence from others. Moreover, fibre cross-sectional variations can arise during fibre drawing from fluctuations in pulling-furnace environmental conditions[28].

By exploiting the mutual cancellation of B_G and B_S a fibre with $B_S - B_G = 0$ could be designed which would be insensitive to a production spread in ellipticity since both B_S and B_G are approximately proportional to ellipticity. However, the necessary control of fibre dopant levels would be difficult to achieve in practice and such a fibre would be extremely temperature sensitive.

Several of the fibres of Table 4.1 exhibit undesired circular-birefringence (rotation) most likely arising from

fibre twists produced during drawing. During pulling the fibre is wound evenly onto a transversely moving take-up drum. The lateral motion of the drum causes the fibre to roll over the drum surface so imparting a torsion to the fibre. This is relieved by viscous flow in the fibre 'hot-zone' and is therefore 'frozen-in' to the drawn fibre as it cools.

The twist which occurs during drawing has been confirmed by drawing a fibre with a rectangular cross-section. A one-axis scanning laser fibre diameter monitor recorded readings alternating between each of the fibre dimensions, indicating that the fibre below the hot-zone was revolving due to the lateral drum motion.

The optical rotation often seen in 'conventional' fibres arising from drawing-induced twist can be reduced by using a separate fibre capstan and take-up drum. Since the capstan would not be required to move laterally, little twist of the drawn fibre would be expected.

In view of the difficulties encountered this far, it remains uncertain that high production yields could be obtained in conventional fibres if continued development took place.

4.4 Twisted and 'Spun' Fibres

The poor reproducibility of ultra-low birefringence in conventional fibres has spurred the development of 'spun' fibres. The basic process and concepts of spinning are now introduced.

Spinning is basically a process whereby a twist is imparted to a fibre whilst in its molten state. In practice the twist can be introduced by simultaneously rotating or spinning the preform about its axis during standard fibre drawing[17]. At the high forming

temperature the fibre is in a molten or viscous state and cannot support any significant torsional shear stress arising from the preform rotation[29]. Upon subsequent cooling then, the applied twist is 'frozen' into the 'spun' fibre. The now-permanent frozen-in fibre twist is given the term 'spin' and can be regarded effectively as a twist imparted without torsional stress. This is distinct from 'twist' applied to the cold fibre where torsional stress *is* supported[30]. This stress introduces an additional twist-induced circular birefringence[31, 18] proportional to the fibre twist rate by means of the photo-elastic effect. Except for this important difference, the basic concepts of spin and twist are in fact identical. In the following conceptual model this distinction is omitted since it does not affect the intrinsic mechanism.

A fibre with no applied twist or spin, with intrinsic linear birefringence $\Delta\beta$ can be modelled as a series of simple linearly-birefringent plates with their principal axes aligned along the fibre length. If the fibre is then spun, the local principal axes of birefringence precess along the fibre length. The fast axis direction at point A approaching apposition with the slow axis direction at point B one quarter-turn of twist further down the fibre. As a simple model, the spun fibre can be divided up into discrete untwisted sections, each having a length of a quarter of a spin period and rotated with respect to each other by 90^{o} (Figure 4.2). At each junction between sections an interchange of fast and slow axes occurs so that the birefringence of the first section is cancelled by that of the opposite sense in the second section. This model, albeit a crude one, clearly demonstrates that the mechanism of spinning a fibre is an averaging effect on the intrinsic birefringence in the fibre by which a small overall fibre retardation may be obtained.

To predict the overall fibre retardation as a function of fibre length, the more refined model shown in Figure 4.3 must be adopted. On this model, the spin rate is implicitly assumed to be much greater than the fibre intrinsic birefringence $\Delta\beta$. Consideration of the series of retarders with rapidly spiralling fast axes, for each fibre length, intuitively gives an overall retardance with a principal axis position ϕ equal to half the total spin angle along that length (see Figure 4.3(a)). The retardation with respect to ϕ oscillates about zero along the fibre, with an amplitude which depends on the birefringence of each individual section (Figure 4.3(b)). Clearly, the shorter the spin period with respect to the birefringence beat length L_p in the unspun fibre, the smaller the birefringence in each section will be and thus the smaller the overall retardation oscillation amplitude.

In contrast to the case of an unspun fibre, the overall retardation in a spun fibre never builds up to an appreciable level over a long fibre length. A highly-twisted fibre also appears to have almost zero overall linear birefringence, but a residual twist-induced rotation appears[18]. However, in a tightly spun fibre this rotation does not arise and a very small linear *and* circular birefringence results. In the limit of a large spin rate the fibre becomes in effect a perfectly isotropic fibre, the spin restoring an overall average circular symmetry of the locally-anisotropic waveguide structure. This spin averaging effect produces a highly reproducible ultra-low birefringence in 'spun' fibres.

4.5 The Analysis of Twisted Fibres

We now consider the detailed analysis of twisted and spun fibres to quantify the basic concepts introduced in the previous section.

The polarisation behaviour of twisted birefringent media has been considered by several authors[32, 33] particularly with application to twisted cholesteric liquid crystals[34] and insect photo-receptors[35]. In the case of fibres many authors have used perturbation theory and coupled-mode analysis to predict the properties of twisted fibres either directly in terms of output polarisation parameters[36, 37, 38, 39, 40] or by graphical representation on the Poincaré sphere[18, 38]. Monerie and Jeunhomme[41] also used coupled-mode analysis and calculated the polarisation mode-dispersion in a twisted fibre. However it is important that any analysis relates the measured universally applicable fibre parameters[32, 42], of retardation R, rotation Ω and principal axis ϕ to the twist[43, 44]. This has been demonstrated by Papp and Harms[44] but it is not possible to include the twist-induced rotation (Section 4.4) or to calculate polarisation mode-dispersion[15] in their analysis.

In view of all these difficulties, the author and his co-workers[45] developed a coupled-mode analysis based on the method by McIntyre and Snyder[35].
This method has the following important advantages:

(i) it is simple, intuitively appealing and versatile, being easily adopted to solve other fibre mode-coupling problems (see Chapter 5).

(ii) it relates directly to the fibre properties R , Ω and ϕ.

(iii) the inclusion of twist-induced rotation is possible, allowing a better understanding of the difference between spun and twisted fibres.

(iv) the calculation of polarisation mode-dispersion in both twisted and spun fibres is possible.

(v) the results may also be represented in the form of an output polarisation-ellipse or plotted on the Poincaré sphere for comparison with other methods[18].

McIntyre and Snyder[35] use a plane-wave approximation to analyse a uniformly-twisted birefringent medium by modelling it as a stack of rotated birefringent plates and employing coupled-mode theory. For a twisted fibre, these retardation plates are interspersed by optical rotation elements which represent the torsional stress-induced rotation[46] per unit length, $\alpha = g'\xi$ for a twisted fibre. Here, ξ is the right-handed twist rate in radians per metre and g' the proportionality constant which has been found experimentally to be ~ 0.08[18, 31]. On the other hand, for the permanent twist in a spun fibre no torsional stress is present; thus $\alpha = 0$. Figure 4.4 shows the new model where each retarder-rotator pair δz thick is rotated by an angle $\delta\Omega$ with respect to the preceding pair.

The electric field equation[35] for Section A in matrix form, using Jones calculus to represent the retarder and rotator, is written:

$$\left[\overline{E}_A\right] = \begin{bmatrix} \cos\ \alpha\delta z & -\sin\ \alpha\delta z \\ \sin\ \alpha\delta z & \cos\ \alpha\delta z \end{bmatrix} \cdot \begin{bmatrix} e^{i\beta_x z} & 0 \\ 0 & e^{i\beta_y z} \end{bmatrix} \cdot \begin{bmatrix} a_x\ \hat{x}_A \\ a_y\ \hat{y}_A \end{bmatrix} \tag{4.1}$$

where β_x and β_y are the propagation constants of the two orthogonally-polarised light components, a_x and a_y are the field amplitudes and $\hat{x}_A$ and $\hat{y}_A$ are unit vectors, in the x_A and y_A directions. Similarly, the electric field at the input to plate B is:

$$\left[\overline{E}_B\right] = \begin{bmatrix} e^{i\beta_x z} & 0 \\ 0 & e^{i\beta_y z} \end{bmatrix} \cdot \begin{bmatrix} (a_x + \delta a_x)\ \hat{x}_B \\ (a_y + \delta a_y)\ \hat{y}_B \end{bmatrix} \tag{4.2}$$

The vector systems in sections A and B are related by:

$$\hat{x}_A = \hat{x}_B \cos \delta\Omega \quad - \hat{y}_B \sin \delta\Omega \tag{4.3}$$

$$\hat{y}_A = \hat{x}_B \sin \delta\Omega \quad + \hat{y}_B \cos \delta\Omega \tag{4.4}$$

The fields $\bar{E}_A$ and $\bar{E}_B$ are now matched at the boundary between the two sections A and B. Assuming a linear twist, using equations (4.3), (4.4) and taking the limit $\delta z \to 0$, yields the two coupled-mode equations:

$$\frac{dA_x}{dz} - i\beta_x A_x = (\xi-\alpha) A_y \tag{4.5}$$

$$\frac{dA_y}{dz} - i\beta_y A_y = -(\xi-\alpha) A_x \tag{4.6}$$

where

$$A_x = a_x e^{i\beta_x z} \tag{4.7}$$

$$A_y = a_y e^{i\beta_y z} \tag{4.8}$$

If no twist-induced rotation is present, as in a spun fibre, $g'\xi = \alpha = 0$, the analysis is identical to that of McIntyre and Snyder[35, 47]. It has been implicitly assumed that $|(\beta_x - \beta_y)/(\beta_x + \beta_y)| \ll 1$ and $\xi \ll |\beta_x|, |\beta_y|$ to neglect the power transfer between forward and backward-travelling waves.

The solution to the coupled-mode equations (4.5) and (4.6), describing the plane-wave propagation along the twisted fibre, is written as:

$$\begin{bmatrix} A_x(z) \\ A_y(z) \end{bmatrix} = \begin{bmatrix} G & -H^* \\ H & G^* \end{bmatrix} \begin{bmatrix} A_x(0) \\ A_y(0) \end{bmatrix} \tag{4.9}$$

where

$$G = \left(\cos \gamma z + i \frac{\rho}{\sqrt{1+\rho^2}} \sin \gamma z\right) e^{i\beta_s z} \tag{4.10}$$

$$H = -\frac{1}{\sqrt{1+\rho^2}} \sin\gamma z . e^{i\beta_s z} \tag{4.11}$$

and

$$\rho = \frac{\beta_x - \beta_y}{2(\xi-\alpha)} = \frac{\Delta\beta}{2(\xi-\alpha)} \tag{4.12}$$

$$\gamma = \tfrac{1}{2} \sqrt{\Delta\beta^2 + 4(\xi-\alpha)^2} \tag{4.13}$$

$$\beta_s = \tfrac{1}{2} (\beta_x + \beta_y) \tag{4.14}$$

Here, the asterisk denotes complex conjugation, and $\Delta\beta$ the intrinsic birefringence of the untwisted fibre in radians per metre. Equation (4.9) expresses the output vectors $A_x(z)$ and $A_y(z)$ in terms of the twisted co-ordinate system $x(z)$, $y(z)$.

The twisted stack of local retarders and rotators representing the fibre in Figure 4.4 may be universally described[32] by a retarder and rotator equivalent model.

To obtain the parameters $R(z)$, $\phi(z)$, $\Omega(z)$ in this model the matrix elements G and H in equation (4.9) are written as[42]:

$$G = \cos\frac{R}{2}\cos(\Omega-\xi z) + i\sin\frac{R}{2}\cos(2\phi+\Omega-\xi z) \quad (4.15)$$

$$H = \cos\frac{R}{2}\sin(\Omega-\xi z) + i\sin\frac{R}{2}\sin(2\phi+\Omega-\xi z) \quad (4.16)$$

Therefore, neglecting the common phase factor $e^{i\beta_s z}$ equations (4.10), (4.11), (4.15) and (4.16) gives[45]:

$$R(z) = 2\sin^{-1}\left[\frac{\rho}{\sqrt{1+\rho^2}}\sin\gamma z\right] \quad (4.17)$$

$$\Omega(z) = \xi z + \tan^{-1}\left[-\frac{t}{\sqrt{1+\rho^2}}\tan\gamma z\right] \pm n\pi \quad (4.18)$$

$$\phi(z) = \frac{\xi z - \Omega(z)}{2} \pm \frac{m\pi}{2} \quad (4.19)$$

where

$$\alpha = g'\xi \quad (4.20)$$

and $m, n = 0, 1, 2, \ldots$

In its untwisted state, the fibre has been assumed to exhibit only linear birefringence $\Delta\beta$ arising from core ellipticity and thermal stress. However, as seen in Section 4.3, many fibres may already be twisted during drawing and exhibit a degree of intrinsic circular rotation[48] α_o, which can be treated as a twist-independent term α_o in the parameter α (equation (4.20)).

The two modes A_x and A_y are in fact coupled by the twist[41] as is evident from the coupled-mode equations (4.5) and (4.6). The coupling coefficient for the plane-wave approximation used[35] is real and given by

$$(\xi - \alpha) = \xi(1 - g') = \xi(1 - \frac{g}{2}) \qquad (4.21)$$

where g is the proportionality constant for twist-induced optical activity[18] (i.e. twice the optical rotation defined by g'). A full analysis of twisted fibres, taking into account the waveguiding effect[36] has been shown[45] to give a coupling coefficient $(\xi - \alpha)$, provided $V > 1.5$ and the fibre ellipticity does not exceed 5%. The plane-wave approximation is valid in the (loss-less) twisted waveguide at high V-values provided the cladding surrounding the core in which part of the guided light propagates[19] also twists with the core[35].

4.6 Physical Interpretation of the Twist Analysis

The twist analysis of the previous section describes the polarisation properties of a length z of uniformly twisted birefringent fibre in terms of a discrete equivalent retarder R and principal-axis orientation ϕ, followed by a discrete optical-rotator element with rotation Ω.

In this section the interpretation of these results is described in detail.

4.6.1 Principal axes in a twisted fibre

In a twisted birefringent fibre, there are no *true* 'fast' and 'slow' axes. The properties of net retardation R and rotation Ω derived are complex functions of both $\Delta\beta$ and ξ. Neverthless, a "pseudo-fast axis" ϕ has been derived for the twisted fibre.

However, some care is required in the interpretation of ϕ, the principal axis orientation, since the retardation R given by equation (4.17) can be both positive and negative. The angle ϕ is interpreted as the azimuthal direction to which the retardation R is referred, being the fast axis when the retardation R is positive and the slow axis when R is negative. The actual 'fast' mode "flips" its direction 90° each time the retardation R given by equation (4.17) passes through zero.

4.6.2 Normal modes in twisted fibres

The coupled linearly-polarised modes A_x, A_y described by equation (4.9) are not the true modes of a twisted fibre, since they rotate with the twist angle and exchange energy as they propagate. However, in a twisted fibre, there always exists a pair of true normal modes[35] or polarisation-eigenstates[41] which propagate along the fibre without change or power coupling. In a loss-less twisted fibre these modes are obtained by diagonalising the coupled-mode equations (4.5) and (4.6) [35], to give:

$$U_{1,2} = \left[\hat{x}(z) - i(\rho \pm \sqrt{1+\rho^2})\, \hat{y}(z) \right] \exp\left\{ i(\beta_s \pm \gamma) z \right\} \qquad (4.22)$$

where ρ and γ are given by equations (4.12) and (4.13) respectively. The normal modes U_1 and U_2 are in general orthogonally elliptically-polarised and rotate with the twist; they do not intuitively relate to the measurable fibre properties R, Ω, ϕ. For this reason the above linearly-polarised coupled modes have been used to obtain R, Ω and ϕ.

Nevertheless, the normal modes are often extremely useful when considering polarisation mode-dispersion[45] or the effects of external influences on twisted fibres[24] (see Chapters Six and Five respectively). The existence of normal modes in twisted fibres has been

verified experimentally[49].

4.6.3 Evolution of polarisation along a twisted fibre

In addition to deriving the fibre birefringence properties R, Ω and ϕ, it is also useful to study the evolution of the actual polarisation state along a twisted fibre. The fibre output polarisation is a primary consideration while using a polarisation sensitive detection system[50].

As an example, we consider the case of a loss-less fibre with a linearly-polarised input at an azimuth θ_o to the x(o) axis. The ellipticity ζ and the angle ψ of the output polarisation ellipse relative to the x(o) axis are given by[35, 47]:

$$\psi = \xi z + \tfrac{1}{2}\tan^{-1}\left[\frac{\sin 2\theta_o \cos 2\gamma z - \frac{1}{\sqrt{1+\rho^2}}\cos 2\theta_o \sin 2\gamma z}{\frac{1}{1+\rho^2}\cos 2\theta_o(\cos 2\gamma z+\rho^2) + \frac{1}{\sqrt{1+\rho^2}}\sin 2\theta_o \sin 2\gamma z}\right] \pm n\pi \qquad (4.23)$$

$$\zeta = \tan\left(\tfrac{1}{2}\sin^{-1}\left\{\frac{2\rho}{\sqrt{1+\rho^2}}\sin\gamma z.(\sin 2\theta_o \cos\gamma z - \frac{1}{\sqrt{1+\rho^2}}\cos 2\theta_o \sin\gamma z)\right\}\right) \qquad (4.24)$$

Thus the state of polarisation (SOP) oscillates between left and right-elliptical polarisation along the fibre length z with a simultaneously rotating azimuth ψ. The parameters ψ and ζ may also be plotted on the Poincaré sphere to give an interesting visual description of the behaviour of a twisted fibre[18] and yield, in general, cycloidal trajectories on the sphere. The typical result (Figure 4.5) demonstrates the similarity and agreement between the present analysis and that of Ref 18.

From this figure and equation (4.24), two particular situations of interest arise.

(i) There is always a certain value of θ_o for which the output polarisation is linear i.e. $\zeta = 0$, for a given length z of fibre. Then θ_o must correspond to the principal axis ϕ for this length of fibre, that is, the "linear-output/linear-input" condition. Linearly-polarised output is only obtained when the input is polarised parallel to the principal axis i.e. $\theta_o = \phi$ and furthermore is rotated by an angle $\psi = \xi z$ (equation (4.23)) with respect to the input polarisation direction. In Figure 4.5, points where this condition is satisfied are marked 'A'.

(ii) At points periodically spaced along the fibre, given by $\sin\gamma z = 0$ the output is also linearly-polarised, for <u>all</u> input angles θ_o. This corresponds to zero total retardation of the fibre R(z) given by equation (4.17) where the fibre acts as a pure rotator. In the example shown in Figure 4.5 this condition is satisfied at points marked 'B'.

The Poincaré sphere illustrates immediately how the polarisation state evolves along the fibre, this evolution depending on the actual values of ξ, $\Delta\beta$ and θ_o.

Two special cases of twist are now considered to highlight the rather subtle but important characteristic differences between a spun fibre and a twisted fibre.

4.6.4 <u>Small twists</u>

The calculated retardance as a function of length z from equation (4.17) is shown in Figure 4.6, for various $\Delta\beta/\xi$ values[45]. In the limit of small twists relative to the intrinsic birefringence ($\xi << \Delta\beta$)

the principal-axis orientation $\phi(z) \simeq 0$ from equation (4.19), while the retardance $R(z) \simeq \Delta\beta z$ is linear with length, shown in Figure 4.6 for $\Delta\beta/\xi = 4000$. Also, the rotation $\Omega \simeq \xi z$ (equation (4.18)). In other words, little modification of the original birefringence $\Delta\beta$ occurs, the principal axis ϕ remaining approximately coincidental with the minor axis of the core ellipse - the 'fast' axis of the untwisted fibre[45].

Alternatively, the evolution of the polarisation state can be examined, the equations for the polarisation ellipse (4.23) and (4.24) reducing in this case of

$$\rho = \frac{\Delta\beta}{2(\xi-\alpha)} >> 1^{47} \text{ to}$$

$$\psi \simeq \xi z + \tfrac{1}{2} \tan^{-1} \left\{ \tan 2\theta_o \cos \Delta\beta z + O(1/\rho) \right\} \qquad (4.25)$$

and

$$\zeta \simeq \tan \left[\tfrac{1}{2} \sin^{-1} \{\sin 2\theta_o \sin \Delta\beta z\} \right] + O(1/\rho) \qquad (4.26)$$

These equations represent elliptical-polarisation in general resulting from the intrinsic phase retardation $\Delta\beta z$. Thus, launching linearly-polarised light parallel to the net retarder principal axis i.e. $\theta_o = \phi \simeq 0$ results in a polarisation state at the fibre output which is approximately linear along the entire fibre length but which rotates as if locked to the fibre twist[18, 35, 45]. On the Poincaré sphere then, the trajectory of the SOP oscillates with a very small amplitude as it slowly moves around the equator, following the twist.

It is evident that in the case of small twists the torsion-induced circular birefringence 2α has a negligible effect, being effectively swamped by the large intrinsic linear birefringence given by equation (4.17)[18].

In the limit of $\rho >> 1$, the normal modes given by equation (4.22) become linearly-polarised along the twisting x(z) and y(z) axes respectively[35]. Again it is immediately evident that linearly-polarised light launched into one of the modes *remains uncoupled* and therefore linearly-polarised, but nevertheless rotates in synchronism with the twist[47, 49, 51]. This is the basis of the linear "polarisation-maintaining" ability of high linear-birefringence fibres which are insensitive to moderate fibre twists[52] (see Section 5.2.1).

4.6.5 Large twists

In the limit of a large twist rate relative to the birefringence i.e. $\xi >> \Delta\beta$, the retardance predicted by equation (4.17) becomes

$$R(z) \simeq \frac{\Delta\beta}{(\xi-\alpha)} \sin\left[(\xi-\alpha)z\right] \qquad (4.27)$$

while the rotation Ω and principal axis ϕ predicted by equations (4.18) and (4.19) become

$$\Omega(z) \simeq \alpha z \qquad (4.28)$$

$$\phi(z) \simeq \frac{(\xi-\alpha)z}{2} \qquad (4.29)$$

In this case, the intrinsic fibre retardance is considerably reduced by the twist and the overall retardation R(z) becomes oscillatory about zero along the fibre length, as shown in Figure 4.6 for $\Delta\beta/\xi = 0.04$. Thus accounting for the rotation α, the results of the conceptual model presented in Section 4.4 are confirmed by the more detailed analysis.

Considering the output polarisation ellipse, equations (4.23) and (4.24) for the case $\rho << 1$ reduce to

$$\psi \simeq \theta_o + \alpha z \tag{4.30}$$

$$\zeta \simeq \frac{\Delta\beta}{2(\xi-\alpha)} \sin\left[(\xi-\alpha)\ z\right].\sin\left[2\theta_o - (\xi-\alpha)z\right] \tag{4.31}$$

These equations and also equations (4.27) to (4.29) show that by launching linearly-polarised light into the fibre *at any azimuth* θ_o results in a near-linear output rotated by an angle αz with respect to the input direction[45]. In fact the SOP along the length consists of an oscillation between very slightly left-and right-elliptically-polarised light rotating in orientation along the fibre. The trajectory on the Poincaré sphere runs rapidly round the equator due to the rotation $\Omega(z)$, with a small amplitude of oscillation which can be regarded as resulting from the small but finite retardation R(z) present.

Effectively a high twist rate rapidly couples the two modes A_x and A_y[41] thereby averaging the birefringence $\Delta\beta$ to zero, to leave the twist-induced rotation alone. In the limit of large twists i.e. $\rho << 1$, the normal modes (equation (4.22)) are oppositely circularly-polarised with a difference in propagation constants of $2(\xi-\alpha)$. Linearly-polarised light launched into the fibre will excite both these modes equally, resulting in linear output state but rotated through an angle αz, as above[49]. In contrast, circularly-polarised light will excite only one mode and travel unperturbed along the fibre. The fibre will "maintain" circular polarisation[18, 53] under external influences[54], provided that the fibre is sufficiently twisted to induce a large rotation (see sub-section 5.2.2).

4.7 Experimental Verification of the Twist Analysis

The evolution of polarisation along a twisted fibre described by equations (4.23) and (4.24) has already been shown to agree closely with Ulrich's method[18]. Similarly, the normal modes agree with those calculated[49] by Sakai and Kimura[37] and confirmed experimentally by these authors[49, 55]. Nevertheless the predicted birefringence properties R, Ω and ϕ must be verified experimentally in twisted fibres. Measurements were made at 633nm with the fibres hanging vertically, as described in the previous Chapter, to ensure a uniform applied twist.

The first experiment was performed on a conventional low-birefringence fibre (GSB4 in Table 4.1). The birefringence of $\sim 8^{o}$/m in the sample selected, enabled investigation of the interesting limit of large twists (Section 4.6.5), while avoiding mechanical limitations on maximum twist angle. The results for the optical rotation Ω and principal axis position ϕ are shown in Figure 4.7(a) and Figure 4.7(b) respectively, for ratios of twist to birefringence $\xi/\Delta\beta$ up to ~90. As predicted by equation (4.28), for the case of large twists, the rotation Ω is linear with twist rate ξ, a left-handed rotation being induced by a right-handed twist[18, 31]. The slope of the line gives $g' = 0.073$, a value in excellent agreement with the results of other investigations[56, 31, 18], and theoretical calculations[18, 37]. This particular fibre is evidently already twisted since there is a rotation α_o present at zero twist which, as predicted in Section 4.5, merely acts as a fixed offset of the twist-induced rotation αz.

The principal axis ϕ is also linear with twist angle as predicted by equation (4.29) showing considerable departures from the untwisted position which is assumed to lie along one of the core elliptic axes. Ignoring α_o it is found that

$2\phi + \Omega = \xi z \pm m\pi$ as predicted by equation (4.19).

In this experiment, the retardation (not shown) remained below $\pm 10^{o}/m$ for all twist rates and could not therefore be measured accurately. Moreover at points where the retardation was particularly small, corresponding to $(2n+1)\frac{\pi}{2}$ of total twist, the principal axis ϕ was subject to considerable error (see Figure 4.7 (b)).

Because of the difficulty of measuring such low retardations accurately, a second experiment was performed on a fibre (VD214) with a silica core and B_2O_3/SiO_2 cladding, a linear birefringence of $\sim 123^{o}/m$ and very small rotation[2, 23]. In view of the higher birefringence, a correction was made using Jones Calculus to allow for the untwisted birefringent fibre sections at each end of the twisted test fibre.

The results for retardance R are shown in Figure 4.8(a). Note the rapid reduction in overall birefringence that can be obtained as the twist rate is increased up to a ratio $\xi/\Delta\beta \simeq 5$. Also shown is the theoretical prediction of equation (4.17) which gives excellent agreement in spite of a slight difference in periodicity, thought to arise from an uncertainty in the values of $\Delta\beta$ and z in the sample of fibre used.

The rotation Ω is shown in Figure 4.8(b), together with the curve predicted by equation (4.18). It can be seen that at large twist rates the rotation asympotically approaches proportionality to the twist with a slope of $\sim$ 0.073, i.e. g', as predicted by equation (4.28) for large twist rates $\xi >> \Delta\beta$ (see Section 4.6.5). Similarly, the principal axis position ϕ, shown in figure 4.8(c) shows close agreement with the theoretical prediction of equation (4.19).

These experiments thus provide clear verification of the analysis of Section 4.5.

4.8 Spun Fibres

4.8.1 Introduction

The above theoretical analysis has already shown that by tightly twisting a fibre the intrinsic birefringence can be reduced dramatically. Such a fibre is thus suitable for use in the current monitor device[31], where ultra-low linear birefringence is required[4]. The maximum applied twist rate is however limited by fibre fatigue failure and moreover, results in a large, temperature-sensitive[31, 56] torsion-induced circular birefringence $g\xi z$. In Section 4.4 it was noted that 'spun' fibres exhibit the same advantages of low birefringence with the additional benefit of negligible circular birefringence.

In this section, the properties, fabrication and other features of 'spun' fibres are examined in detail.

4.8.2 Birefringence properties of spun fibres

As previously described, drawing a fibre while simultaneously rotating the preform produces a simple precession or twist of the axes of asymmetry in the fibre, which is subsequently frozen-in to the fibre. It is assumed that the actual intrinsic birefringence $\Delta\beta$ arising from the normal core non-circularity and thermal stress effects, remains unaffected. The preceding analysis of twisted fibres may therefore be applied to a spun fibre, with the proviso that since no appreciable torsional stress is supported in the viscous fibre preform hot-zone at the drawing and spinning temperature ($\alpha = 0$).

As with twisted fibres, a high spin rate $\xi'(\xi' >> \Delta\beta)$ will provide the dramatic reduction in intrinsic birefringence necessary for the production of ultra-low birefringence fibres.

Using equations (4.27) to (4.29), the polarisation characteristics of a tightly spun fibre are given by

$$R(z) = \frac{\Delta\beta}{\xi'} \sin(\xi' z) \tag{4.32}$$

$$\Omega(z) = -\frac{\Delta\beta^2}{8\xi'} z \simeq 0 \tag{4.33}$$

$$\phi(z) = \frac{\xi' z}{2} \tag{4.34}$$

A spun fibre thus has very small amounts of retardation and rotation. In the limit of very large spin, the fibre behaves as a perfectly isotropic waveguide and can transmit any polarisation state without change, provided no external influences exist. Thus on the Poincaré sphere, for any input polarisation state, the general cycloidal trajectory derived in sub-section 4.6.3 reduces to a spot on the sphere. Consequently, the waveguide asymmetries caused by ellipticity and thermal stress can be averaged to produce near perfect overall symmetry by rapidly spinning the fibre about its axis. Naturally, at finite spin rates, a small amount of polarisation anisotropy remains and the evolution of the polarisation state for linearly-polarised light input is, from equations (4.23) and (4.24)

$$\psi \simeq \Theta_o - \frac{\Delta\beta^2}{8\xi'} z \tag{4.35}$$

$$\zeta = \frac{\Delta\beta}{2\xi'} \sin \xi' z . \sin\left[2\Theta_o - \xi' z\right] \tag{4.36}$$

Thus the trajectory on the Poincaré sphere is again an oscillation between very slightly left- and right-elliptically polarised light, which rotates slowly around the sphere. Here only a very small second-order rotation $\Omega(z)$ (equation (4.33)) of the polarisation (equation (4.35)) exists, in direct contrast to the case

of a fibre twisted tightly after drawing which exhibits a substantial rotation (equation (4.28)).

In a tightly spun fibre the normal modes (equation (4.22)) are oppositely circularly-polarised, rotating with the twist, with a difference in propagation constants of $\sim 2\xi'$. Linearly-polarised incident light excites both modes equally giving a linear output, but with very small net rotation. As in a highly-twisted fibre, circularly-polarised light travels without change alone the fibre. However since there is only a second-order circular birefringence, a spun fibre possesses little ability to maintain circular-polarisation. A small modulation of the spin rate ξ' will result from any twist arising from the drawing drum (Section 4.3). However since $\xi' >> \Delta\beta$, this modulation will not introduce any rotation in contrast to conventional fibres. The adoption of a fibre pulling capstan to reduce these effects, described in Section 4.3, would seem to be unnecessary for spun fibre manufacture.

As predicted in Section 4.4, so long as $\xi' >> \Delta\beta$, the averaging mechanism of spinning will guarantee ultra-low overall birefringence in every spun fibre manufactured. In practice, by ensuring that the spin rate always far exceeds the likely range of $\Delta\beta$ values expected in the unspun ('conventional') fibres, the actual $\Delta\beta$ value is of no concern. The resultant tolerance towards $\Delta\beta$ in a tightly spun fibre leads one to expect a very high degree of reproducibility for ultra-low birefringence in 'spun' fibres. Furthermore, low birefringence may be attained along an entire length of fibre, regardless of any variations in $\Delta\beta$ arising from preform or fibre geometry variations along the length.

Peak retardations below measurable levels (i.e. less than 10^{-2} radians) may be obtained in a spun fibre if the ratio of spin rate ξ' to intrinsic birefringence $\Delta\beta$ is greater than one hundred. It is relatively easy to produce conventional fibres with beat lengths of 1m

or more[2]. Satisfying the above guideline thus requires a 1cm spin pitch, which may be obtained in practice without difficulty. A 1m-beat length fibre spun with a pitch of 1cm would have a residual rotation Ω of $\sim 7.8 \times 10^{-3}$ rad/m or one complete turn in ~800m. In the case of ultra-low birefringence fibres of the type shown in Table 4.1, a 5-10 cm pitch is sufficient to produce immeasurably small overall retardations.

Any spun fibre meeting the criterion $\xi'/\Delta\beta > 100$ is ideally suitable for use in the Faraday ammeter device[6, 57].

4.8.3 Fabrication of spun fibres

The actual spinning procedure was mainly developed[17, 45, 58] at Southampton University and is described briefly in this Section.

The preform, typically made by the CVD process, is attached to the shaft of a speed-controlled DC motor, which is gimbal-mounted at the top of the fibre drawing tower in place of the usual preform chuck (Figure 4.9). The lower end of the preform is accurately centred inside the pulling furnace using a spring-loaded iris diaphragm which also serves as a furnace gas-seal. Normal fibre drawing is commenced and once stable conditions have been established, the spinning motor is run up to the required speed. Rotation rates of up to 2000 rpm have been achieved with accurately centred, straight preforms, which at a typical pulling speed of $\sim 0.5\ ms^{-1}$ gives a spin pitch of ~1.5cm in the fibre. Typical motor speeds are in the range of 600 rpm, however. The primary-coating process and automatic diameter control system[28] are used in the normal fashion.

If the preform is not straight or accurately centred prior to spinning, centrifugal forces act to cause the viscous glass in the furnace hot-zone to "throw-out" still

further away from the centre to eventually touch the walls of the graphite resistance-furnace. An additional problem is that the eccentric drawing region at the end of preform sets the drawn fibre into vibration. The rapid fibre movement within the measurement zone of the scanning-laser fibre diameter-monitor can be sufficient to cause loss of fibre diameter control. Hot zone "throw out" can however be substantially reduced by using a lower furnace temperature ($\geq 1800^{o}C$) to increase the fibre drawing tension, which also gives improved diameter control. It then becomes possible to spin unstraight preforms to produce fibres with sustained ~1cm spin pitches and controlled diameters ($\pm$ 0.3μm) in lengths of several kilometers.

Consideration of the viscosity of the fluid fibre hot-zone[29] shows that there is almost complete relaxation by viscous flow of elastic torsion in the drawn fibre during spinning, even at the unusually low pulling temperatures required for good diameter control. This results in negligible applied twist in the fibre wound on the drum as verified by paying out the fibre from the drum and allowing the end to hang freely, whereupon no untwisting of the fibre was observed[24, 59]. The preform spin rate w is thus taken-up almost entirely by the viscous hot-zone to give a fibre with a spin pitch s given by

$$s = \frac{v}{w} = \frac{2\pi}{\xi'} \qquad (4.37)$$

where v = pulling speed in ms^{-1}. The spinning motor speed w is linked to the fibre drawing speed v so that despite variations in drawing speed caused by the diameter control, a constant fibre spin pitch s is obtained.

An alternative method of producing a fibre spin has recently been proposed[60] using a rotating fibre drawing drum as opposed to the preform. The effect is the same, however and avoids the problems associated with the spinning hot glass, but only at the expense of considerably

more complex drawing and fibre coating apparatus.

The spinning process has been fully developed and it is now routinely possible to manufacture spun fibres in large quantities.

4.8.4 Experimental properties of spun fibres

Fibre preforms similar to those shown in Table 4.1 are normally used to manufacture spun fibres. To demonstrate the effect of fibre spinning, both spun and unspun sections of fibre were each drawn from various preforms of this type. The unspun sections, used as controls, were obtained by stopping the spinning motor and taking a fibre sample from the fibre section immediately adjacent to the spun section of fibre.

Table 4.2 shows the properties measured using a polariser and analyser in various spun and unspun fibres, showing the marked effect of fibre spinning on the birefringence properties. In all the fibres, spinning gives a reduction in linear birefringence approaching two orders of magnitude. In reality, the spun fibre birefringence was typically at or below measurement limits so that the actual reduction may be much larger in many cases. Spun fibres also consistently exhibit negligible levels of rotation as predicted in sub-section 4.8.2.

Evidently from Table 4.2, the theoretically predicted spun fibre birefringence properties are verified in practical spun fibres. The consistently low retardation and rotation confirms the prediction of very high reproducibility of ultra-low polarisation anisotropy in spun fibres.

4.8.5 Local anisotropy in spun fibres

It has been assumed throughout the discussion of spun fibres that spinning produces little modification of the local anisotropy $\Delta\beta$ within the fibre itself but only a simple frozen-in fibre twist which averages the anisotropy to restore a near-perfect symmetry to the waveguide structure. If this were true, a spin fibre, although exhibiting low overall retardation, would still have high birefringence on a local scale. The *consistently* low birefringence seen in practical spun fibres leaves little doubt of the validity of the above assumption. Nevertheless, it is conceivable that spinning could also produce ultra-low birefringence by actually smoothing the elliptical cross-section to reduce the local anisotropy itself in the revolving molten preform hot-zone. This would give rise to a low birefringence not only on a macroscopic scale but also on a local scale within the fibre. Moreover, such an effect should also be expected to be highly variable from fibre to fibre.

If the spin averaging mechanism does occur, twisting a spun fibre after drawing in a direction as to oppose the spin, should reduce the averaging effect[59, 61]. This would cause the original anisotropy to fully reappear at a point where the applied twist exactly negates the spin. The analysis presented in Section 4.5 shows that a spun fibre should behave as a twisted fibre but with zero torsion-induced rotation α. An applied twist ξ acts as an additional twist but in contrast, has an associated rotation $\alpha = g'\xi$. Using the twist analysis of Section 4.5, the retardation and rotation of a spun fibre with a spin rate ξ' (taken to be negative) and an applied twist ξ are given by

$$R(z) = 2 \sin^{-1}\left[\frac{\rho_1}{(1+\rho_1^2)^{\frac{1}{2}}} \sin \gamma_1 z \right] \qquad (4.38)$$

$$\Omega(z) = (\xi+\xi')z + \tan^{-1}\left[\frac{-1}{(1+\rho_1^2)^{\frac{1}{2}}}\ \tan\ \gamma_1 z\right] \qquad (4.39)$$

where

$$\rho_1 = \frac{\Delta\beta}{2\left[\xi(1-g') + \xi'\right]} \qquad (4.40)$$

$$\gamma_1 = \tfrac{1}{2}\sqrt{\Delta\beta^2 + 4\left[\xi(1-g') + \xi'\right]^2} \qquad (4.41)$$

and $\Delta\beta$ is the intrinsic birefringence in the unspun fibre.

As the applied twist opposes the spin the net precession of the axes is progressively reduced and the intrinsic local birefringence consequently becomes more apparent. At a twist rate ξ_c given by

$$\xi_c\ (1-g') = -\xi' \qquad (4.42)$$

the retardation R given by equation (4.38) rises and peaks at a value R = $\Delta\beta z$, while the rotation $\Omega(z)$ from equation (4.40) and (4.42) is given by

$$\Omega(z) = (\xi_c+\xi')z = g'\xi_c\ z \qquad (4.43)$$

At this point, the applied twist ξ_c is such that the rotation is equal to the remaining net twist $(\xi_c+\xi')z$ in the fibre. The plane of polarisation of the light rotates in synchronism with the twist so that light polarised parallel to the local axes of the intrinsic birefringence at the input remains oriented parallel to these rotating axes along the fibre length. Effectively all the local axes along the fibre are "aligned" to the linearly-polarised light and the fibre exhibits its full birefringence $\Delta\beta$, in addition to a net rotation $g'\xi_c z$.

Increasing the applied twist ξ beyond ξ_c results in a return to the averaging effect of the net positive applied twist, to give negligible levels of retardation. Note that if ξ acts in the same sense as the spin (i.e. ξ is negative) the retardation remains negligibly small for all applied twist rates.

An experiment was performed to verify these predictions using a spun fibre (VD348) at 633nm of length 1.262m. The retardance was measured using the polariser-and-analyser technique described in Chapter Three, as a function of applied twist. Figure 4.10 shows the experimental result, showing, as predicted above, a peak in retardation of $14.42^{o}/m$, corresponding to the local birefringence $\Delta\beta$ in the spun fibre. This compares well with the value $\Delta\beta = 32^{o}/m$ measured in an unspun section 100m down the fibre and is within the normally-expected variation of intrinsic birefringence along the fibre length. From the applied twist necessary to produce this peak retardation the fibre spin pitch $s = 2\pi/\xi'$ was found, using $g' = 0.073$[45] (Section 4.7) in equation (4.42) to be 5.24cm. This value agrees with the nominal value of 5.0cm shown in Table 4.2 within the calibration error of the preform spinning motor speed-control. The close agreement verifies that almost complete relaxation of torsion occurs in the cold fibre by means of viscous flow in the fibre hot zone, as discussed in sub-section 4.8.3. The determination of the spin pitch in a spun fibre by this means requires prior knowledge of the nominal pitch since the range of twist over which the retardation reappears is very narrow.

Using the values $\Delta\beta = 14.42^{o}/m$ and $s = 5.24$cm, the theoretically predicted retardation given by equation (4.38) also shown in Figure 4.10, showing the excellent agreement with the experimental results. The reappearance of the birefringence with applied twist is an important feature of spun fibres which could be exploited in a fibre angle sensor. It also shows conclusively that a

spun fibre retains a local anisotropy approximately equal to the intrinsic fibre birefringence, with apparently little modification of the fibre cross-sectional geometry. Further confirmation of this fact is provided by the cross-sections of both the spun and unspun sections of a highly-elliptical fibre[62] shown in Figure 4.11(a) and 4.11(b) respectively, which are evidently almost identical. Figure 4.12 compares the transverse-sections of these fibres to clearly show the elliptical core and cladding spiralling along the spun fibre. The unspun fibre had a high birefringence due to its elliptical cross-section with a beat length of 19mm. However, in the spun fibre, since the spin pitch of ~1.2mm is far shorter than the beat length i.e. $\xi' >> \Delta\beta$ there was, as expected, negligible birefringence. This illustrates how even a high birefringence fibre may be spun to produce low birefringence, using a sufficiently short spin pitch obtained in practice at greatly-reduced fibre drawing speeds.

From the above experiments it is clear that the repeatable reduction in birefringence obtained in a spun fibre can be attributed largely to the averaging effect of the precession of the fibre axes of symmetry and not to changes in fibre cross-sectional geometry or smoothing of anisotropic stress.

4.8.6 Other features

Apart from their ultra-low birefringence, spun fibres have several other features pertinent to their potential applications.

(i) Temperature and wavelength sensitivity

As a consequence of the intrinsic overall geometric symmetry of a tightly spun fibre, the ellipticity and thermal stress effects contributing to the intrinsic local fibre anisotropy $\Delta\beta$ are of little consequence to the overall fibre properties. Thus spun fibres are insensitive to variations

in temperature which affects only the value of $\Delta\beta$. Evidence of this was provided by varying the temperature of a length of spun fibre using the tube furnace described in Chapter Three; no change in the fibre birefringence was observed.

The birefringence of a spun fibre will remain low despite variations in $\Delta\beta$ arising from a change in source wavelength; thus spun fibres have negligibly small polarisation mode-dispersion, as with all low-birefringence fibres, as will be shown in Chapter Six.

(ii) Fibre attenuation

Figure 4.13 shows a typical spectral attenuation curve for a fibre in both spun and unspun conditions. This fibre (VD386) was similar to the conventional low-birefringence fibres of Table 4.1, having a B_2O_3/SiO_2 cladding/ GeO_2/SiO_2 core structure, optimised for low birefringence $\Delta\beta$ rather than for low attenuation. Nevertheless, within experimental error (~0.5 - 1dB/km), negligible increase in loss over a wide spectral range is observed in the spun fibre over that of the unspun fibre. This was confirmed by OTDR attenuation measurements[63]. Similar results may be obtained in all spun fibres, even with fibre spin pitches as short as 1cm. In as much as spinning places little constraints on any other parts of the fibre fabrication process and furthermore guarantees ultra-low birefringence with virtually any value of $\Delta\beta$, there is effectively enormous flexibility in the choice of preform design for an ultra-low birefringence spun fibre. Essentially, ultra-low birefringence could be obtained equally well using a preform optimised for loss or one optimised for a low $\Delta\beta$ value. There is every reason to expect that simultaneously ultra-low attenuation and ultra-low birefringence

spun fibres will be made in the future.

(iii) Chromatic dispersion

It is possible to compensate the material chromatic dispersion in a single-mode fibre using the waveguide and profile dispersion of the propagating modes in a fibre, to give zero first-order chromatic dispersion at any given wavelength longer than ~1.3μm [64]. Fibre polarisation mode-dispersion then becomes the major limitation of fibre bandwidth[15]. At longer wavelengths such as 1.55μm where a silica-based fibre has its lowest loss, a fibre numerical aperture (NA) greater than 0.15 is needed for chromatic dispersion optimisation, while the fibre core diameter must be very closely controlled to within 0.1μm [64]. In conventional low-birefringence fibres, the high NA required for chromatic dispersion optimisation would pose a severe problem for low-birefringence reproducibility. If as well as zero dispersion, joint loss, bending loss and cabling loss optimisation[64] is required, the additional attainment of ultra-low birefringence and polarisation mode-dispersion appears to be a remote possibility in a conventional fibre. However spinning could be used to obtain the required ultra-low birefringence and polarisation mode-dispersion, independently of and supplementary to, the normal preform design and fibre diameter control necessary for loss and chromatic dispersion optimisation. The exciting possibility of potentially ultra-low loss, ultra-low birefringence, ultra-high bandwidth fibres with low joint, bending and cabling losses for advanced telecommunications immediately springs to mind. Such a fibre would naturally have a great market potential for submarine cable systems and coherent (heterodyne) fibre systems[65].

(iv) Environmental sensitivity

We will show in Chapter Five that, as with any low-birefringence fibre, a spun fibre is extremely sensitive to environmental effects such as bending, applied stress or twists. These effects upset the spun fibre near-perfect circular symmetry on a local scale to induce the same birefringence or rotation effects as in conventional low-birefringence fibres.

Although a spun fibre is almost perfectly isotropic and can therefore transmit any polarisation state without change, it cannot maintain that state under conditions of external effects since power transfer readily occurs between the normal modes. Thus a spun fibre has little polarisation-maintenance ability, but it is of course highly suited to various fibre sensors such as the Faraday current monitor[3, 57]. The negligible intrinsic birefringence in a spun fibre is exceedingly useful in the design and stable operation of fibre sensors, filters and isolators which use controlled birefringence fibre elements[8-14].

4.9 Summary

In this Chapter, the two types of low-birefringence fibre have been discussed. The production yield of 'conventional' low-birefringence fibres is extremely low because the sources of intrinsic fibre birefringence, namely anisotropic thermal stress and core ellipticity, are difficult to control during the CVD fibre fabrication process. In 'spun' fibres, this lack of control is of no consequence because spinning (performed by simply rotating the preform during fibre drawing) imparts a frozen-in twist to the fibre guaranteeing that any intrinsic polarisation anisotropy arising from stress or ellipticity, whatever its value, is averaged to give near-perfect waveguide symmetry.

The extremely high reproducibility of ultra-low birefringence expected has been demonstrated in practical spun fibres.

A new analysis of twisted and spun fibres has been developed relating directly to the properties of net retardation and rotation usually measured in a fibre and furthermore highlighting the important differences between twisted fibres and spun fibres. A highly-twisted fibre can exhibit low linear-birefringence only at the expense of a substantial twist-induced circular-birefringence. In contrast, a spun fibre exhibits negligible linear and circular birefringence provided the spin rate far exceeds the intrinsic birefringence in the fibre arising from stress or ellipticity. Spinning has been verified as being a process of averaging the intrinsic anisotropy with negligible modification of the anisotropy itself on a local scale, by applying a reverse twist to a spun fibre, whereupon the full retardation of the corresponding unspun fibre reappeared.

The invention of fibre spinning means that ultra-low birefringence fibres can now be produced on a routine basis in the laboratory. Spinning provides ultra-low birefringence in any type of fibre, so permits great flexibility of preform design, which could be set for optimal loss and bandwidth characteristics, for example. It is not difficult to envisage that low-loss, high-bandwidth spun fibres exhibiting negligible birefringence or polarisation mode-dispersion will find widespread application in future advanced fibre telecommunications systems. For the present however, spun fibres, with their ultra-low birefringence and high environmental sensitivity, are being widely used in fibre sensors and other optical devices.

4.10 References

1. Schneider, H., Harms, H., Papp, A., and Aulich, H.: "Low-birefringence single-mode optical fibres: preparation and polarisation characteristics", Appl. Optics, 17, 1978, pp. 3035-3036.

2. Norman, S. R., Payne, D. N., Adams, M. J., and Smith, A. M.: "Fabrication of single-mode fibres exhibiting extremely low polarisation birefringence", Electron. Lett., 15, 1979, pp. 309-311.

3. Harms, H., Papp, A., and Kempter, K.: "Magneto-optical properties of index-gradient optical fibres", Appl. Optics, 15, 1976, pp. 799-801.

4. Smith, A. M.: "Polarisation and magneto-optic properties of single-mode optical fibre", Appl. Optics, 17, 1978, pp. 52-56.

5. Papp, A., and Harms, H.: "Magneto-optical current transformer. Parts I-III", Appl. Optics, 19, 1980, pp. 3729-3745.

6. Smith, A. M.: "Optical fibres for current measurement applications", Opt. Laser Tech., February 1980, pp. 25-29.

7. Kaminov, I. P.: "Polarisation in optical fibres", IEEE J. of Quantum Electron., QE-17, 1981, pp. 15-22.

8. Lefevre, H. C.: "Single-mode fibre fractional wave devices and polarisation controllers", Electron. Lett., 16, 1980, pp. 778-780.

9. Johnson, M.: "Single-mode fibre birefringent filters", Optics Lett., 5, 1980, pp. 142-144.

10. Yen, Y., and Ulrich, R.: "Birefringent optical filters in single-mode fibre", Optics Lett., 6, 1981, pp. 278-280.

11. Stanford University, unpublished work.

12. Day, G. W., Payne, D. N., Barlow, A. J., and Ramskov Hansen, J. J.: "Faraday rotation in coiled, monomode optical fibres: isolators, filters and magnetic sensors", Optics Lett., 7, 1982, pp. 238-240.

13. Rashleigh, S. C.: "Acoustic sensing with a single-coiled monomode fibre", Optics Lett., 5, 1980, pp. 392-394.

14. Rashleigh, S. C.: "Magnetic-field sensing with a single-mode fibre", Optics Lett., 6, 1981, pp. 19-21.

15. Marcuse, D., and Lin, C.: "Low dispersion single-mode fibre transmission - the question of practical versus theoretical maximum transmission bandwidth", IEEE J. of Quantum Electron., QE-17, 1981, pp. 869-878.

16. Adams, M. J., Payne, D. N., and Ragdale, C. M.: "Birefringence in optical fibres with elliptical cross section", Electron. Lett., 15, 1979, pp. 298-299.

17. Barlow, A. J., Payne, D. N., Hadley, M. R., and Mansfield, R. J.: "Production of single-mode fibres with negligible intrinsic birefringence and polarisation mode-dispersion", Electron. Lett., 17, 1981, pp. 725-726.

18. Ulrich, R., and Simon, A.: "Polarisation optics of twisted single-mode fibres", Appl. Optics, 18, 1979, pp. 2241-2251.

19. Adams, M. J.: "An Introduction to Optical Waveguides", Wiley, 1981.

20. Imada, K., Sugawara, Y., Kobayashi, T., Yamada, T., and Tokuda, M.: "Cabling of ultra-low loss optical fibres", Proc. 4th European Conference on Optical Communication, 1978, Genoa, Italy.

21. Miller, S. E., and Chynoweth, A. G.: "Optical Fibre Telecommunications", Academic Press, 1979.

22. Calligaro, R. B.: Unpublished work.

23. Norman, S. R.: Ph.D. Thesis, University of Southampton, 1981, Ch. 2.

24. Payne, D. N., Barlow, A. J., and Ramskov Hansen, J.J.: "Development of low- and high-birefringence optical fibres", IEEE J. Quantum Electron., QE-18, 1982, pp. 477-488.

25. Shibata, N., Jinguji, K., Kawachi, M., and Edahiro, T.: "Non-destructive structure measurement of optical fibre preforms with photo-elastic effect", Jap. J. Appl. Phys.,18, 1979, pp. 1267-1273.

26. Sasaki, I., Payne, D. N., and Adams, M. J.: "Measurement of refractive-index profiles in optical-fibre preforms by spatial filtering technique", Electron. Lett., 16, 1980, pp. 219-221.

27. Akamatsu, T., Okamura, K., and Ueda, Y.: "Fabrication of graded index fibres without an index dip by chemical vapour deposition method", Appl. Phys. Lett., 31, 1977, pp. 515-517.

28. Hadley, M. R., Payne, D. N., and Mansfield, R. J.: "Identification of sources of diameter fluctuations in smooth optical fibres by analysis of their spatial power spectrum", paper presented at Sixth European Conference on Optical Communication, 1980, York, UK.

29. Mansfield, R. J.: University of Southampton, Private communication.

30. Timoshenko, S. P., and Goodier, J. N.: "Theory of Elasticity", McGraw-Hill, 1970.

31. Rashleigh, S. C., and Ulrich, R.: "Magneto-optic current sensing with birefringent fibres", Appl. Phys. Lett., 34, 1979, pp. 768-770.

32. Jones, R. C.: "A new calculus for the treatment of optical systems" (Parts I-VII), J. Opt. Soc. Am., 31, 1941, pp. 488-503.

33. Stokes, A. R.: "The Theory of the optical properties of inhomogeneous materials", Spon Press.

34. Azzam, R. M. A., and Bashara, N. M.: "Simplified approach to the propagation of polarised light in anisotropic media - application to liquid crystals", J. Opt. Soc. Am., 62, 1972, pp. 1252-1257.

35. McIntyre, P., and Snyder, A. W.: "Light propagation in twisted anisotropic media - application to photo-receptors", J. Opt. Soc. Am., 68, 1978, pp. 149-157.

36. Fujii, Y., and Sano, K.: "Polarisation coupling in twisted elliptical optical fibre", Appl. Optics, 19, 1980, pp. 2602-2605.

37. Sakai, J., and Kimura, T.: "Birefringence and polarisation characteristics of single-mode optical fibres under elastic deformations", IEEE J. of Quantum Electron., QE-17, 1981, pp. 1041-1051.

38. Fujii, Y.: unpublished work.

39. Namihira, Y., Kudo, M., and Mushiake, Y.: "Polarisation characteristics of twisted single mode optical fibre", Trans. IECE Jap., J64-C, 1981, pp. 180-187.

40. Kusano, K., and Nishida, S.; "Polarisation properties of optical waves in a twisted elliptical fibre", Trans. IECE. Jap. J64-C, 1981, pp. 173-179.

41. Monerie, M., and Jeunhomme, L.: "Polarisation mode coupling in long single-mode fibres", Opt. Quantum Elect., 12, 1980, pp. 449-461.

42. Kapron, F. P., Borrelli, N. F., and Keck, D. B.: "Birefringence in dielectric optical waveguides", IEEE J. of Quantum Electron., QE-8, 1972, pp. 222-225.

43. Matsumura, H.: "Birefringence and optical activity in phosphosilicate glass fibres", University of Southampton, internal report (unpublished) November 1976.

44. Papp, A., and Harms, H.: "Polarisation optics of liquid-core optical fibres", Appl. Opt., 16, 1977, pp. 1316-1319.

45. Barlow, A. J., Ramskov Hansen, J. J., and Payne, D.N.: "Birefringence and polarisation mode-dispersion in spun single-mode fibres", Appl. Optics, 20, 1981, pp. 2962-2968.

46. Hecht, E., and Zajac, A.: "Optics", Addison-Wesley, 1974.

47. McIntyre, P.: Ph.D. Thesis,, Australian National University, Canberra, 1976.

48. Gambling, W. A., Payne, D. N., and Matsumura, H.: "Birefringence and optical activity in single-mode fibres", paper presented at Topical Meeting on Optical Fibre Transmission II, Williamsburg, February 22-24 1977.

49. Sakai, J., Machida, S., and Kimura, T.: "Existence of eigen-polarisation modes in anisotropic single-mode optical fibres", Optics Lett., 6, 1981, pp. 496-498.

50. Ulrich, R.: "Polarisation stabilisation on single-mode fibre", Appl. Phys. Lett., 35, 1974, pp. 840-842.

51. Papp, A., and Harms, H.: "Polarisation optics of index gradient optical waveguide fibres", Appl. Optics, 14, 1975, pp. 2406-2411.

52. Stolen, R. H., Ramaswamy, V., Kaiser, P., and Pleibel, W.: "Linear polarisation in birefringent single-mode fibres", Appl. Phys. Lett., 33, 1978, pp. 644-701.

53. Jeunhomme, L., and Monerie, M.: "Polarisation-maintaining single-mode fibre cable design", Electron. Lett., 16, 1980, pp. 921-922.

54. Barlow, A. J., and Payne, D. N.: "Polarisation maintenance in circularly birefringent fibres", Electron. Lett., 17, 1981, pp. 388-389.

55. Machida, S., Sakai, J., and Kimura, T.: "Polarisation conservation in single-mode fibres", Electron. Lett., 17, 1981, pp. 494-495.

56. Smith, A. M.: "Birefringence induced by bends and twists in single-mode optical fibre", Appl. Optics, 19, 1980, pp. 2606-2611.

57. Smith, A. M.: "Polarisation properties of a very low birefringence optical fibre produced by a novel technique", CERL, Internal report, 1980.

58. Ashkin, A., Dziedic, J. M., and Stolen, R. H.: "Outer diameter measurement of low birefringence fibres by a new resonant backscatter technique", Appl. Optics, 20, 1981, pp. 2299-2303.

59. Barlow, A. J., Ramskov Hansen, J. J., and Payne, D.N.: "Anisotropy in spun single-mode fibres", Electron. Lett., 18, 1982, pp. 200-202.

60. Arditty, H. F.: Paper presented at International Conference on Fibre Optic Rotation Sensors and Related Technologies, M.I.T., USA, November, 1981.

61. Barlow, A. J., Payne, D. N., Hadley, M. R., and Mansfield, R. J.: "Production of single-mode fibres with negligible intrinsic birefringence and polarisation mode-dispersion", paper presented at Seventh European Conference on Optical Communication, Copenhagen, Denmark, 1981.

62. Birch, R. D.; Private Communication.

63. Hartog, A. H.: University of Southampton, Private Communication.

64. Ragdale, C. M.: Ph.D. Thesis, University of Southampton, 1982.

65. Barlow, A. J., Payne, D. N., Varnham, M. P., and Birch, R. D.: "Polarisation characteristics of fibres for coherent detection systems", paper presented at colloquium on "Coherence in Optical Fibre Systems" IEE, London, 25 May, 1982.

Fibre No.	Δ'	N.A.	Core Ellipticity e	Retardance @ 633nm	Rotation @ 633nm	Beat Length @ 633nm	Bire-fringence B	Predicted Ellipticity Bire-fringence B_G
GSB2	0.0034	0.082	<1%	2.6 °/m	-	140m	4.57×10^{-9}	7.05×10^{-9}
GSB3	0.0046	0.14	3%	148 °/m	3.3 °/m	2.4m	2.60×10^{-7}	3.79×10^{-7}
GSB4	0.0063	0.164	2.8%	3.5-55°/m	1-10 °/m	6.5-105m	6×10^{-9} - -9.7×10^{-8}	6.70×10^{-7}
GSB5	0.0032	0.116	9%	165 °/m	6 °/m	2.2m	2.9×10^{-7}	5.32×10^{-7}
GSB6	0.0017	0.085	10%	15 °/m	13 °/m	24m	2.64×10^{-8}	1.74×10^{-7}
GSB7	0.0031	0.114	260%	>2000 °/m	4 °/m	0.18m	3.52×10^{-6}	5.95×10^{-6}

Table 4.1 Measured properties of low-birefringence "conventional" fibres. Also shown isthe core-ellipticity birefringence B_G predicted from ref. 5.

FIBRE NUMBER		UNSPUN FIBRE	SPUN FIBRE	FIBRE SPIN PITCH
337 (633 nm.)	retardation rotation	450 °/m. ~50 °/m.	2·3 °/m. ~0 °/m.	5·0 cm.
302 (633 nm.)	retardation rotation	60 °/m. 4·3 °/m.	< 1 °/m. ~0 °/m.	1·0 cm.
333 (1064 nm.)	retardation rotation	- -	< 2 °/m. ~0 °/m.	3·9 cm.
319 (1064 nm.)	retardation rotation	232 °/m. 1·1 °/m.	< 4 °/m. 0·4 °/m.	0·92 cm.
319 (1300 nm.)	retardation rotation	208 °/m. 4 °/m.	~4 °/m. 0·6 °/m.	0·92 cm.

Table 4.2 Comparison of birefringence in unspun and spun fibres.

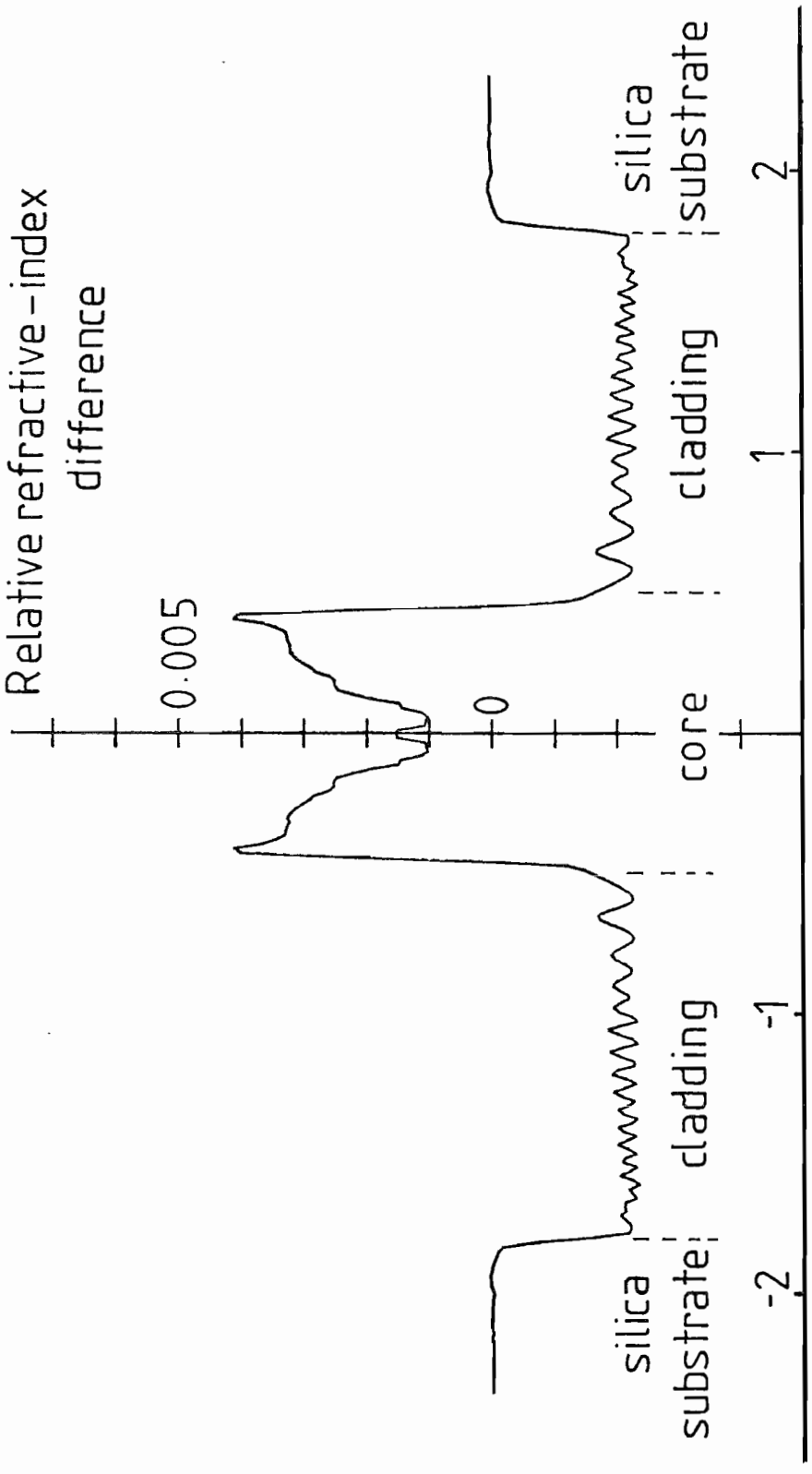

Figure 4.1 Refractive-index profile obtained by spatial filtering in preform GSB4, showing a large central index-dip in the core.

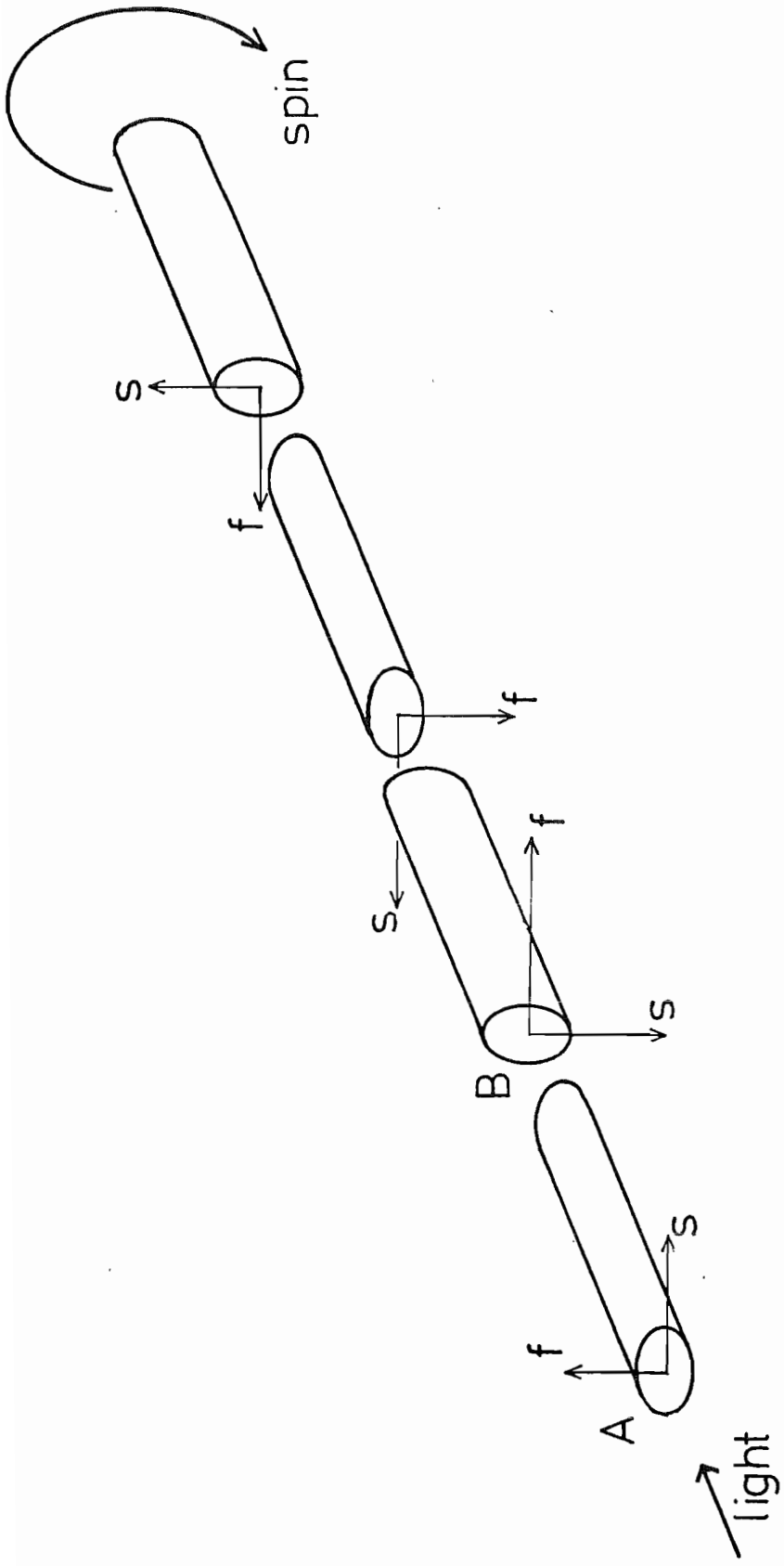

Figure 4.2 Simplified conceptual model to illustrate the averaging effect of spin on birefringence. 'f' and 's' denote "fast" and "slow" axis of each birefringent fibre section.

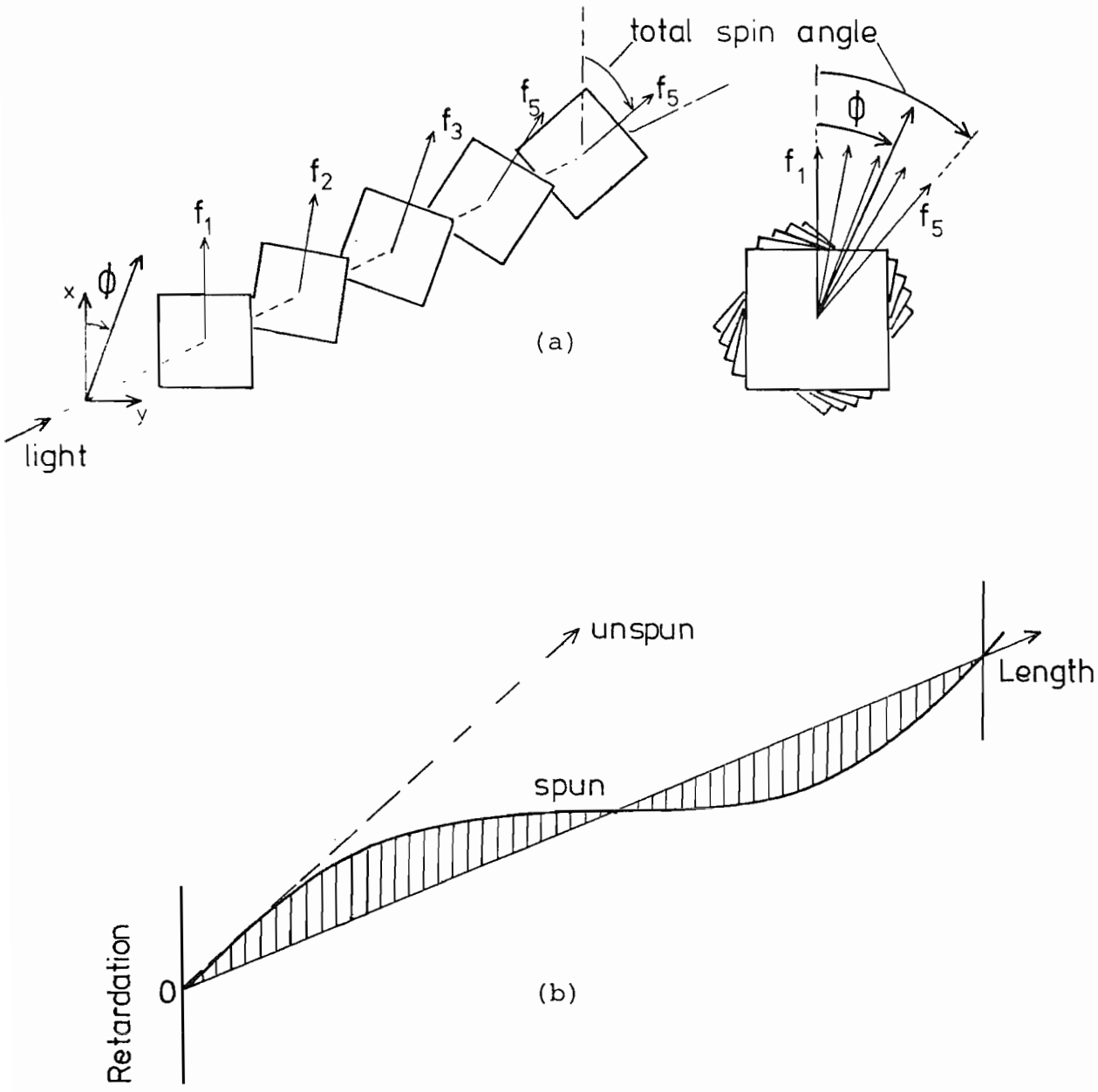

Figure 4.3 (a) Spun fibre model to illustrate the spiralling local fast axis and overall fibre principal axis equal to half the total spin angle.
(b) The overall retardation predicted in a spun fibre as a function of length.

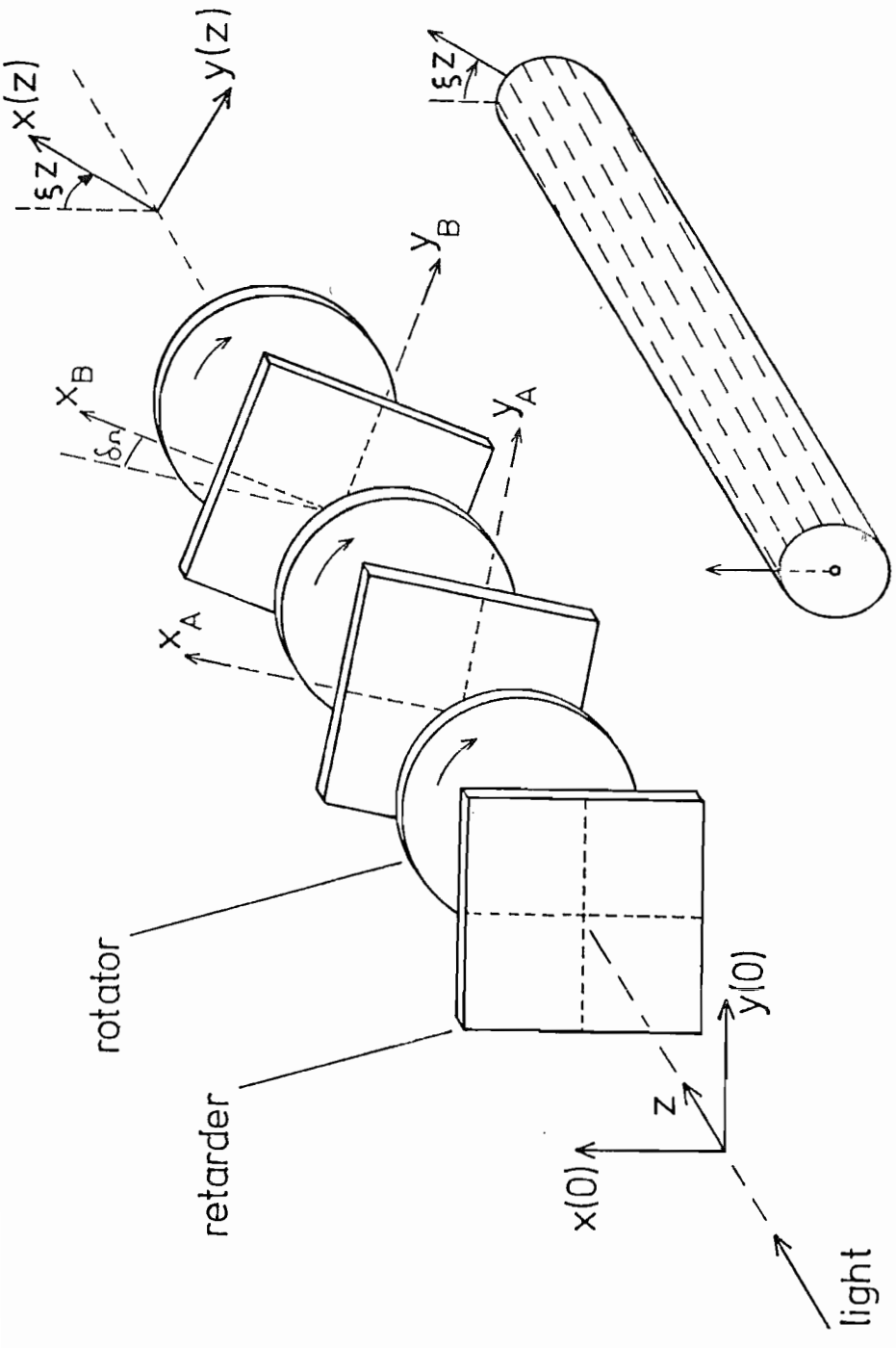

Figure 4.4 Schematic representation of model used for twisted fibre analysis.

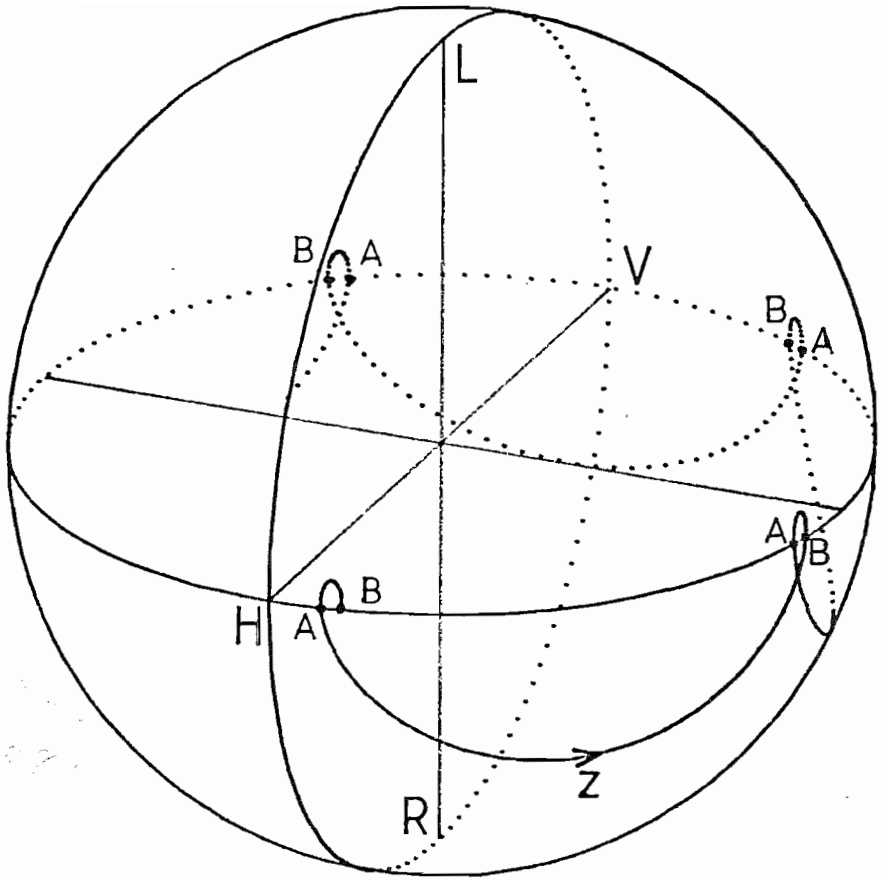

Figure 4.5 Polarisation evolution in a twisted fibre as a function of fibre length z, shown on the Poincaré sphere. Input angle $\theta_o = 5^o$, $\Delta\beta = 244.6^o/m$, $\xi = 24^o/m$. Total fibre length = 5m.

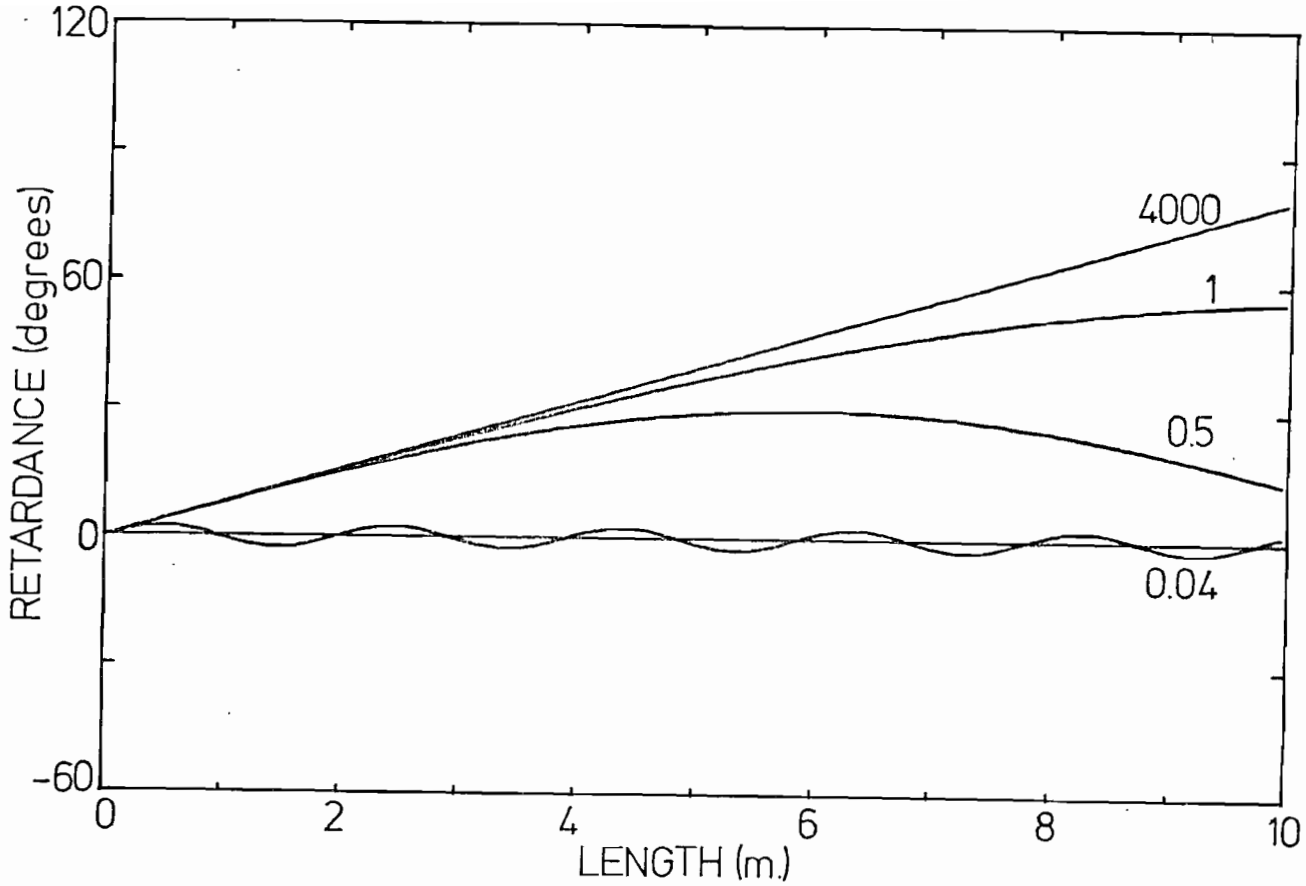

Figure 4.6 Calculated twisted fibre retardance as a function of length for various twist rates ξ given by the values of $\Delta\beta/\xi$ shown. Curves are plotted for an intrinsic linear birefringence of 8^{o}/m.

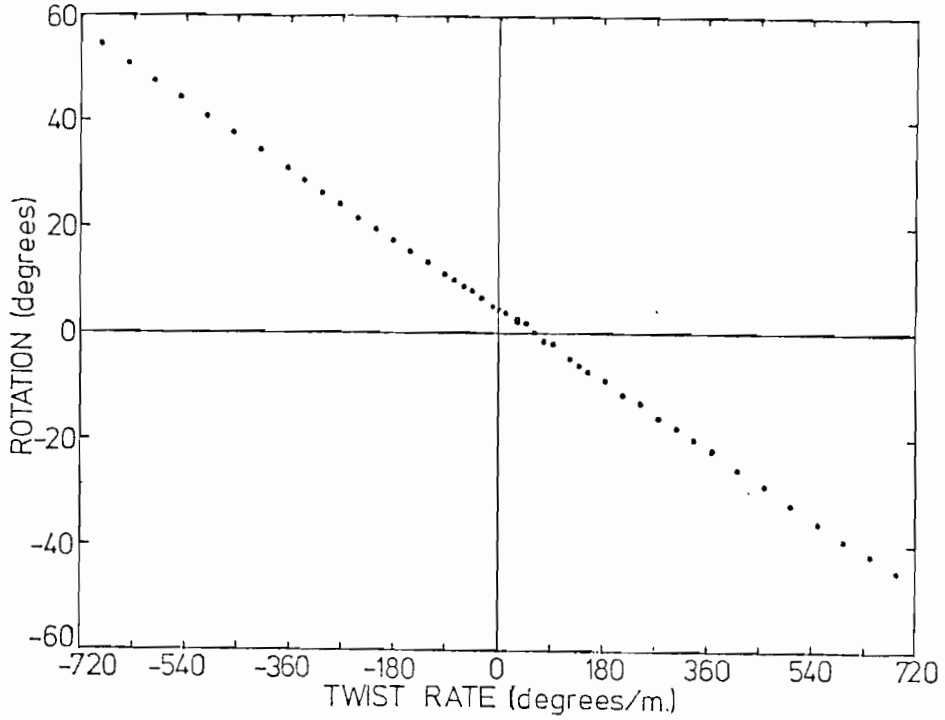

(a)

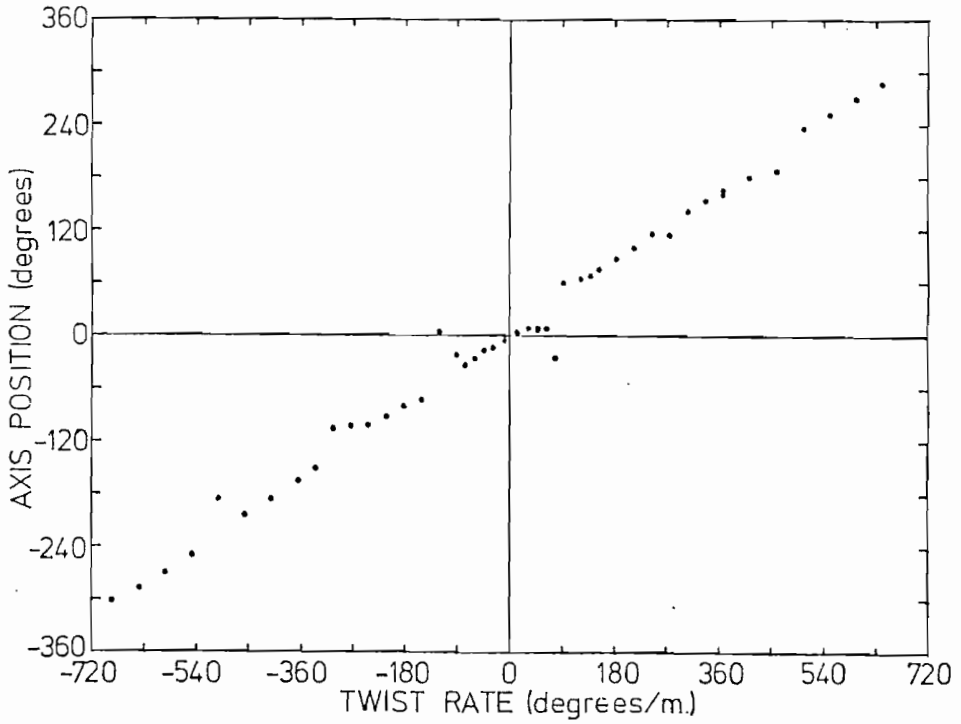

(b)

Figure 4.7 Large twists: measured parameters in fibre GSB4 as a function of fibre twist rate: fibre length = 0.983m; (a) rotation $\Omega(z)$
(b) principal axis position $\phi(z)$.

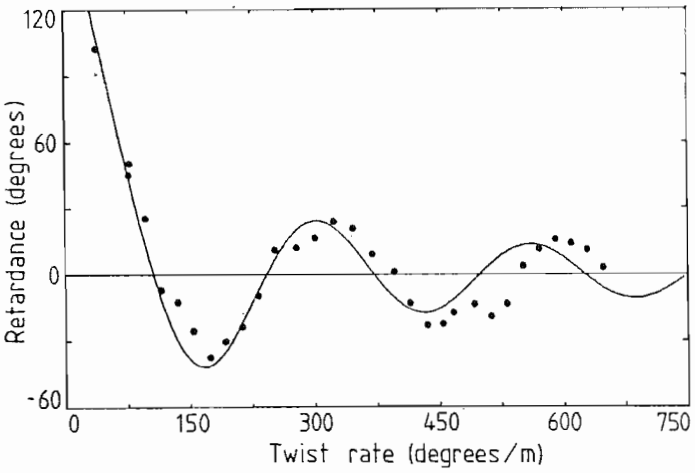

(a)

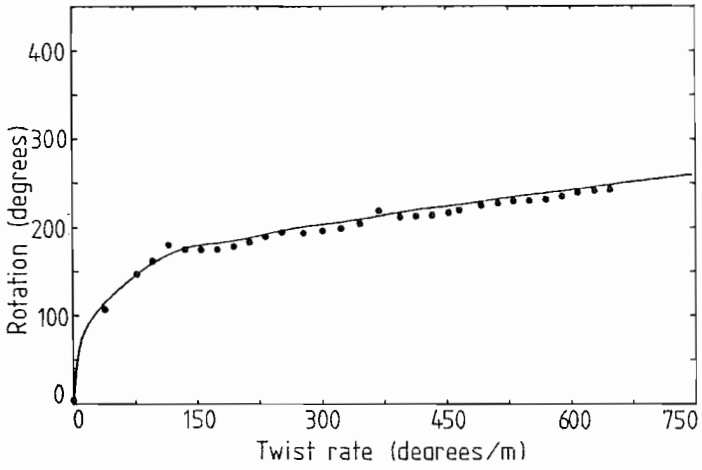

(b)

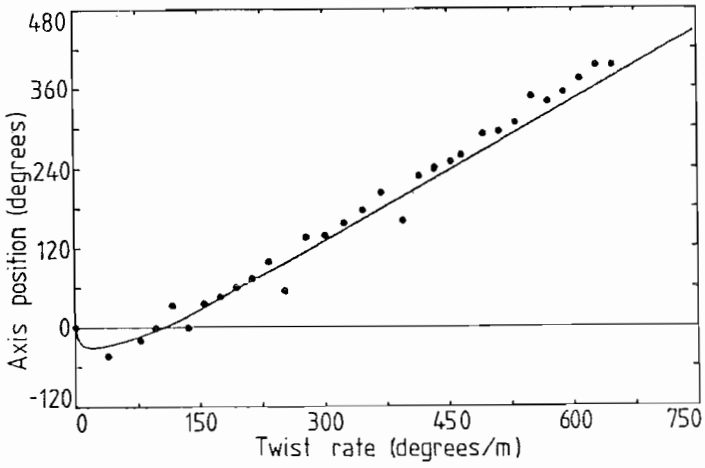

(c)

Figure 4.8 Small twists: (a) retardance, (b) rotation and (c) principal axis measured in fibre VD214 as a function of twist rate. Solid lines are calculated for g' = 0.073, $\Delta\beta$ = 123°/m and L = 1.544m.

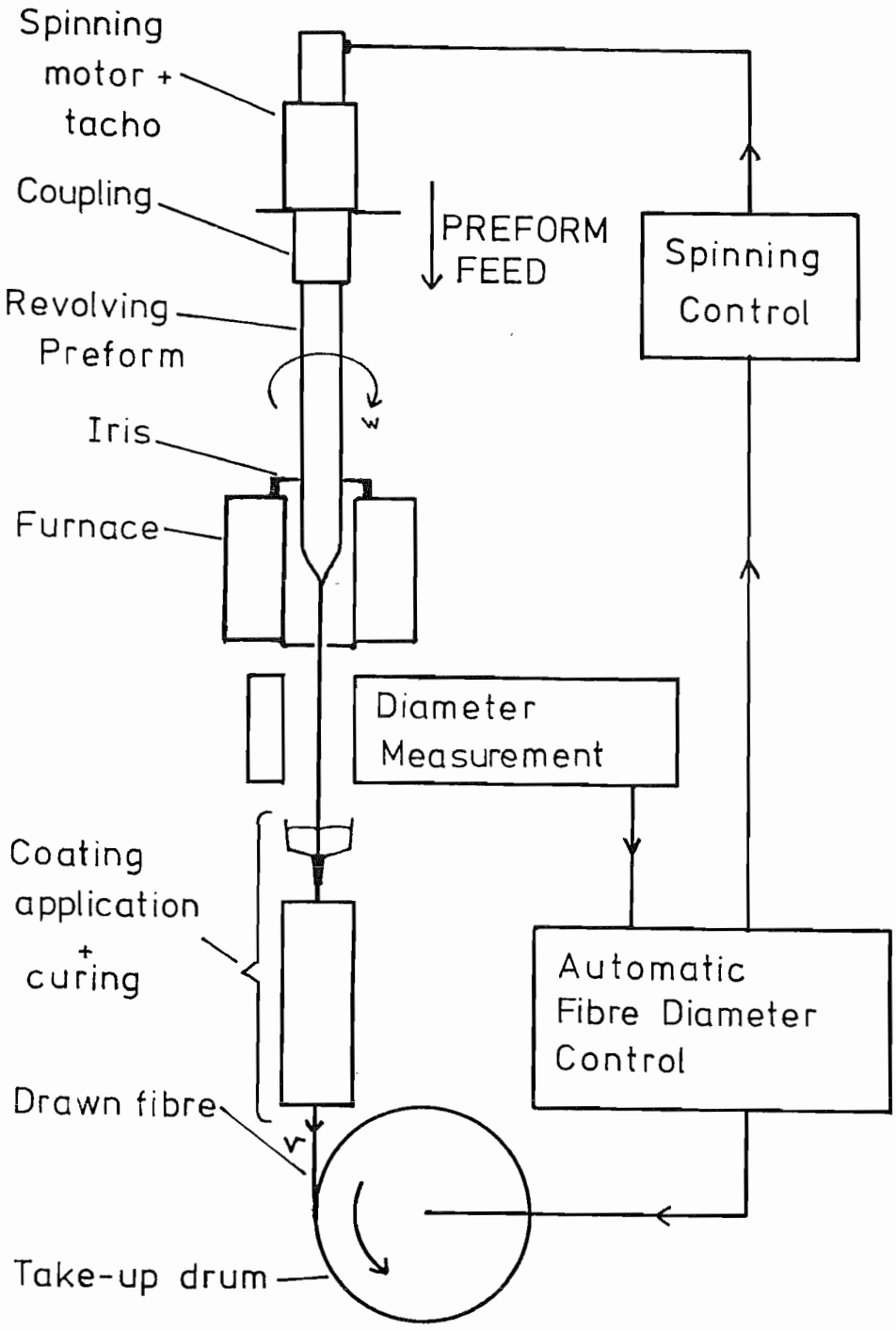

Figure 4.9 The fibre spinning process.

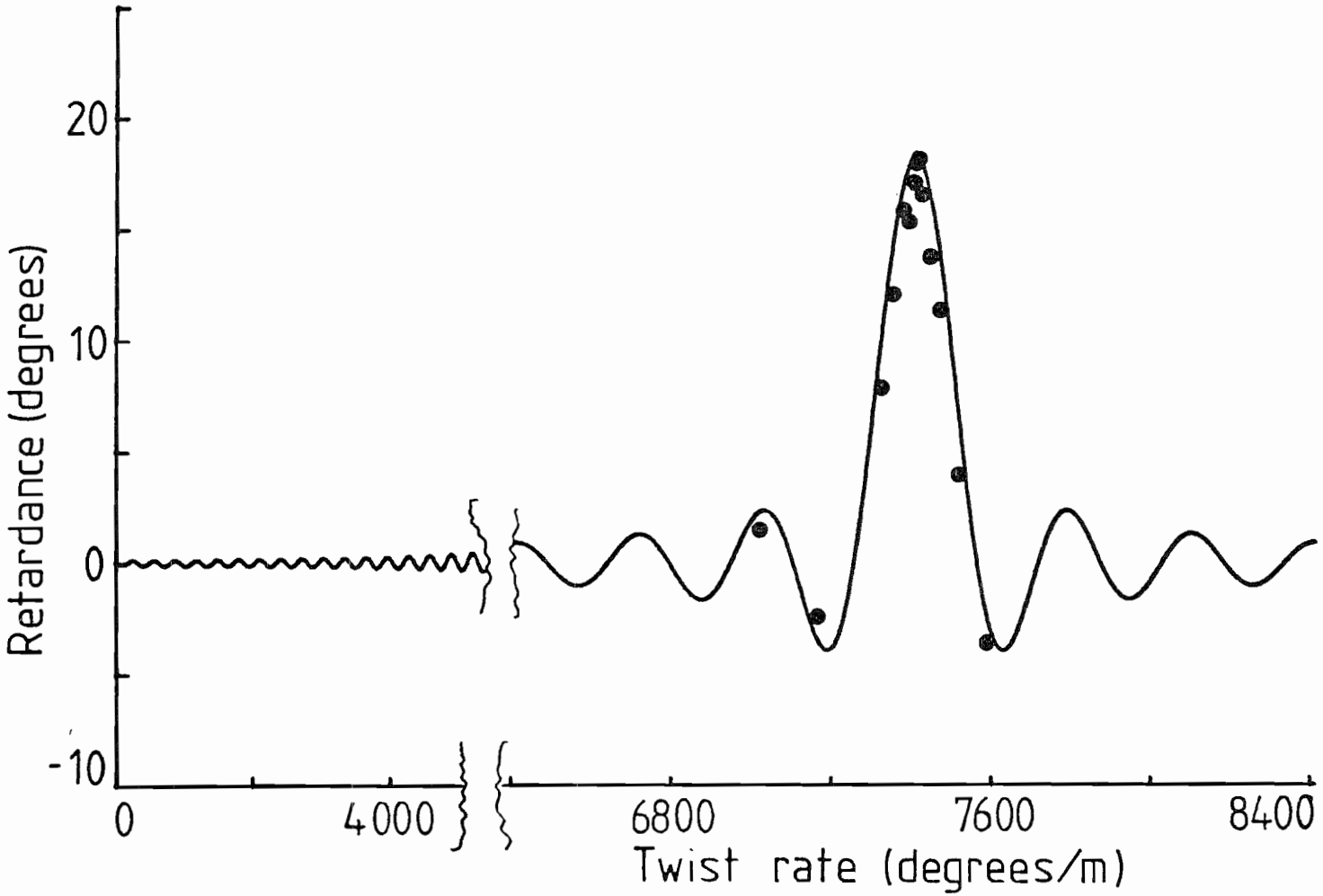

Figure 4.10 Retardance as a function of twist rate in 1.262m of VD348 spun fibre. Solid line is calculated using $\Delta\beta = 14.42^{o}/m$, s = 5.24cm.

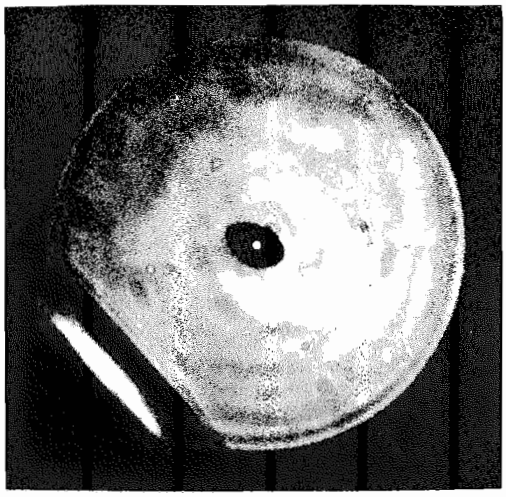

(a)

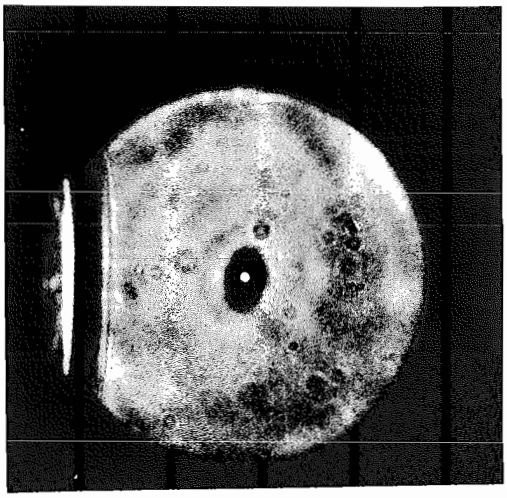

(b)

Figure 4.11 Cross-sections of an elliptical-core fibre when (a) spun with a spin pitch of ~ 1.2mm and (b) unspun.

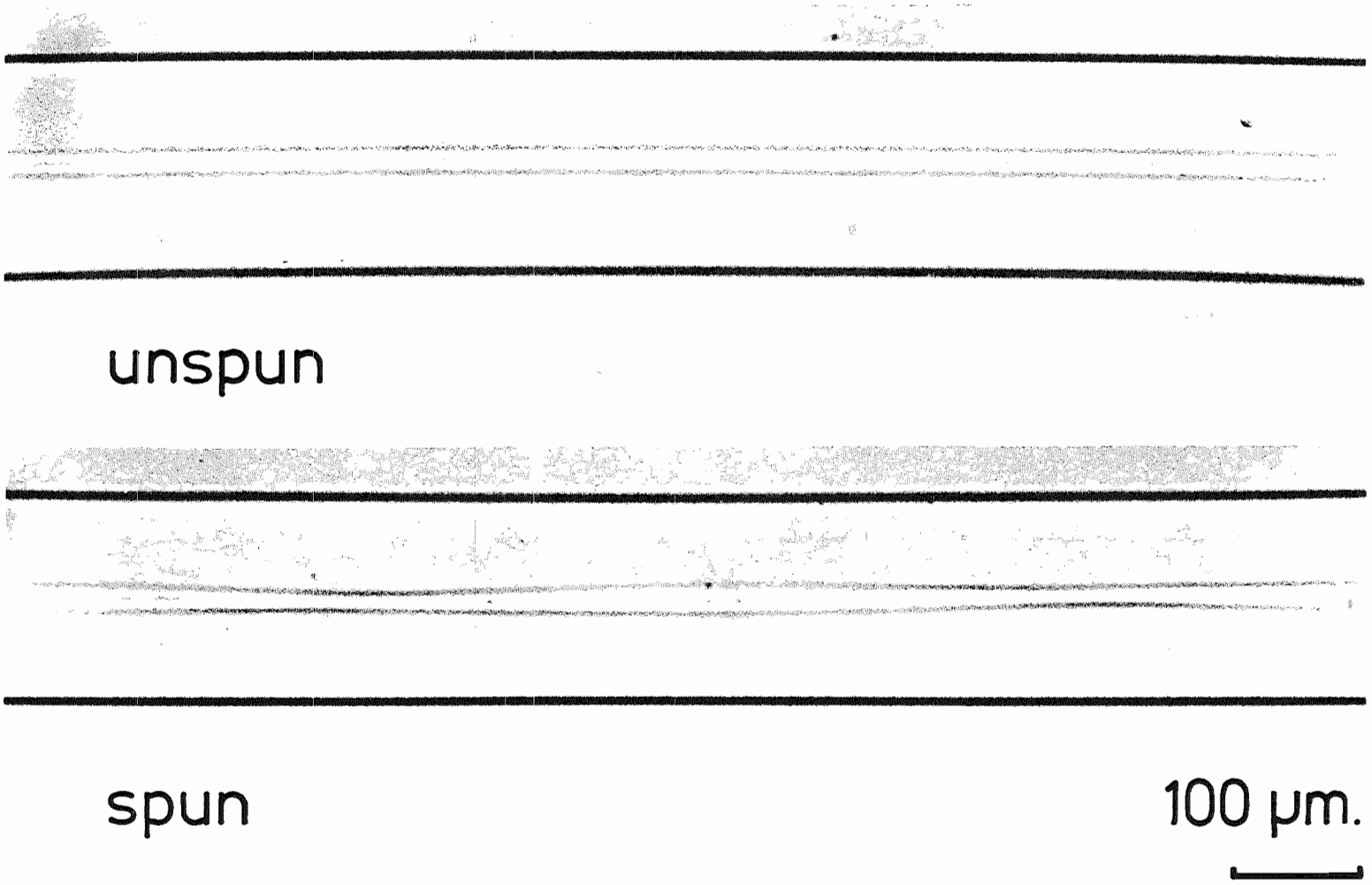

Figure 4.12 Comparison of the transverse sections of an elliptical core fibre when unspun and when spun with a pitch of ~1.2mm.

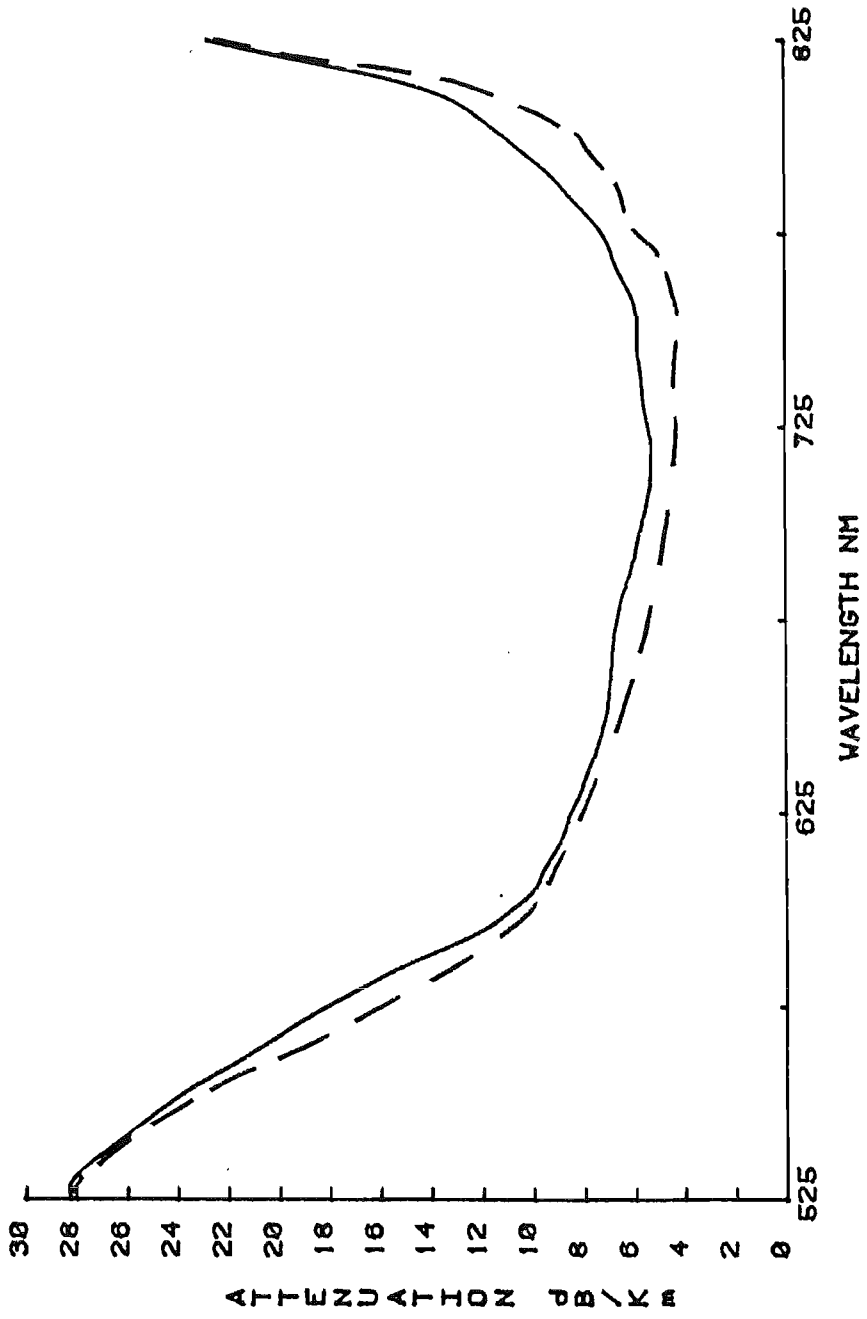

Figure 4.13 Spectral attenuation curves for fibre VD386 in unspun (lower curve) and spun (upper curve) conditions.